104
102

EVALUATING ABRASIVE WEAR RESISTANCE OF EXTRUDER TOOLING MATERIALS USING THE DRY SAND RUBBER WHEEL ABRASION TEST

by

William G. Halley

Thesis submitted to the faculty of the
Virginia Polytechnic Institute and State University
in partial fulfillment of the requirements
for the degree of

MASTER OF SCIENCE

in

Materials Engineering

APPROVED:

R.E. Swanson, Chairman

N.S. Eiss, Jr.

J.L. Lytton

August, 1990

Blacksburg, Virginia

EVALUATING ABRASIVE WEAR RESISTANCE OF EXTRUDER TOOLING MATERIALS USING THE DRY SAND RUBBER WHEEL ABRASION TEST

by

William G. Halley

Committee Chairman: R.E.Swanson
Materials Engineering

(ABSTRACT)

A series of experiments was performed on groups of samples made from materials currently used to manufacture tooling for extruders to determine if the ASTM G65 dry sand rubber wheel abrasion test could be used as an accelerated test to evaluate candidate materials. Samples were tested in the heat treated condition and after surface modification by plasma ion nitriding. The range of materials tested included medium and high alloy steels and steel bonded carbide composites. The abrasives used were AFS 50/70 test sand and Dresser Glasgrain crushed fused silica.

Evaluation of test wear scars and wear debris from the tests using AFS 50/70 showed that delamination was the primary wear mechanism for the composite materials, with some ploughing and microcutting, while ploughing and microcutting were the primary mechanisms in the wear of the steels. Evaluation of parts made from a composite material which were removed from service indicated that matrix erosion was the primary wear mechanism. Tests with Glasgrain fused silica as the abrasive yielded wear scars with the same morphology as the parts returned from service, but the very poor flow

characteristics of this material caused inconsistency in the supply of this abrasive to the contact region.

Interrupted tests showed that the wear rate was constant for the steels in the non-nitrided condition. After nitriding, the wear rate increased with test duration. The nitriding was found to act as a barrier coating providing an initial period of very low wear until the nitride layer is broached. The wear rate then increases to approximate the wear rate of the non-nitrided samples.

It was found that the friction force alters the location of the maximum normal force, shifting the point of greatest contact force toward the entry end of the wear scar.

ACKNOWLEDGMENTS

The author would like to thank the members of my committee, Dr. R.E. Swanson, Dr. N.S. Eiss and Dr. J. L. Lytton for their help and guidance throughout the course of my research and studies.

Many people at Virginia Tech and at Windward International, Inc have contributed to this research and the knowledge that I have gained at Virginia Tech. At Virginia Tech I would like to thank Stephanie Chanat, Todd Serafin, Rich Hays, Ken Imrich, Jinmyun Jo, Michel Laurant, Pascal Guerin, Chris Turman, Christophe Dehan, Kathy Rohr, and Karen Swanson. At Windward Bill Wood, Bobby Williams and formerly N. Wayne Stagner have all been very helpful. To all of you plus all the other people who have helped my thanks; I couldn't have done it without you.

TABLE OF CONTENTS

Page No.

LIST OF FIGURES ix

LIST OF TABLES xvi

1.0 INTRODUCTION 1

1.1 Terminology 1

1.2 Extruders 5

1.3 Tribosystem 9

1.3.1 Extruder 10

1.3.2 Resin 11

1.3.3 Filler 11

1.3.4 Operating parameters 12

1.3.5 Worn parts 16

2.0 REQUIREMENTS OF TEST 18

3.0 MATERIALS 21

3.1 CPM 10V 21

3.2 FerroTiC CM45 22

3.3 Thyssen 4122 22

3.4 Ferrotitanit 23

3.5 FerroTiC CM25 23

3.6 AISI 4150 24
3.7 D-2 tool steel 24
3.8 Ion nitrided samples 25
3.8.1 The samples 25
3.8.2 The process of ion nitriding . . . 26
3.9 Abrasives 29
3.9.1 AFS 50/70 standard testing sand . 29
3.9.2 Glasgrain crushed fused silica . . 30

4.0 WEAR TEST APPARATUS 32
4.1 Apparatus 32
4.2 Truing the wheel 33

5.0 TEST PROCEDURE 38
5.1 Rockwell C hardness tests 38
5.2.1 Weighing the sample 39
5.2.2 Mounting the sample 39
5.3.3 Wear testing 40
5.3.4 Calculating the volume wear loss . 41
5.4 Wear debris collection 41
5.5 Wear testing with Glasgrain 43

6.0 ABRASIVE WEAR 47
6.1 The effect of the sample 54
6.2 The load per abrasive particle 55

6.2.1 Spherical particles 56
6.2.2 Elongated particles 59
6.3 Wheel hardness 60
6.4 Abrasive particle transport modes 61
6.5 Operating parameters 63

7.0 RESULTS 68
7.1 Metallography 68
7.1.1 Thyssen 4122 68
7.1.2 D-2 tool steel 68
7.1.3 CPM 10V 69
7.1.4 FerroTiC CM45 69
7.1.5 FerroTiC CM25 70
7.1.6 Ferrotitanit 71
7.2 Rockwell C 71
7.3 Microhardness depth profiles 72
7.3.1 Thyssen 4122 73
7.3.2 CPM10V RC 55 74
7.3.3 CPM10V RC 59 75
7.3.4 AISI 4150 75
7.4 Wear tests 76
7.4.1 Thyssen 4122 76
7.4.2 D-2 tool steel 78
7.4.3 FerroTiC CM45 80
5.4.4 FerroTiC CM25 81

7.4.5 Ferrotitanit 82
7.4.6 CPM10V RC 55 83
7.4.7 CPM10V RC 59 84
7.5 ION NITRIDED SAMPLES 86
7.5.1 CPM10V RC 55 ion nitrided 87
7.5.2 CPM10V RC 59 ion nitrided 89
7.5.3 Thyssen 4122 ion nitrided 91
7.5.5 AISI 4150 ion nitrided 94
7.6 Interrupted testing 95
7.7 Low Speed Tests 97

8.0 DISCUSSION 100
8.1 Steels 101
8.2 Composites 101

9.0 CONCLUSIONS 107

10.0 RECOMMENDATIONS FOR FUTURE WORK 111

References: 112

LIST OF FIGURES

Page No.

Figure 1: Schematic of an extruder barrel showing liners and saddles 121

Figure 2: Worn saddle returned from service 122

Figure 3: Worn saddle region of a linerless barrel . . 123

Figure 4: Worn mixing element removed from service . . 124

Figure 5: Surface morphology of high wear region of saddle 125

Figure 6: Surface morphology of low wear region of a saddle 126

Figure 7: Sample configuration and orientation 127

Figure 8: Typical AFS 50/70 sand grains 128

Figure 9: AFS 50/70 sand grain showing crystal terminations 129

Figure 10: Size distribution Glasgrain fused silica (equivalent spheres) 130

Figure 11: Typical particles of Glasgrain fused silica 131

Figure 12: Schematic of the dry sand rubber wheel test apparatus 132

Figure 13: Tool bit holder and micrometer feed for truing wheel 133

Figure 14: Grinding attachment for truing test wheels . 134

Figure 15: Rockwell test locations 135

Figure 16: "Galled" region of D-2 steel wear scar

abraded by Glasgrain fused silica showing exposed carbides 136
Figure 17: "Polished" region of D-2 wear scar abraded by Glasgrain showing linear scratches 137
Figure 18: Wear scar surface of FerroTiC abraded by Glasgrain fused silica 138
Figure 19: Effect of asperity tip radius on critical angle 139
Figure 20: Static normal force distribution along contact region. 140
Figure 21: Dynamic normal force distribution along contact region. 141
Figure 22: Interrupted test samples showing movement of the wear scar with test duration. 142
Figure 23: Microstructure of Thyssen 4122. 143
Figure 24: Microstructure of D-2 tool steel. 144
Figure 25: Microstructure of CPM10V. 145
Figure 26: Microstructure of FerroTiC CM45. 146
Figure 27: Nonuniform distribution of titanium carbides in FerroTiC CM45. 147
Figure 28: Microstructure of FerroTiC CM25. 148
Figure 29: Microstructure of Ferrotitanit. 149
Figure 30: Microhardness versus depth profiles for ion nitrided samples. 150
Figure 31: Typical surface appearance of Thyssen 4122

ion nitrided samples. 151
Figure 32: Variations in nitride layer thickness on Thyssen 4122. 152
Figure 33: Ion nitride layer on CPM10V RC 55 samples. . 153
Figure 34: Two different surface appearances of the ion nitrided CPM10V RC 59 samples. 154
Figure 35: Microstructures of the gray and black ion nitrided CPM10V RC 59 samples showing lack of nitride layer on the gray sample and thin layer on the black sample. 155
Figure 36: Wear scar on Thyssen 4122. 156
Figure 37: Microchip wear debris from Thyssen 4122. . . 157
Figure 38: Acicular plowing wear debris from Thyssen 4122. 158
Figure 39: Sand grain fragment with transferred metal. 159
Figure 40: Wear scar on D-2 tool steel. Debris at bend in scratch contains silica and may indicate fracture of a sand grain. 160
Figure 41: Ridge of plowed metal on a D-2 wear scar showing transverse cracks. 161
Figure 42: D-2 wear debris containing microchips and cigar shaped particles. 162
Figure 43: Mechanisms for formation of cigar shaped particles. 163
Figure 44: Wear scar on FerroTiC CM45 showing exposed

titanium carbides shifted in the matrix. 164
Figure 45: Wear sheet detaching from FerroTiC CM45 wear scar. 165
Figure 46: Plate shaped particles in wear debris from FerroTiC CM45. 166
Figure 47: Microchip type particles in wear debris from FerroTiC CM45. 167
Figure 48: Cigar shaped particle in wear debris from FerroTiC CM45. 168
Figure 49: FerroTiC CM45 plate type wear particle becoming rounded into a cigar shaped particle. . . 169
Figure 50: Macrograph of FerroTiC CM25 wear scar showing pits and striations. 170
Figure 51: Wear scar on FerroTiC CM25. 171
Figure 52: Microchips in wear debris from FerroTiC CM25. 172
Figure 53: Plate type wear debris from FerroTiC CM25. . 173
Figure 54: Wear scar on Ferrotitanit. Note cracks in surface. 174
Figure 55: Loosely attached wear sheet on Ferrotitanit. 175
Figure 56: Sheet or plate type wear particles typical of Ferrotitanit. 176
Figure 57: Small microchip containing a titanium carbide particle found in the wear debris from Ferrotitanit. 177

Figure 58: Pits in wear scar of CPM10V RC 55. 178
Figure 59: CPM10V RC 59 wear scar. 179
Figure 60: Crack in bottom of "L" shaped pit in CPM10V RC 59 (arrow). 180
Figure 61: Large gouge in wear scar of CPM10V RC 59 with longitudinal crack at right edge. 181
Figure 62: Wear debris from CPM10V RC 59 consisting mostly of sheet or plate type particles, with occasional microchips (arrow). 182
Figure 63: Wear particle from CPM10V RC 59 which may have formed by wedging. 183
Figure 64: Cracks (arrow) in wear scar of ion nitrided CPM10V RC 55. 184
Figure 65: Pits in wear scar of ion nitrided CPM10V RC 55 (same region as Figure 64). 185
Figure 66: Loosely attached wear sheet in wear scar of ion nitrided CPM10V RC 55. 186
Figure 67: Sheet type wear particle in debris from ion nitrided CPM10V RC 55. 187
Figure 68: Microchip attached to silica fragment in debris from ion nitrided CPM10V RC 55. 188
Figure 69: Used sand grain with wear debris. 189
Figure 70: Enlarged view of crystal terminations on sand grain in Figure 69, showing microchips (arrows). . 190
Figure 71: Wear scar on a gray sample of ion nitrided

CPM10V RC 59 showing several cracks at the edge of wear sheets (arrows). 191
Figure 72: Unworn surface on a gray sample of ion nitrided CPM10V RC 59 showing several cracks. . . 192
Figure 73: Entry region of wear scar on a black sample of ion nitrided CPM10V RC 59 showing surface layer spalling off. 193
Figure 74: Center of wear scar on a black sample of ion nitrided CPM10V RC 59. 194
Figure 75: Transition in appearance of wear scar on ion nitrided Thyssen 4122. 195
Figure 76: Linear scratches on nitride layer of wear scar on ion nitrided Thyssen 4122. 196
Figure 77: Sheet of loosely attached smeared metal in wear scar on ion nitrided Thyssen 4122. 197
Figure 78: Wear sheet, with scratches, in debris from ion nitrided Thyssen 4122. 198
Figure 79: Microchip with thick center region in debris from ion nitrided thyssen 4122. 199
Figure 80: Sharply defined microcutting type scratches in nitride layer at ends of wear scar on ion nitrided AISI 4150. 200
Figure 81: Smeared and dented plowing type scratches in nitride layer at the ends of wear scar on ion nitrided AISI 4150. 201

Figure 82: Interrupted tests on D-2, showing a linear relationship of wear to sliding distance. 202
Figure 83: Interrupted tests on ion nitrided Thyssen 4122, showing a nonlinear relationship of wear rate to sliding distance. 203

LIST OF TABLES

Page No.

Table I NOMINAL COMPOSITION (weight percent) 116

Table II HEAT TREATMENT (DEGREES C) 117

Table III WEAR VOLUME LOSS (MM^3) 118

Table IV ROCKWELL HARDNESS VALUES 119

Table V 200 GRAM KNOOP MICROHARDNESS VERSUS DEPTH PROFILES 120

1.0 INTRODUCTION

1.1 Terminology

Before delving into the description of the specific problem addressed by this research, it is necessary to introduce some terminology. Much of the terminology of tribology has widely used general definitions which many people understand, however when these words are used in discussing aspects of tribology they have much more restrictive definitions. For example: What is abrasive wear? Webster's New Universal Unabridged Dictionary defines wear: "to become impaired, consumed, or diminished by constant use". Abrasion is defined as: "a wearing away by rubbing or scraping".[1] Combining these gives a definition of abrasive wear as becoming consumed or impaired by rubbing. This definition is not very useful in describing a specific problem as it is too broad. Many authors have narrowed the definition. Haworth [2] defines abrasion as "...removal of metals by the cutting or scrubbing action of extraneous abrasive materials." This definition is too narrow since abrasive machining is routinely applied to nonmetals and because the abrasive materials may not be extraneous. Avery [3] defines abrasion as "...the field where stresses imposed by hard (usually non-metallic) particles cause surface metal loss by scratching, grinding, gouging or chipping." Again

this refers only to metals. Avery further categorizes abrasion into three types: gouging, grinding, and scratching. Gouging abrasion involves high impact stresses, resulting in loss of large chunks of the abraded material. Without specifically saying so, Avery apparently includes chipping in the gouging category. Grinding abrasion, though occurring at a much lower stress than gouging abrasion, is still a high stress condition which causes crushing of the abrasive particles. The grinding he is referring to is rock crushing, such as ball milling of ore. Grinding, of the abrasive machining type, fits into the third category, scratching abrasion. In this category, the abrasive particle size is not significantly altered.

A number of standard definitions for tribological terms have been established. For instance, the Organization for Economic Co-operation and Development defined abrasion, or abrasive wear, as "Wear by displacement of material caused by hard particles or hard protuberances." [4]

The ASTM G40-88 terminology standard defines abrasive wear as " Wear due to hard particles or hard protuberances forced against and moving along a solid surface." This definition encompasses all of the key features of abrasion without being excessively limiting. It includes both the force which tends to make the hard particles penetrate the solid surface as well as relative motion. The situation

where abrasion results from hard protuberances, or asperities, on an opposing solid surface is commonly referred to as "two body abrasion". When abrasion is due to separate hard particles between two solid surfaces, the accepted terminology is "three body wear". Another distinction is that of one pass versus multiple pass abrasion. In one pass abrasion, the hard particles or asperities travel through the contact region only once. In multiple pass abrasion, the particles or asperities pass repeatedly through the contact region. In the case of three body abrasion, the particles either remain between the surfaces, or having escaped, re-enter the contact region. It should be noted that most cases of "one pass abrasion" are really limited exposure abrasion. Only in very special cases, such as impingement erosion or simulated asperity tests can it be reasonably assumed that any one particle or asperity has only a single encounter with the abraded surface. Thus in the usual case where the abrasion path is many times the size of the abrasive particle, a given particle will probably have many encounters with the abraded surface. Each of these encounters has the potential to alter the abrasive particle, so that the during a particle's final encounter the size, shape, or angularity of the abrasive particle may differ greatly from its initial encounter.

The abrasive condition which Avery called "grinding

abrasion" is commonly referred to as "high stress abrasion", while Avery's "scratching abrasion" is generally referred to as "low stress abrasion". The difference between these two is the effect of the abrasion process on the abrasive. In high stress abrasion, the abrasive particles or protuberances are crushed while in low stress abrasion, the particles or protuberances are essentially unchanged. Thus the properties of the abrasive, as well as the properties of the wearing surfaces, are important in determining the type of abrasion which predominates. These are only general classifications since there are probably no situations where either all or none of the abrasive particles or protuberances are crushed.

The term "hard" has been used repeatedly in the above definitions, however it has not been defined itself. In regard to abrasion, hard is a relative term. Thus the expression "hard particles" means particles which are harder than one or both solid surfaces. Babichev [5], Khruschov [6], and Richardson [7] have found that the wear rate is very low if the hardness of the particles is less than approximately three-fourths of the maximum hardness of the abraded surface, and that above about five fourths of the maximum hardness of the abraded surface the wear rate does not vary with increased particle hardness. The range from $^{3}/_{4}$ to $^{5}/_{4}$ of the maximum hardness of the solid surface represents a transition range in which the wear rate varies

with particle hardness.

1.2 Extruders

Extruders have been used in polymer processing since the middle of the nineteenth century, both in Europe and in the United States. These were simple machines, consisting of a single Archimedean screw in a pipe. These machines were used to process gutta percha and rubber, with use extended to casein, nitrocellulose and polyvinyl chloride as they became available. The first screw type extruder designed specifically for thermoplastic materials appears to have been built by Troester of Germany in 1935. [8] These simple, single screw machines proved to be an efficient means of forming some materials into useful shapes, of performing simple mixing and even of cooking the product, in the case of some food stuffs. However, these mechanisms depend on friction of the extrudate against the inside of the barrel to convey the material through the machine, and what mixing occurs is limited to the material in any given portion of the channel. To overcome these limitations, the co-rotating twin screw extruder was developed by Roberto Columbo of Italy. [9] The original intent was to provide positive displacement, thus removing the need for friction which had restricted the compositions which could be extruded.

It was soon discovered that the twin screw extruder

could be an efficient mixer if the degree of intermeshing and conjugation were controlled. This mixing action could be further enhanced by including kneading elements in the screw design. [10,11] Homogenization of the material in the machine could be controlled by cross channel flow. These machines were able to create filled polymers of different compositions. However, some of the filler materials were highly abrasive and some of the polymers were themselves corrosive or emitted corrosive materials. In addition to the chemical species inherent in the polymers, numerous chemicals were added, either to enhance some quality of the polymer (flame retardants, plasticizers) or to ease some step in manufacture (lubricants). Many of these chemicals were aggressive toward the machine parts they contacted. The corrosion and wear products can be contaminants in the extrudate, however the biggest problem is loss of efficiency due to increased clearance between the mixing elements and between the screws and the housing. This increased clearance causes a loss of production volume and loss of product quality through loss of mixing action.

The design engineers' search for better solutions to various end use problems has led to the development of numerous polymeric formulations. Many of these materials contain fillers of one type or another. Particle and short fiber filler materials combine several characteristics which

render them of special value. These filler shapes provide useful increases in physical properties while remaining suitable for extrusion processing and injection molding. In addition to physical properties such as strength, proper choice of filler material, particle shape, and loading level can allow tailoring of thermal and electrical properties. The fillers may also serve to replace some of the more expensive polymer, thus reducing the cost of the final material.

One composite material which takes advantage of the ability to tailor properties to a specific end use is electronic molding compound. This is the material used to encapsulate integrated circuits, that is, it forms the visible part of the classic "chip" which has become ubiquitous in our society. This application requires a material which is strong, tough, resistant to the environment, and not corrosive toward electronic components such as silicon, metallization, or the metal leads and pins. In addition it should have a coefficient of thermal expansion close to that of silicon, have reasonably good thermal conductivity, have high dielectric strength, good flame resistance, and be readily injection moldable and inexpensive. The material which meets these requirements is an epoxy resin filled with approximately 70 percent crushed, fused silica. This material is used in large quantities

(75,000 tons in 1988 [12]), therefore a continuous, as opposed to batch, manufacturing process is advantageous. This material can be, and is, made in twin screw compounding extruders. Since the silica is used in part to modify the linear coefficient of thermal expansion and dielectric strength of the resin, the uniformity of distribution of the filler particles in the resin is important. The uniformity of the mixture deteriorates as the clearance between the mixing elements in the extruder increases, therefore wear of the machine parts can lead to both a loss of production volume and to the production of unsuitable material. Since this resin is a thermoset, it cannot be salvaged by reprocessing, as might be the case with thermoplastic materials. It is therefore necessary to err on the side of caution in regards the life of the extruder parts to avoid expensive errors.

Wear of machine parts is a critical factor in production of a quality product at a reasonable cost, yet this material is an aggressive wear environment due to the silica filler. Extruder tooling contributes to total extrudate cost through cost of purchase and through productivity (machine downtime and quality). The most wear resistant tooling currently is made of expensive, difficult to machine, tool steel bonded carbide composite materials. These parts have a high purchase cost, however they offer significantly longer

service life than alternate materials. Because of the cost/life tradeoff, there exists a need to either further extend the service life of the metal matrix composite materials or to find alternative materials which could give equivalent life at a lower initial cost. There is also a need to develop an accelerated test to evaluate candidate materials.

The purpose of this research is to develop a test which can then be used to evaluate potential materials and surface treatments for service in twin screw mixing extruders.

1.3 Tribosystem

Czichos [13] proposed a system approach for evaluation of tribological problems. He suggested that only by considering all components of a tribological system could any hope of understanding be achieved. Before a valid simulation of a situation can be created, it is necessary to find out what is to be simulated. Since parts of a tribological system almost always affect each other, they can not be evaluated separately. Thus in abrasive wear it is not enough to consider just the characteristics of the wearing part, but also those of the abrasive, the counterface and the environment.

In the development of an accelerated test which can adequately represent an extruder, it is necessary to examine

an extruder as a tribological system. This requires consideration of the various mechanical parts of the extruder, the epoxy resin, additives to the resin, and the silica filler. The normal operating parameters, such as temperature and rotational speed, also must be included. Examination of worn parts removed from service and verbal reports from extruder operators also constitute valuable input, but must be evaluated judiciously.

1.3.1 Extruder

A twin screw mixing extruder consists of two screws rotating inside a barrel. Each screw is an assembly of separate sections, or segments, mounted on a central mandrel. The mandrels are driven by a motor-gearbox system. Torque is transmitted to the screw segments by one or more keys in key-ways, or by splines. The barrel may consist of a single piece bored lengthwise, but more normally is split axially into two halves which can be hinged open for cleaning, maintenance or repair ("clamshell barrel"). Each half may consist of a single piece or there may be separate barrel liners, held in place by "saddles", which function as keystones. These features are illustrated in Figure 1. The length of the barrel is divided into zones, each equipped for heating and cooling. Normally the entry zone is heated to melt the resin while the other zones are cooled to remove

excess heat. During initial start-up with a cold machine external heat may be supplied to all zones in order to reach operating temperature quickly.

1.3.2 Resin

In the case of electronic molding compound the resin is an epoxy of the epoxidized cresol novolac type with an ortho-cresol formaldehyde novolac hardener. A percentage of epoxidized phenol novolac may be included to increase the speed at which curing takes place. Flame retardant additives to the resin generally include an organo-bromine compound and antimony oxide, which combine under heat to form antimony oxihalides. Other additives include molding lubricants, pigments, and coupling agents. Coupling agents used with silica fillers are generally epoxy functional silanes. The coupling agents improve the bond between the epoxy and the silica particles, resulting in improvement of mechanical properties and resistance to moisture infiltration.[14,15]

1.3.3 Filler

Crushed fused silica is the filler material most widely used in the manufacture of electronic molding compound. This material combines a very low coefficient of linear thermal expansion with acceptable thermal conductivity. It is also

relatively inexpensive. This material is manufactured by melting carefully selected and cleaned silica sand, solidifying the melt, and crushing and grinding it to size. The result is an amorphous material with an extremely angular particle shape.

1.3.4 Operating parameters

Operating conditions for a typical 127 millimeter (five inch) nominal diameter extruder manufacturing electronic molding compound are 149°C (300°F) and 150 RPM. This gives a tip velocity of 1 meter per second (3.3 feet per second). This rotational velocity is only approximate. It will vary from machine to machine and plant to plant. It typically will be higher for smaller diameter machines because the higher surface area to volume ratio allows extraction of more heat. It is also increased as wear occurs to compensate for loss of shear intensity and pumping efficiency, and to maintain product quality and production volume.

Screw segments which are removed from service and then returned to service need to be cleaned of polymer prior to reuse. Standard practice includes placement of the segments in an oven at 425 to 480° C (800 to 900° F) to char the epoxy. The residue can then be wiped off. Occasionally, especially in smaller shops, the extruder barrel is hinged open and the epoxy is set on fire in the barrel. This is not

considered good practice because, aside from the health hazards, danger of fire, and contamination of everything in the building, it is not possible to control the temperatures to which the extruder parts are exposed. This practice may account for the anomalously short wear lives of some tooling.

In a properly set up extruder, the screws do not touch each other or the barrel liner during normal operation. Minimum clearance between new components is usually on the order of 0.13 millimeters (0.005 inches), and can be expected to increase with wear. Particle size analysis of the crushed fused silica gives an equivalent sphere size of 0.013 millimeters (0.0005 inches), thus the occurrence of metal-silica-metal contact is rare. This lack of metal-silica-metal contact is further evidenced by examination of parts removed from service, where it is noted that the most wear occurs at the peak of the saddles and on the corners of mixing elements, rather than the barrel surface and the outer diameter of the elements. The high wear regions tend to be regions with larger than minimum clearance, but also regions where the extrudate is forced to change direction. Although these regions of high wear have a reduced probability of direct, hard contact, they are regions of intense shearing of the polymer. Since direct metal-silica-metal contact is probably a rare occurrence anywhere in the extruder, these high shear regions represent the areas which experience the

highest average normal force of the silica against the metal parts. However, since direct contact is not occurring, this force results from compression of the polymer and the resistance of the polymer to silica particle motion.

Because of the relatively large separation between the screw and barrel, the extruder can be considered in the simplest form as multiple cases of a tribological system consisting of polymer-silica-metal. For instance, when considering wear of a mixing element, the only effect of the barrel is to constrain the polymer and alter the apparent viscosity.

The force required to embed a silica particle in the epoxy resin, which is the force contributing to wear by loading the silica particles against the metal surface, is a result of both polymer characteristics and operating parameters. Many of these factors vary with position along the length of the extruder. The epoxy initially is a granular solid, which melts to form a highly viscous liquid. As the temperature increases, the viscosity decreases. In competition with the decrease in viscosity due to increased temperature, the apparent viscosity increases as the silica is incorporated. In the early stages of mixing, the mixture is inhomogeneous, resulting in a variable apparent viscosity. Cross linking begins, which also increases the viscosity. The temperature varies both axially and radially. In the

entry stages, it is necessary to supply heat to melt the resin by heating the barrel. However, cross-linking is exothermic and the later sections of the extruder barrel are water cooled. Thus in the entry stages the temperature is highest at the barrel surface while in the later stages the temperature is lowest at the barrel surface. The temperature will also show a local variation related to the intensity of shearing, being higher in regions of intense shear. The apparent viscosity also increases with increased shear rate. In addition to the factors affecting viscosity, there is a surface energy factor in the early stages of the extruder. Because the silica and epoxy are separate powders, any penetration of the silica into the epoxy entails formation of new surface. Initially this surface may be an increase in the air-epoxy surface area resulting from denting of the epoxy surface by the silica particles, but eventually new epoxy-silica surface must form if mixing is to occur. This surface energy factor is additive to the viscosity derived force. In other words, it will require less energy to move a particle embedded in epoxy than to move a particle on the epoxy surface.

Corrosion of the extruder tooling by the polymer also needs to be considered. Where corrosion occurs in conjunction with a wear process loss of materials is often much more rapid than would be expected from either the wear

resistance or corrosion resistance capabilities of the material. Many researchers [16,17,18,19] have found that the synergistic effect of corrosive wear can result in weight loss rates as much as four times greater than expected, thus even minor corrosion effects can become important. Although pure epoxy is relatively inert, it can contain contaminants from the manufacturing process, especially chloride ions, which are aggressive. Organo-bromine compounds are also included as flame retardants which can emit bromide ions and may contain other halide ions as impurities. However, corrosion weight loss tests of typical extruder tooling materials in electronic molding compound, performed by Michael J. Ward, showed that this material is essentially inert toward iron base materials [20]. Based on these results, corrosion is assumed to not be a significant factor in the wear of extruder tooling used in the manufacture of electronic molding compound.

1.3.5 Worn parts

Examination of field worn parts shows that wear occurs initially, and most severely, on the ridge of the saddle and on the outer corners of the mixing elements. Wear of the saddle is illustrated in Figure 2 and the equivalent region of a linerless barrel is shown in Figure 3. The wear regions on a typical mixing element are shown in Figure 4. Note that

the machining marks are still visible on the outer diameter of this element.

The only used elements which were available for sectioning and examination by scanning electron microscopy (SEM) were made from tool steel bonded carbide material. These parts showed no indication of the parallel scratch type of abrasion such as is typical of grinding operations. They did show exposed carbides in relief above the matrix material. This was true both in regions of relatively high wear and relatively low wear. This is readily apparent in Figures 5 and 6, which show the surface of high and low wear regions of the saddle section shown in Figure 2. This indicates that the wear mechanism is probably the same in both regions with the difference in wear loss resulting from either differences in intensity or differences in opportunity. It is not known how this saddle section correlates with the screw segments. For instance the high wear region may correspond to a mixing segment, with high shear stress, while the low wear region is a screw (feeding/conveying) segment with low shear stress, but this is not known for certain.

2.0 REQUIREMENTS OF TEST

Consideration of the material flow in an extruder indicates two requirements of a test intended to simulate the conditions in the extruder. These requirements are that the test has a one-pass system and that the abrasion flow be unidirectional. Because the material flows through a two screw extruder as a result of its positive displacement pumping action, each portion of the extruder is only exposed to a particular abrasive particle once. This indicates that a one pass type of test would be preferable. Also, since the material only flows in one direction, a unidirectional test is better than an oscillatory test.

The fact that even the minimum clearance between the screws and the barrel is much larger than the silica particle size indicates that the conditions during extrusion of electronic molding compound are primarily of the low stress type. It is probable that occasional fracture of a silica particle occurs, either due to an exceptionally large particle or as the result of the formation of a "log jam" of several particles, however it is unlikely that these events are common. In general the stress applied to the silica particles is a result of the force necessary to move it through the epoxy, which is not likely to be large enough to fracture the silica particles. Note that although high

pressures are attainable in an extruder, the resulting stresses applied to the silica particles would be hydrostatic in nature and would not cause fracture. The uniaxial and shear stresses which could cause fracture of the particles are limited to the force (stress x area) necessary to move the particle through the molten epoxy. These stresses are related to the viscosity of the melt and to interactions with other particles. This indicates that the test should be of the low stress type and that the abrasive particles should be restrained yet able to move under load. The fact that there is less than a complete monolayer of sand makes it more likely that all of the particles are forced against the sample surface regardless of their actual size. Even with the restricted size range of AFS 50/70 sand, it is possible that a small grain among several larger grains would bear less than its share of the applied load, however the open arrangement makes this less likely. The abrasive particles are free to rearrange themselves with respect to each other and to the surfaces of the parts in the extruder. A three body type of test utilizing loose abrasive particles would therefore be more appropriate than a test utilizing two body, fixed abrasive test. The particles are constrained to a degree by the viscosity of the epoxy, so that the test should provide for resilient constraint of the abrasive.

Summarizing the above paragraphs, the test should have

the following characteristics:

1) be one pass
2) be unidirectional
3) be low stress
4) utilize three body abrasion
5) offer resilient constraint of the particles

In addition, the test should allow the wear debris to be collected for analysis, use samples of relatively simple shape, and be of fairly short duration.

A test which meets these criteria is ASTM G65 - Dry sand rubber wheel abrasion test. This test offers the additional benefit of being standardized, thus the work necessary to establish that the test method is capable of producing repeatable test results has already been performed. The ASTM G65 standard test was chosen to evaluate the materials in this study.

3.0 MATERIALS

Materials chosen to be evaluated in this study consist of materials which are currently used to manufacture extruder screw segments, competitive materials from new manufacturers or new materials from existing manufacturers, and a standard material. These materials were tested heat treated in accordance with standard practice for screw segment application. In addition, those materials which are candidates for use in the ion nitrided condition were tested after ion nitriding.

The materials currently used for screw segments are CPM10V, FerroTiC CM45, and Thyssen 4122. Ferrotitanit and FerroTiC CM25 were evaluated as competitors of CPM10V and FerroTiC CM45 while AISI 4150 was evaluated as a replacement for Thyssen 4122. D-2 tool steel was included as the standard material since this is the material used to qualify the ASTM G65 standard. The nominal chemical analyses of these materials is presented in Table I.

3.1 CPM 10V

CPM10V is a product of Crucible Specialty Metals Inc. This material is produced by hot isostatic pressing (HIP) of the appropriate powders. Carbides form during the HIP process. Luken [21] reported that the carbides are

vanadium carbides of the MC type, containing equal proportions of vanadium and carbon, regardless of the heat treatment. CPM10V is utilized at two hardness levels, nominal Rockwell C 55 and nominal Rockwell C 59, which result from different heat treatments. The heat treatment parameters are given in Table II. Twelve samples at each nominal hardness level, each 0.5 X 1.0 X 3.0 inches, were supplied by Windward International, Inc. in the heat treated state. Sample configuration is illustrated in Figure 7a.

3.2 FerroTiC CM45

FerroTiC CM45 is manufactured by Alloy Technology, Inc. This material is manufactured by liquid phase sintering of powdered matrix alloy and titanium carbide powder. The nominal composition includes 45 volume percent titanium carbide. Windward International, Inc. supplied material as partial cylinders cut from round bar, each of which was diamond sawed into a slab with parallel flat sides and a piece with one flat side and one semicircular side. This is illustrated in Figure 7a. Each of these pieces were then heat treated to parameters provided by Windward. The heat treatment specifications are given in Table II.

3.3 Thyssen 4122

Thyssen 4122 is a medium chromium stainless steel

produced by conventional ingot metallurgy steel making practice. This material is produced by Thyssen Edelstahlwerke AG. of Germany. Although this material is not normally used in abrasive applications without surface hardening treatments such as nitriding or boriding, it was evaluated to create a baseline for comparison so as to be able to evaluate the effectiveness of surface treatments. This material is used in the annealed state. Twelve samples, each 12.7 X 25.4 X 76.2 millimeters (0.5 X 1.0 X 3.0 inches) as shown in Figure 7a, were supplied by Windward International, Inc.

3.4 Ferrotitanit

Ferrotitanit, a direct competitor to FerroTiC CM45, is also manufactured by Thyssen Edelstahlwerke AG. Twelve samples each 12.7 X 25.4 X 76.2 millimeters (0.5 X 1.0 X 3.0 inches), were supplied by Windward International, Inc. in the heat treated state. Sample configuration is illustrated in Figure 7a. Heat treatment parameters are listed in Table II.

3.5 FerroTiC CM25

FerroTiC CM25 was manufactured by Alloy Technology, Inc. specifically for evaluation in this study. This material was manufactured by liquid phase sintering of powdered matrix alloy and titanium carbide powder. This material is

essentially FerroTiC CM45 with a reduced percentage of titanium carbide, 25 volume percent rather than 45 volume percent. FerroTiC CM25 is proposed as a lower cost competitor to FerroTiC CM45 and Ferrotitanit. Twelve samples each 12.7 X 25.4 X 76.2 millimeters (0.5 X 1.0 X 3.0 inches) as shown in Figure 7a, were supplied in the heat treated state by Alloy Technology Inc. Heat treatment parameters are proprietary, however they are probably similar to those for FerroTiC CM45 since the matrix alloy is the same.

3.6 AISI 4150

AISI 4150 is a medium carbon low alloy steel produced by conventional ingot metallurgy steel making practice. Samples of this material were provided by Windward International, Inc. as 12.7 X 25.4 millimeter (0.5 X 1.0 inch) flat bar stock, sawed into 76.2 millimeter (3 inch) lengths as shown in Figure 7b, and heat treated. After these samples were prepared and wear tested, the vendor notified Windward International that the material was not AISI 4150 but was of uncertain composition. The wear results from these samples were therefore discarded as meaningless. This unfortunately eliminated the baseline for comparison of the ion nitrided 4150 results.

3.7 D-2 tool steel

D-2 is a high carbon, medium chromium tool steel produced by conventional ingot metallurgy steel making practice. This material was purchased as 12.7 X 25.4 millimeter (0.5 X 1.0 inch) flat bar stock from commercial warehouse inventory, however it was supplied as 12.7 X 25.4 millimeter (0.5 X 1.0 inch) flat stock sawed from 12.7 millimeter (0.5 inch) thick plate, as shown in Figure 7c. These samples were heat treated to ASTM G65 specification. The heat treatment parameters are given in Table II. These samples were protected from oxidation during heat treatment by wrapping them in newspaper and stainless steel foil before austenitizing. Heat treatments were performed in a Sybron Corporation Thermoline 2000 furnace. Temperature was monitored using an Omega Engineering, Inc. model 115KC digital thermometer and chromal-alumel thermocouple.

3.8 Ion nitrided samples

3.8.1 The samples

Groups of ten to twelve samples of CPM10V heat treated to Rockwell C 55, CPM10V heat treated to Rockwell C 59, heat treated AISI 4150, and annealed Thyssen 4122 were prepared by Windward International and then sent to a commercial ion nitriding firm for nitriding. These samples were all ion nitrided at 525 °C (975°F) for 36 hours.

3.8.2 The process of ion nitriding

There are two processes referred to commercially as "ion nitriding". These are ion implantation and plasma ion nitriding, also called glow nitriding. These two processes have nothing in common except the name and the use of nitrogen. Ion implantation is a low temperature process in which nitrogen ions are accelerated through an electric field and ballistically implanted into the target. Because this is a low temperature process almost no diffusion takes place. The nitrogen therefore ends up almost entirely as interstitials, with no formation of nitride precipitates. The nitrogen concentration resulting from implantation is a Gaussian distribution about the maximum concentration, which occurs at a depth below the surface determined by the accelerating voltage. The width of the distribution generally increases as the depth of implantation, or the accelerating voltage, increases [22].

Nitrogen implantation can reduce both friction and wear, and as a result of the non-equilibrium structure the nitrogen migrates ahead of the wear surface, enhancing wear resistance to depths greater than the original implantation depth [23]. However, at the high ion doses needed for wear performance enhancement, problems are encountered with sputtering of the target and deposition of materials

sputtered from tooling used to support the target during implantation [24].

Plasma ion nitriding [25,26,27], on the other hand, is a relatively high temperature process in which nitrogen ions are deposited on the target surface and travel into the material by thermally activated diffusion. This results in the maximum nitrogen concentration at the surface. Because this is a high temperature process, alloying elements can diffuse through the lattice resulting in the formation of complex nitride precipitates. Plasma nitriding is performed by placing the target in a chamber containing low pressure nitrogen or a nitrogen/hydrogen mixture. A voltage is applied between the target and the anode, usually the chamber walls. This voltage causes electrons to leave the cathode (target), ionizing the nitrogen. The electrons, both the primary electrons from the cathode and electrons dislodged from nitrogen atoms during ionization, quickly move toward the anode, leaving the more sluggish ions and creating a positive charge in the plasma. Thus there are two sources of the electric field which the positive ions experience. The ions are attracted by the negative applied voltage and repelled by the positive charge on the plasma, resulting in the ions accelerating toward the target. Collisions in the plasma result in changes in the energy of individual ions with resulting shifts in electron orbits. These shifts give

rise to the characteristic visible glow near the cathode. The thickness of the glow is a result of the applied current, gas pressure , and the separation of the anode and cathode. Varying the gas pressure determines how closely the plasma will conform to the target surface. This phenomenon is used to mask off regions, such as holes, that are not to be nitrided, however it can also cause problems in the form of bridging and hollow cathode effect. In bridging, portions of the surface are not nitrided because the plasma does not "adhere" to the surface, thus few ions are deposited in these regions. The hollow cathode effect occurs when electrons become trapped in a confined volume of plasma, greatly increasing the local ion density and causing overheating of the surface surrounding the confined region. This often occurs inside holes and tubes which are in the transition size between bridged and nonbridged plasma, hence the name.

Energy is transferred to the target primarily through loss of kinetic energy of ions and energetic neutrals during collisions with the target. This kinetic energy is converted to heat in the target. It is possible to provide all of the heat needed to nitride the target from the plasma, however it is normal commercial practice to use auxiliary heaters to decrease the cycle time. The use of auxiliary heating allows both the voltage and current to be used to control the nitriding conditions, so long as care is taken that

overheating does not result.

As alluded to in the discussion of the hollow cathode effect, plasma nitriding is sensitive to the geometry of the chamber and load. This is because the concentration of ions, electrons and radicals in the plasma are a result of the balance between the rate at which these species are created in the plasma and the rate at which they are lost to the target and chamber walls. Therefore the chemistry of the plasma is strongly effected by the surface to volume ratio. In a job shop atmosphere this will vary from load to load. It should also be noted that the target surface area of interest is the effective area, that is the area being nitrided, which is found by subtracting any bridged regions and mechanically protected regions from the total surface area. This also enters into the applied current values, since the value of interest is the effective current density. Thus, in considering the area, only that area which is interacting with the plasma should be included. This net area may be considerably smaller than the total area, either intentionally or unintentionally.

3.9 Abrasives

3.9.1 AFS 50/70 standard testing sand

Two abrasives were utilized in this work. AFS 50/70

test sand is the standard abrasive specified in the ASTM G65 specification. This material was purchased from U.S. Silica Corporation, Ottawa, Illinois, an ASTM approved source. This sand is described by ASTM as a rounded grain, subangular silica sand. The individual grains are rounded when viewed at low magnification, but show many surface irregularities at higher magnification. Crystal terminations are present on many of the grains. It is believed that these crystal facets formed much more recently than the sand grain itself. In other words the sand deposit from which this sand was mined is in the process of converting into sandstone by the process of dissolution and redeposition of silica. The main effect of the crystal terminations is to provide areas with much smaller radius of curvature than would be expected from the sand grain size, in effect making the sand more angular. Morphology of typical grains is shown in Figure 8 and the crystal terminations are illustrated in Figure 9.

3.9.2 Glasgrain crushed fused silica

Dresser Glasgrain fused silica is the type of crushed, fused silica used by at least one major company in the manufacture of electronic molding compound. This material is manufactured by melting carefully selected silica sand, cooling the melt, and then crushing and grinding to final size. Samples of this material were submitted to Particle

Data, Inc. for particle size analysis. Analysis was performed using Elzone equipment. This apparatus pumps conducting fluid containing the particles through an orifice. A voltage is applied across the orifice. As a nonconducting particle passes through the orifice it replaces some of the conducting fluid, creating a voltage drop. The equipment measures this drop and calculates the size sphere required to cause an equivalent drop. The results of this analysis are reported as equivalent sphere diameters. The mean equivalent diameter was 12 micrometers, with a spread of 0.2 to 80 micrometers. The complete distribution is shown graphically in Figure 10. Typical particles are shown in Figure 11.

4.0 WEAR TEST APPARATUS

4.1 Apparatus

Wear tests were conducted in accordance with ASTM G65 procedure "A" utilizing a Dietert Division of George Fisher Foundry Systems, Inc. model 4853 abrasion testing machine. This device is shown schematically in Figure 12. This device consists of a wheel (8 inches) in diameter by 12.7 millimeter (0.5 inch) thick of AISI 1020 steel to which is attached a 12.7 millimeter (0.5 inch) thick by 12.7 millimeter (0.5 inch) wide tire of chlorobutyl rubber with a Shore Durometer A 60 +-2 hardness. The overall diameter of the wheel-tire assembly is 22.86 centimeters (9 inches). The sample, a 12.7 x 25.4 x 76.2 millimeter (0.5 x 1.0 x 3.0 inch) block, is affixed in a holder such that one of the 25.4 x 76.2 millimeter (1.0 x 3.0 inch) faces contacts the wheel perimeter, with the mid-length of the sample on the horizontal radius and the length of the sample parallel to the circumference of the wheel. Care must be taken that the plane of the sample face is parallel to the wheel axis, so that the contact patch is rectangular. The normal force is applied by a weight acting on a system of levers. The normal force specified for procedure "A", the procedure utilized in this study, is 130 Newtons (30 pounds).

The abrasive particles are fed by gravity flow from a

hopper through a nozzle into the interface between the wheel and the sample. Flow rate is regulated by the size of the nozzle opening. Flow rate should be in the range of 250 to 350 grams per minute (0.55 to 0.75 pounds/minute). Flow rate measurements of the nozzle used for testing showed an average of 305.7 grams per minute.

In procedure "A" the duration of the test is 6000 revolutions of a new wheel, or 4309 meters (14,138 feet). The number of revolutions is increased to maintain a constant sliding distance as the wheel diameter is reduced through wear of the wheel and resurfacing of the worn wheel. Test duration is controlled by a electromechanical counter which is preset to the required number of revolutions and switches off the motor when the preset number is reached.

The wear tester, as delivered, had no provision for dealing with the spent abrasive. The acrylic housing surrounding the wear wheel was therefore modified to adapt to the hose from a Sears shop vacuum. This provided positive removal of the used sand and also any dust which was formed. Any dust which passed through the filter in the vacuum was vented into a fume hood through a system of flexible plastic ducts.

4.2 Truing the wheel

Resurfacing and trueing of the wheel is necessary for

several reasons. First, it is necessary that the outside diameter of the wheel be concentric with the wheel axis to avoid a cyclic oscillation in the applied load. The specified limit is 0.05 millimeter (0.002 inch) maximum deviation from concentric. It is also necessary that the wheel surface be parallel to the sample face, which is held parallel to the wheel axis by the sample holder. The wheel surface needs to be consistent from test to test in order to give repeatable results, and the wheel surface needs to be flat edge to edge. Circumferential grooving is especially bad as it tends to get worse with use. Very light grooves in the wheel cut grooves in the sample face which then deepen the grooves in the wheel in a positive feedback system which results in an invalid test and a wheel which has to be heavily resurfaced, causing reduced wheel life. Other surface defects tend to "wear out", resulting in one invalid test, but leaving the surface suitable for additional testing.

ASTM recommends two methods of truing test wheels. Both involve mounting the wheels in a lathe. The preferred method uses a specially ground tool bit to cut the wheel surface, while the second method involves grinding the surface. Both of these methods have a common problem in that, since the wheels are trued and then mounted on the test machine, they do not account for the effect of the clearance between the

wheel and the shaft. On the machine used in these tests, this clearance was sufficient to result in excessive eccentricity of the wheel. In addition, the cutting method tends to result in circumferential grooves in the wheel surface, and to yield a slightly concave wheel surface as less material is removed from the wheel edges than is removed from the mid-width region. This is a result of increased deformation of the rubber because of less constraint. Lighter cuts produce rolls of rubber similar to those produced from rubber erasers, rather than cleanly cut shavings, and to leave a sticky surface to which sand adheres, giving invalid test results. The grinding method produces extensive circumferential grooving and also tends to give a sticky surface.

To circumvent the first of these problems, that is the excessive eccentricity, both of these two methods of truing were adapted to use with the wheel mounted on the test machine. A mechanism which mounted onto a modified sample holder and could traverse a carbide tool bit across the wheel face was developed and built. In conjunction with the tool bit holder, there is a device which mounts on the weight arm and provides micrometer depth of cut control. These devices are shown in Figure 13. Although this device did successfully solve the eccentricity problem, it did not eliminate the surface problems encountered with tool bit

truing on the lathe.

Subsequently, a device which utilized a Dremel Mototool high speed grinder and mounted on a modified sample holder was built. This device, shown in Figure 14, also utilized the previously built micrometer feed. This device produced a sticky surface with numerous circumferential grooves, which was not suitable for use in testing. Efforts to cool the wheel during truing, first with water and then with ice, did not solve the problems, but did lead to the development of a procedure that worked. The procedure which was developed involves chilling the wheel and then truing it with the tool bit device. The wheel is removed and placed in a freezer until it reaches -20° C (0° F). The time required was not determined, but rather a two hour minimum period was chosen because the wheel was at -20° C (0° F) when checked after that time. The wheel is then removed from the freezer and quickly mounted on the test machine. The tool bit is then traversed across the wheel, having been previously mounted. The depth of cut is set utilizing the micrometer feed device. The rate of traverse is important. The tool bit must move fast enough to avoid frictional heating of the rubber surface and slow enough to avoid formation of circumferential grooves. Experience has shown that two cuts can be made successfully, after which the wheel surface becomes too warm and the eraser debris type of action begins, which results in

a sticky surface. The only time more than two cuts have been required is when extensive corner rounding of the wheel surface has occurred while testing soft materials. In this case most of the required material is removed prior to freezing the wheel.

In addition to this technique for truing wheels, a technique for remedying minor surface problems has been utilized. This consists of mounting a section of an eight inch bastard file in the sample holder and running it for 2000 revolutions under a 45 Newton (10.1 pound) normal force. This removes the sticky surface which results from an interruption in sand flow. Although it was not tried, this procedure would probably also remove the sticky surface layer which results from grinding the wheel. For this technique, it is necessary to use a new file section each time, as the files are rapidly dulled.

The rate of revolution called for in the ASTM specification is 200 RPM +- 10 RPM. This was set and maintained using a General Radio Strobotac. In addition, one set of tests on D-2 samples was run at 83 RPM. This set of reduced speed tests was performed to evaluate the effect of sliding speed on the wear rate. The rate of revolution was chosen to match the velocity of the tips of mixing elements on a 127 millimeter (5 inch) diameter extruder operating at 150 RPM, a typical operating speed.

5.0 TEST PROCEDURE

5.1 Rockwell C hardness tests

Rockwell hardness has been a criterion for wear resistance since before the earliest wear models. To the early engineer or blacksmith, and to most people even today "Hard" and "Wear resistant" are synonymous.

Rockwell C hardness tests were run on each sample to verify consistency of heat treatments and as a potential way to rank materials. To avoid making indents in the region to be abraded and yet still determine the hardness in this region, three Rockwell tests were run at each of six locations around the periphery of each sample, except for the crescent shaped FerroTiC CM45 samples where geometry only allowed two test locations. The test locations are shown in Figure 15a.

The nitrided AISI 4150 samples were only 50.8 millimeters (2 inches) long, so that three Rockwell tests were taken on either side of the sample midsection, the region where the wear scar would fall, as shown in Figure 15b. All the other ion nitrided samples were Rockwell tested following the procedure used for the non-nitrided samples.

5.2 Wear test procedure

5.2.1 Weighing the sample

A sample, having been previously Rockwell tested, was cleaned in acetone, rinsed in ethanol and dried using a hot air hand drier. The sample was handled using stainless steel tongs. It was then weighed to milligram accuracy using a Mettler PM 400 electronic balance and the weight was recorded as the beginning weight. Three separate weighings were carried out, with the balance re-zeroed before each weighing, and the average value was recorded. These individual readings never varied more than 0.003 gram maximum difference (high-low reading), and often were identical.

5.2.2 Mounting the sample

After weighing, the sample was placed in the sample holder and lightly clamped. The thickness of the sample-sample holder assembly was checked using a 12 inch (30.5 centimeter) Mitutoyu dial caliper. If the edge-to-edge variation in thickness was less than 0.076 millimeter (0.003 inch), the sample holder was tightened to secure the sample. However, if the variation was 0.076 millimeter (0.003 inch) or more, the sample was removed and both the sample and the holder were checked for contamination. The procedure was repeated. If the variation was still too great, shims were added to the edges of the sample. This procedure was adopted

after it was found that slight irregularities in the edges of the sample from machining could cause the sample to tilt in the holder, forcing the wear face out of alignment with the wheel face and causing a trapezoidal wear scar.

5.3.3 Wear testing

Once the sample was properly mounted in the holder, the holder was attached to the weight arm, which was supported away from the wheel face by the weight arm prop. The revolution counter was then preset to the appropriate number of revolutions, the sand hopper was filled, and the vacuum system and the Strobotac were turned on. Then the sand flow was started, and the weight arm was lifted to allow the prop to swing out of the way. The wheel was started turning, and the weight arm was quickly but gently lowered to bring the sample into contact with the wheel face. At this point the wheel speed was checked with the strobotac and adjusted if necessary. The test then proceeded with frequent checks of sand flow and wheel speed. Although the machine would easily meet the required wheel speed criterion, it was found that it was possible to hold the speed within +-2 RPM with close monitoring. When the preset number of revolutions was reached and the motor shut off by the counter, the weight arm was immediately lifted and supported on the prop. It is important that the sample be lifted away from contact with

the wheel immediately. If it is allowed to rest against the wheel for even a short time, the hot sample will create a small flat spot on the wheel and will embed some sand in the rubber. The sample holder was removed from the machine and the sample released from the holder. The sample was rinsed with ethanol, which quickly evaporated. The sample was then reweighed using the same procedure of multiple weighings and the final weight was recorded. The difference between the beginning and final weight was the weight loss due to abrasion. This figure was then used to calculate the wear volume loss according to

$$\frac{WEIGHTLOSS}{DENSITY} * 1000 = MM^3$$

where the density is in grams per cubic centimeter. These density values are presented in Table III.

5.3.4 Calculating the volume wear loss

The mean volume wear loss is then calculated for each group of samples. The coefficient of variance, given as the standard deviation / mean, is then calculated. According to ASTM G65, the test results are valid as long as the coefficient of variance does not exceed 7 percent.

5.4 Wear debris collection

Wear debris was collected magnetically by placing a large electromagnet in the stream of sand exiting from the sample/wheel interface. The magnet used was obtained from Edmund Scientific Company and has a reported surface pull (lifting capacity) of 136 kilograms (300 pounds). The surface of the magnet was covered with Fisher Scientific glassine weighing paper. After each group of tests of a given type of material, the debris was transferred from the glassine to a piece of 3M Company Scotch Removable Magic Tape #811. This tape was subsequently attached to a cover glass using two small pieces of 3M Company Scotch Double Stick tape, and coated with a gold-palladium sputter film for examination by SEM. A Tousimis Research Corporation SamSputter-2A sputter coater was used to deposit the films.

No effort was made to determine the weight of debris recovered, as the majority of the debris collected by this technique consisted of fragments of silica. There are two possible explanations for the silica becoming attached to the magnet. The silica fragments, and even some whole sand grains, have adherent metal particles which help transport the silica toward the magnet. The presence of adherent metal has been observed in many instances by SEM. The other possibility is that the silica is electrostatically attracted to the glassine rather than the magnet.

5.5 Wear testing with Glasgrain

A few tests were performed on D-2 samples using Dresser Glasgrain fused silica as the abrasive. The small particle size and the high angularity of the particles combine to give this material extremely poor flow characteristics. The first attempt at testing with this abrasive, which involved simply replacing the AFS 50/70 sand with Glasgrain failed completely. The Glasgrain quickly bridged both the opening in the sand nozzle and the exit opening in the abrasive hopper, and abrasive flow ceased. Before proceeding, the moisture content of the Glasgrain silica was checked to see if absorbed moisture from the atmosphere could have contributed to the flow problems. This was checked by weighing a beaker to 0.001 gram accuracy, adding approximately 40 grams of silica and reweighing the beaker plus silica, then drying in an oven at 100°C for one hour and reweighing the beaker and silica. This procedure showed a moisture content of 0.083 percent. In addition, the flow characteristics of the dried silica were no better than before drying. From this it was concluded that the poor flow characteristics were inherent in the material.

For the next test a vibrator mechanism consisting of an eccentric weight mounted on a small electric motor was constructed and mounted on the hopper. At the same time a

light weight trough was constructed and equipped with a vibrator to replace the sand nozzle. The vibrator mechanism for the trough consisted of the voice coil-magnet assembly from an audio speaker driven by a variable frequency oscillator and amplifier. This system allowed both the amplitude and frequency of vibration to be varied. Pretest trials of the vibrator mechanisms showed that the eccentric weight vibrator on the hopper was only minimally successful. Initially abrasive flowed from the hopper, but eventually bridging occurred. After bridging, the vibration served only to compact the abrasive, making removal of the blockage more difficult. The trough mechanism, however, was totally successful. It provided a consistent, though small, flow of abrasive, even when the flow of abrasive into the trough was intermittent. The flow rate was determined to be approximately 10.5 grams per minute maximum. The trough mechanism was attached to the wear test apparatus in place of the sand nozzle. A rectangular section funnel was constructed to serve as a guide tube to direct the abrasive into the wheel-sample interface region. It was thought that a test could be run by feeding small quantities of abrasive into the trough manually and allowing the trough to smooth out and regulate the delivery rate.

A D-2 sample was cleaned, weighed, and mounted in the sample holder. The test was initiated. During the test it

was observed that a "prow" of silica formed on the front face of the sample immediately above the wheel which deflected the flow of abrasive toward the wheel edges. Periodically this accumulation would break away and pass through the wear region, but would quickly reform. The wear scar was divided longitudinally into zones which had two distinctly different appearances. One zone near the midwidth of the wear scar had a rough, almost galled, appearance, while the regions on either edge appeared polished. Figures 16 and 17 show that the galled appearance results from chromium carbides which stand proud above the surrounding matrix, while the polished regions show long linear grooves resulting from microcutting. This may result from abrasive starvation of the central region as a result of the prow formation, or the prow may act as a size selective filter, diverting larger particles toward the wheel edges while retaining smaller particles.

A second test was run during which the sample was mechanically vibrated by tapping the sample holder with a steel rod. This vibration prevented the prow formation, however at the completion of the test is was found that there was a layer of compacted silica on the wear scar region. Wear volume was greatly reduced compared to the initial test.

A third test was run in which a small flow of water was introduced into the guide tube. This prevented the

accumulation of silica on the sample, either as a prow or as a compacted layer. It also prevented the adherence of silica to the wheel face as had occurred during the previous tests. However, it was impossible to introduce the abrasive slurry to the sample - wheel interface region in a uniform distribution. Some of the abrasive solution was ejected from the sides of the entry portion of the wear region, so that it is probable that a portion of the abrasive never entered the wear region. The wear scar appeared highly polished.

In addition to the D-2 samples, one sample of FerroTiC CM45 was run using the dry abrasive feed technique without sample vibration. As can be seen in Figure 18, the carbides are in slight relief above the matrix. It is possible that a much longer duration test would develop a surface morphology similar to the field worn FerroTiC.

6.0 ABRASIVE WEAR

Early work in abrasion considered only two wear mechanisms. These were plowing and microcutting. Plowing occurred when an asperity plastically deformed the material being abraded without any material being removed. Eventual loss of material occurred when the ridges of deformed material accumulated cold work from repeated deformations and fractured. Models included a probability factor which accounted for the number of contacts necessary to cause a wear particle to form. Microcutting results in the immediate formation of a wear particle, in the form of a chip, from a single asperity contact. These two mechanisms can be considered as variations of the same mechanism, since a contact that does not result in microchip formation may result in plowing, with the only difference due to chance orientation of the abrasive asperity relative to the abraded surface. However they may also be considered as competing processes since microchip formation may remove some or all of the accumulated plastic deformation before a wear particle can form as a result of plowing and work hardening of the surface may alter the probability of microchip formation.

Additional wear mechanisms also need to be considered. For instance in three body wear rolling fatigue may occur. In addition to the purely rolling fatigue encountered in

rolling element bearings, abrasion introduces sliding fatigue which results from macroscopically elastic sliding contact. This latter source of fatigue stress may be simply additive to the rolling fatigue, or it may function as a separate mechanism, initiating failure at different locations. These fatigue processes eventually result in the formation of wear particles, either by surface spalling or by the delamination wear mechanism. Adhesion can also occur, in which material from the abraded surface attaches to the abrasive asperities and then either is lost or reattaches to the abraded surface.

Composite materials consisting of hard particles in a softer matrix introduce several additional potential abrasive - abraded surface interactions. For instance in these materials there is an impact character to both rolling and sliding contact, as abrasive asperities bounce from one hard particle to the next. In the extreme case the impact may serve to drive the hard particle into the matrix, initiating a crack in a single occurrence, much as a wedge will split wood. The hard particles may also serve to concentrate the contact stress, turning a nominally elastic contact into microscopically plastic contacts. These fatigue mechanisms can combine to cause delamination wear in which flakes or sheets of material detach from the abraded surface.

There are mechanisms which are peculiar to composite

materials other than delamination. The hard particles in the composite interact with the abrasive and protect the softer matrix. The size, spacing, particle-matrix interface strength, and matrix strength all affect the type of interactions which occur. If the abrasive particles are small relative to the mean free distance between hard particles the abrasive may attack the matrix and wear can occur by a process of matrix erosion and subsequent particle loss. Larger abrasive may remove hard particles from the composite by pulling them loose if the interface strength is low or by chipping and fracturing the hard particles if the interface strength is high. If the matrix strength is low the abrasive may penetrate to a depth much greater than the hard particle size, thus removing microchips of the composite material. In this latter case the hard particles have minimal effect on the wear resistance since they only provide a reduction of penetration depth due to dispersion hardening.

In the three body, low stress, abrasion there are four main factors which control the wear rate. These are: the abrasive, the abraded surface (sample), the counterface (wheel), and the operating parameters of load, speed, and environment. These factors are all interrelated and cannot easily be examined individually.

As mentioned previously, Babichev [4, 5], Khruschov [6], and Richards [7] found that for many materials the wear rate

is insensitive to changes in the relative hardness of the abrasive if it is either much harder or much softer than the abraded surface. In the range where the abrasive and the abraded surface have similar hardness values, the wear rate increases with increasing abrasive hardness. This is the same as saying that under the same abrasion conditions, harder materials have better wear resistance, and many other researchers have found similar results. For instance Rabinowicz, Dunn, and Russell [28], Larsen-Badse [29], and Quinn and Hall [30] have found that the wear resistance of quenched and tempered carbon steels is a function of hardness when abraded by a given abrasive. However, this is not always the case. Khruschov [6] found that work hardened metals were not more abrasion resistant than the same metals in the annealed state even though they had higher hardness. He surmised that the wear surface became much more highly cold worked during abrasion, so that cold working the surface prior to abrasion altered the initial, but not the final, state of the worn surface. Richardson [31] established that this was the case by comparing field worn, cold rolled, and trepanned surface hardness values.

Abrasive particle size has also been found to influence the abrasive wear rate for a given sample under given conditions. Avery [32] noted that for a given volume of abrasive, larger particles mean fewer particles. Each

particle then carries a larger load per particle but the number of particles decreases. If the probability of a particle being oriented so that it will actually create a wear fragment remains constant, the wear may decrease. Thus with the trade off of opportunity versus severity it is possible for the wear rate to increase, remain unchanged, or even decrease as grit size increases. Babichev [4, 5], Rabinowicz, Dunn, and Russell [28], Muscara and Sinnott [33], Rabinowicz and Mutis [34], Nathan and Jones [35], and Sin, Saka and Suh [36] have all reported that the wear rate increases with increasing grit size up to a critical grit size and then either remains constant or increases very slowly. This effect has generally been explained as either a tendency for the fine grit to "clog" with debris or to a change in wear mechanism due to a change in the stress at the asperity contact. These researchers all worked with relatively homogeneous materials, either pure metals or heat treated steels. For heterogeneous materials such as high chromium white irons (Zum-Gahr [37]) and metal matrix-ceramic composites (Kulic, Kosel, and Xu [38]) the wear rate may follow the usual trend of levelling off or it may increase significantly at a critical grit size. This uncertainty is a result of interactions between the hard particles in the material (carbides) and the abrasive. When the abrasive particles are small compared to the mean

distance between carbides, wear is reduced on the basis of less exposed abradable material. As the abrasive size approaches the mean free distance, the carbides afford more protection, and wear decreases. At still larger grit sizes, the abrasive particles begin to tear out the carbides, or else fracture them, resulting in accelerated wear.

Abrasive particle morphology has several effects on the abrasive wear process. First, one of the most obvious effects is that more angular particles have an increased tendency to slide rather than roll. Since the types of damage which sliding contact can cause, such as plowing and especially microcutting, is much more immediate than the fatigue type damage incurred by rolling contact, an increase in the tendency to slide should increase the severity of wear. This was confirmed by Swanson and Klann [39] using AFS 50/70 sand and crushed quartz with similar particle size distribution, and by Haworth [2] using a variety of abrasives. Haworth's work showed that softer, highly angular particles may cause more wear loss than harder, rounded abrasive. Increased angularity also decreases the contact radius, at least on a macroscopic scale. Since almost all of the models of sliding wear involving plowing or microcutting mechanisms include the contact radius in calculating the depth of penetration, and thus the volume removed per wear particle formation, a smaller radius which leads to deeper

penetration increases wear. Care must be used when examining the angularity of abrasive particles. As shown in Figures 9 and 10, the angularity of sand particles depends on the scale of observation used. Blau [40] reports that "Ives at the National Bureau Of Standards has noted that the fine features on abraded surfaces of the ASTM G65 test correspond more in size to the micrometer-sized asperities on the sand particles surfaces than to the overall shapes of the particles suggesting that an order of magnitude smaller scale should be considered in correlating abrasion damage with microgeometry of the abrasive particles." Thus it may be the radius of curvature of the microscopic asperities rather than the macroscopic radius of the sand grains themselves that is important.

Mulhearn and Samuels [41], and Murray, Mutton, and Watson [42] found a critical angle of attack, the angle between the forward face of the asperity and the abraded surface, at which the action of sliding asperities changed from plowing to microcutting. Hokkirigawa and Kato [43] confirmed the critical angle, but added a "wedge" mechanism in the case where the contact shear stress approaches the bulk shear strength. In the wedge mechanism a prow forms ahead of the asperity, as in plowing, but detaches during a single occurrence, as in microcutting. As can be seen in Figure 19, increased angularity makes attaining the critical

angle necessary for microcutting to occur much easier.

In abrasion of multi-phase materials containing a hard phase, more angular particles have the potential to get between the hard particles like small abrasives yet still carry the heavy load of a large abrasive particle. There may be a relationship between abrasive particle angularity and hard particle pullout.

More angular particles, with smaller radii of curvature, will increase the contact stress in elastic interactions. The hertzian contact area varies as the 2/3 power of the asperity radius [44], so for constant load the more angular particle will rest on a smaller contact area. This increased stress may influence the occurrence of fatigue wear mechanisms such as delamination wear described by Suh [45,46] or spalling reported by Zum-Gahr [47]

The higher stress associated with increased angularity may also contribute to fracture of hard particles in metal matrix- ceramic particle composites and white irons. Kulic, et al [38], and Fiore et al [48], have found that in the case where the carbides are harder than the abrasive, wear is due to fracture of carbide particles.

6.1 The effect of the sample

The sample is the one intentional variable in a standardized test. The purpose of standardization is to

minimize variability in all factors except the sample to allow assessment of sample characteristics. However, as discussed under abrasive hardness, sample characteristics can affect the type of test being run. If two samples of different hardness are tested, it is possible that one will be soft relative to the abrasive, while the second is hard. In the first case the sample would be abraded, but in the second scenario it is the abrasive particles which would be worn. Since the effect on the abrasive was used to categorize the test, this test has changed from a low stress to a high stress abrasion test simply by changing the sample hardness. Also. since the abrasive is being degraded, the average particle size will decrease and the angularity will probably increase, but could decrease if the initial angularity is high. Especially in composite materials consisting of hard particles in a softer matrix, the large rounded abrasive grit interacts primarily with the hard particles, while the smaller, more angular abrasive fragments have the potential to attack the matrix.

6.2 The load per abrasive particle

The obvious functions of the wheel are to apply a load to the abrasive particles and transport them along the sample face. Haworth [2] and Avery [32] showed that wear loss increased with increasing applied (total) normal load in

rubber wheel abrasive tests. However, the value of interest, especially if comparisons between abrasives are to be made or modeling is to be attempted, is the load on an individual abrasive grain.

To calculate the load per particle, it is necessary to make some assumptions about the contact area. The rubber wheel abrasion test is a semi-conformal test, in that the basic geometry is block on ring, however the ring is flexible and deforms to create a rectangular contact area. As the test progresses, the sample wears, acquiring a concave surface which approaches the undeformed wheel shape. The degree of conformation which develops during a test is of course related to the amount of wear which occurs. For very wear resistant materials the beginning and ending geometry are almost identical but for the least wear resistant materials the ending geometry is essentially conformal. The actual length of the wear scars ranged from 29.2 millimeters (1.15 inch) to 38 millimeters (1.5 inch) on samples with wear volume losses of 13 to 340 cubic millimeters. Choosing a length of 32 millimeters (1.25 inch) gives a projected area of 406.4 square millimeters (0.625 square inch).

6.2.1 Spherical particles

Assume spherical particles for AFS 50/70 sand with a diameter of 0.25 millimeters (0.01 inch). The particle

volume is then 0.008181 cubic millimeters with a weight of 0.0217 milligram (quartz density = 2.653 gram per cubic centimeter) for 46083 grains per gram or 13,824,900 per minute at 300 grams per minute, the median specified flow rate. Assuming a square array for simplicity, 6500 grains of sand would cover the entire abraded surface. The available sand would cover the scar 2130 times per minute.

However, looking at the wheel surface; A 228.6 millimeter (9 inch) diameter by 12.7 millimeter (0.5 inch) wide wheel turning at 200 RPM gives 1,824,147 square millimeters (2827 square inches) of wheel surface per minute or 7.6 grains per square millimeter. This is about half the number required to form a monolayer of sand with the assumed square array. Thus for the wheel surface, a more appropriate array might be a checker board layout with one color squares occupied by sand. This arrangement assures that the rubber will transfer the same force to each grain despite the variation in grain size. Neglecting for the moment the wheel curvature, this gives a load of 0.04 Newton (0.009 pound) per sand grain. This is an average load, the actual load will vary from 0 at the entry and exit ends of the scar to a value roughly 3/2 of 0.04 Newton per sand grain at the center of the scar length. Even this is only an approximation. The actual force exerted by the wheel at any point in the scar is a complex function of the static and dynamic forces applied

to the wheel. Figure 20 shows the static force distribution along the scar, assuming a linear relationship between deformation of the rubber and the required force. It is possible that the rubber is nonlinear, either by itself or as a result of constraint by the steel core. It is also probable that the force varies across the width, at least near the edges. This relatively simple situation becomes more complex when dynamic effects are considered. The friction is proportional to the normal force, so it will vary with the normal force. Since the rubber is elastic, regions below (toward the exit end of the wear scar) the maximum friction force will tend to be stretched by the rotational torque, thinning the rubber and reducing the normal force, while regions above the point of maximum normal force will be compressed, bulging the rubber. The result of all this will be that the point of maximum normal force will be shifted toward the top of the wear scar, at least initially when the sample surface is flat. This is illustrated schematically in Figure 21. Interrupted tests on soft materials with hard nitride layers have shown that initial breakthrough of the nitride layer occurs at a point above the middle of the wear scar, but this region of high wear gradually descends toward the middle as the test progresses. It is thought that this eventual descent is caused by concentration of stress at the sharp edge of the nitride layer. A set of interrupted test

samples of ion nitrided Thyssen 4122 illustrating this effect is shown in Figure 22. The arrows on each sample indicate the extent of the region of penetrated nitride layer (high wear region).

6.2.2 Elongated particles

Examination of scanning electron micrographs of AFS 50/70 sand grains, such as Figure 9, shows that typically the grains are not spherical, but rather they are somewhat elongated. Measurements of maximum width (D) and minimum width (d) on a representative sample of grains from two batches of sand were taken. D was chosen as the longest axis of the grain and then d was taken approximately perpendicular to D. These measurements showed the average D to be 0.381 millimeter (0.015 inch) and the average d to be 0.274 millimeter (0.011 inch) so that the average ratio of widths, D/d, was 1.4, with a range of 1.1 to 1.9, that is D/d for the most spherical and least spherical, respectively. This suggests that a more representative shape might be a cylinder with spherical ends 0.3 millimeter in diameter by 0.4 millimeter long. Such a particle would have a volume of 0.021 cubic millimeters and a mass of 0.0557 milligram, for 17,953 grains per gram or 5,385,900 grains per minute at 300 grams per minute sand flow rate. This figure gives only 2.95 grains per square millimeter of wheel surface, however, each

grain now occupies a rectangle 0.3 X 0.4 millimeter, so only 8.3 grains per square millimeter are required to give complete coverage for the assumed square (rectangular now) array. Thus the coverage is now roughly a third, rather than a half, of the wheel surface. With 3 grains rather than 8 grains per square millimeter of wheel surface, each elongated grain will bare approximately twice the load as a spherical grain. This will either increase the number of microcontacts between the abrasive grain and the abraded surface or it will increase the load, and possibly the depth of penetration, of each the microcontact.

6.3 Wheel hardness

Using a rubber wheel abrasion test similar to ASTM G65, Borik [49] found that the characteristic of the rubber wheel which had the largest effect on wear volume loss was the hardness of the rubber. Using wheels of nominal Shore Durometer of 55, 60, and 65, and testing materials with weight losses of 0.003 to 8 grams Borik found a consistent exponential relationship between wheel hardness and weight loss, with weight loss increasing with increasing wheel hardness. Although he did not present an equation, he reported that "a difference in Durometer hardness of 3 points resulted in wear rate variations amounting to 30% of the total weight loss." Although Borik's test parameters are

different from the ASTM standard, they are similar. Borik used a 178 millimeter (7 inch) diameter wheel at 240 RPM for 5000 revolutions under a 222 Newton (50 pound) load. The largest single difference is that he used neoprene rubber rather than chlorobutyl rubber in the ASTM G65 test. It is not known for certain, however it does seem likely that hardness variation in chlorobutyl rubber would have a similar effect on wear.

Avery [48] reported similar results and concluded that the hardness range allowed by ASTM could result in a 31% difference in weight loss resulting just from rubber hardness.

Interestingly, Xuan, Hong, and Fitch [50], using a journal bearing test rig and abrasive contaminated lubricant, found that the hardness of the journal (sample), bearing (counterface), and abrasive all influenced wear. They found that the critical value of the ratio of journal hardness to abrasive hardness at which journal wear essentially stopped depended on the bearing hardness.

6.4 Abrasive particle transport modes

Sand particles can only travel along the sample surface in one of two ways. They can either slide or roll. As a cause of wear, sliding is much the more aggressive, since sliding can result in microcutting, the most aggressive form

of low stress abrasion. The elongated nature of the sand grains is important in the sliding mode. If the particles were approximately spherical there would be very little tendency for them to slide. Sliding is a much higher friction process than rolling. This friction force, applied at the particle surface, would impart a torque which a sphere could not resist. As a result most of the particles would roll and very little wear would occur. However, since the particles are actually somewhat elongated they will tend to roll as cylinders, that is with their axis perpendicular to the direction of motion. Any greater than average encounter between a particle and the sample as a result of particle nonuniformity or asperities on the particle or sample will most likely not be exactly on the center of the axis length. This encounter will therefore produce a torque which will tend to align the particle axis parallel to the direction of motion. Once this happens rolling will be of an end-over-end tumbling nature, which will require much more force than simple rolling. Thus once the rotation from cylinder rolling to sliding, with the asperity bearing high friction end trailing, occurs the situation becomes metastable, and sliding tends to continue. If tumbling does begin it will tend to dampen out and return either to sliding or cylinder rolling.

There are a number of interactions which can occur

between sand grains. If two rolling grains encounter each other, the mating, or rubbing, surfaces will be traveling in opposite directions. Interactions of asperities on the surfaces may lock the grains together to cause sliding, or they may bang against each other, causing chipping. When a rolling grain meets a sliding grain, the rolling grain may lodge against the sliding grain in a T formation and begin sliding itself or the rolling grain may provide the input to destabilize the sliding grain and cause it to roll. Each of these abrasive-abrasive encounters, as well as the "normal" abrasive-sample encounters, has the potential to chip or fracture the abrasive grains. The resulting subsize abrasive particles may "piggyback" on other abrasive grains, acting as super asperities. However, because the wheel surface is not completely covered by sand grains, these small fragments have the potential to act as additional small, highly angular individual abrasive particles. This may be one mechanism of matrix erosion of composite materials.

6.5 Operating parameters

The main operating parameters which can affect the test results are applied load, sliding speed, and environment. One purpose of standardizing a test is to eliminate this type of variable from the equation, however it is almost impossible to completely eliminate environmental effects from

any test.

The static total applied load is relatively easy to calculate and to verify experimentally. As a result of the tight limitation on wheel eccentricity, the dynamic total applied load does not vary much from the static condition. However the load on an individual particle is difficult to evaluate. In addition to the particle size, particle shape and rubber deformation problems discussed above there are minor fluctuations in sand flow rate which influence the number of particles in the wear scar and also the friction force, which will change the rubber deformation and also introduces an acceleration effect since the change in friction results in a change in wheel rotation speed. All of these effects are minor on a macroscopic scale, however they would not be minor with respect to a single particle. Therefore, although the total applied load is known, the actual load at the particle-sample contact where abrasion occurs is highly variable.

Because the rotational velocity is specified as 200 RPM in ASTM G65, the sliding speed will decrease over the life of the wheel. This allows the grains-per-minute exposure to remain constant. However, the grains per square millimeter of wheel surface will increase as a result of the smaller wheel surface area, as will the total number of grains as a result of the extended test duration. Thus one severity

factor, sliding speed, decreases while two opportunity factors, abrasive particle density and total number of particles, increase. At the 216 millimeter (8.5 inch) minimum diameter specified by ASTM G65, the wheel surface area per minute is 1,722,805 square millimeters (2670 square inches) per minute. This gives 8.02 spherical, or 3.13 elongated, grains per square millimeter. The test duration increases from 30 to 31.76 minute during the life of a wheel, so that at an average flow rate of 300 grams per minute the total sand used increases from 9000 to 9528 grams. The sliding speed decreases from 2.39 to 2.26 meters per second. These are the extreme end points of each range. Each of these small changes probably contributes only a small amount of variation in results and they tend to offset each other, resulting in insignificant effects on the end result.

The reduced speed tests on D-2 indicate that a 60% reduction in sliding speed gives a 30% reduction in wear volume. It should be noted that the sand flow rate was not reduced, nor was the sliding distance, so that both the sand distribution density and the total quantity of abrasive used increased greatly. Haworth [2] found that large increases in sliding speed resulted in large increases in wear volume in the rubber wheel abrasion test, but attributed much of the increase to the high temperatures attained. Nathan and Jones [35, 39] found that for slow sliding speeds in two body

abrasion, the wear rate was essentially constant over a range of 0 to 2.5 meters per second. ASTM G65 sliding speed is 2.39 meters per second maximum with a new wheel, so wear should not vary much with speed. Rabinowicz et.al. [28], in a test using a metal counterface, found that wear loss varied with abrasive flow rate over the range they examined, while Babichev [4, 5], using a rubber wheel tester with different abrasives, found that wear rate varied greatly at low flow rates but was essentially constant above a critical value.

Temperature and relative humidity are the two environmental factors which can affect wear test results. The range of normal room temperatures is small enough so that no appreciable affect on wear test results are found. The other temperature which can influence results is the contact temperature. This is not only the flash, or microcontact temperature, but also the temperature which the bulk of the sample and wheel reach. When comparing different classes of materials such as tool steels and particle reinforced composites, or the same bulk material with a surface treatment such as ion nitrided and non-ion nitrided samples, differences in the samples such as thermal conductivity or emissivity may cause large differences during testing which would not exist in the actual operating environment, where temperature is not due solely to abrasion.

Relative humidity has been shown to have a major affect

on wear rate results. Rabinowicz et.al. [28], using a three body ring on disk apparatus, found that the wear rate increased with increasing humidity. This effect was found to induce variations in wear rate of as much as 20%. Tsuji and Ando [51] investigated the effects of ambient temperature and humidity on metal-to-metal unlubricated sliding wear and found that for steels there was little effect for sliding speeds above 1.5 meters per second up to the maximum tested, 3.5 meters per second. Below 1.5 meters per second, increased humidity could create large variations and the direction of change depended on the ambient temperature. Relative humidity should not be a factor in the results of this research because the tests were run in a relatively short time span during which humidity did not change drastically, and because the sliding speed of 2.4 meters per second is well into the insensitive range found by Tsuji and Ando.

7.0 RESULTS

7.1 Metallography

Sections were cut from a sample of each material for metallographic examination. The specimens were mounted in Beuhler Epomet compression mounting compound. They then were rough ground on either 120 grit silicon carbide paper or 180 grit metal bond diamond lap. Fine grinding was performed by hand with diamond paste on Fisher Scientific filter paper through the sequence of 9 - 6 - 3 - 1 micron. They mounts were thoroughly cleaned between steps. The polished samples were examined using an ausJENA Neophot 21 Metallograph.

7.1.1 Thyssen 4122

As shown in Figure 23, the microstructure consists of coarse grain boundary precipitates which almost continuously outline the grains. Long thin stringers, probably silicate or sulfide type nonmetallic inclusions, were observed in the microstructure, usually accompanied by second phase precipitates.

7.1.2 D-2 tool steel

As illustrated in Figure 24, the microstructure contains large second phase particles, thought to be chromium carbides, and dispersed smaller particles which are thought

to be vanadium and molybdenum carbides. A Kevex Microanalyst 8000 energy dispersive x-ray analysis system (EDS) attached to a JEOL JSM 35 scanning electron microscope confirmed that the chromium content in the large particles was much higher than the matrix. EDS did not indicate significantly higher chromium, vanadium or molybdenum in the small particles, however this probably is due to the small particle size relative to the volume of material which the electron beam excites.

7.1.3 CPM 10V

This material consists of a uniform distribution of vanadium carbides throughout the matrix. Only a few scattered agglomerates of carbides are present. The string of beads appearance of the agglomerates indicate that they resulted when individual carbides grew into each other. There was no visible difference in the microstructures of the two different Rockwell hardness levels. A representative microstructure can bee seen in Figure 25.

7.1.4 FerroTiC CM45

Figure 26 shows that the distribution of titanium carbides is much less uniform in this material than was true for the vanadium carbides in CPM10V. In extreme cases relatively large areas of matrix material are present, as

shown in Figure 27. The Knoop microhardness indents prove that this is not matrix material smeared over the carbides, but rather a carbide-poor region associated with regions which are virtually solid carbide. There are also numerous small pores present in the microstructure in close association with carbide particles. These pores may result from residual porosity from the sintering operation, from the loss of small portions of the matrix during polishing, or from loss of carbide particles or fracture of carbide particles. It is probable that all of these mechanisms are responsible for the pores, however they have very different implications for wear. Fracture of the carbide particles is a polishing artifact and would not effect wear, however loss of matrix or carbides indicates a very low interface strength, which could also lead to loss of carbides during wear. Residual porosity would be involved in fatigue wear mechanisms, where pores might either initiate fatigue cracks or serve to blunt them, depending on the pore size and the plastic zone size at the crack tip.

7.1.5 FerroTiC CM25

This microstructure differs significantly from that of FerroTiC CM45. The titanium carbides are much larger, have a larger size range, and are much more angular. The pores present in this material are much larger and are obviously

residual porosity from sintering. These features are shown in Figure 28.

7.1.6 Ferrotitanit

As can be seen in Figure 29, the microstructure of this material is similar to FerroTiC CM45, except that the carbides in Ferrotitanit are somewhat larger and there are fewer pores.

7.2 Rockwell C

The Rockwell hardness test results are presented in Table IV, along with the respective coefficients of variation. The test results for samples which are wear tested are presented separately, as well as being incorporated into the totals of all samples of a given material. The small values of the coefficient of variation for all groups of samples, except for the FerroTiC CM45 and FerroTiC CM25, indicate that the heat treatments were uniform and there are no unusual variations in microstructures. The somewhat larger coefficients for the two grades of FerroTiC are a result of variations in distribution of carbide particles and/or porosity, rather than heat treatment abnormalities. As was illustrated in Figures 26, 27, and 28, these two materials have a nonuniform distribution of carbide particles due to clustering of carbide particles, and they

contain numerous pores. Both of these characteristics would tend to increase the spread of hardness values.

Rockwells indicated that one sample in the AISI 4150 ion nitrided samples had not been heat treated before nitriding. These Rockwells were not included in the results for the group and the sample was not wear tested, however it was examined metallographically, as discussed later.

Ion nitriding had little effect on the Rockwell hardness values, with the exception of the CPM10V heat treated to RC 59. The reason for this minimal effect is that even where they are present, the nitride layers are very thin relative to the depth of the Rockwell indentations. Thus the Rockwell hardness values represent a bulk or average hardness and do not reflect any hard surface layer. The large drop in Rockwell hardness of the nitrided CPM 10V samples which had been heat treated to RC 59 is a result of overheating during nitriding.

7.3 Microhardness depth profiles

Sections were cut and prepared from the ion nitrided samples as previously described. Knoop microhardness readings (200 gram load, 15 second load duration) were taken at 25 micron (0.001 inch) increments to determine the depth of the nitride layer. The increments were dictated by the need to separate indentations and the tendency for the reading

closest to the surface to be low due to deformation of the material between the indent and the surface. The relatively large load was needed to avoid distortion of the indentation shape in the materials with high carbide fractions.

These same samples were then etched and examined visually using the metallograph. A depth measurement was obtained from the photomicrographs. This depth value is not precise, since it depends on visually estimating the end of the darkened region in the microstructure. This darkening results from a change in etchant attack rate due to modification of the microstructure. The depth observed is somewhat dependent on the etching time, since longer exposure will tend to darken material with lower dosage, and is very subjective at best. However, the technique does reveal thin layers not picked up in the microhardness profiles, thus indicating that some materials which appeared not to be nitrided in fact were.

Results of the microhardness depth profiles and visual depth determinations are given in Table V. The microhardness depth profiles are presented graphically in Figure 30

7.3.1 Thyssen 4122

The ion nitrided Thyssen 4122 samples exhibited a discolored black area along all corners of the sample, as shown in Figure 31. Microsections of these samples showed

that only the face and back of the sample were nitrided; no nitride layer was present on the sample edges or ends. Thus the discolored regions marked the junction between regions in which the "plasma seam" adhered to the surface, resulting in nitriding, and regions which were bridged over and not nitrided. Three of the samples actually wear tested were examined metallographically and were microhardness depth profiled because of the extremely large standard deviation of the wear results, as discussed later. Although the actual values differed, both the visual determination and the microhardness tests indicate a sample to sample variation in nitride layer thickness of 200%. Figures 32 shows the nitride layers on these samples. All of these samples were reportedly nitrided at the same time in the same nitriding chamber load. The differences in nitride layer must therefore be due to variations in the conditions of the plasma inside the reactor. This could reflect geometric effects due to other parts of the nitriding chamber load.

7.3.2 CPM10V RC 55

These samples all had a slight, but uniform, discoloration. The microsection showed a uniform nitride layer on all surfaces. The nitride layer is shown in Figure 33.

7.3.3 CPM10V RC 59

This group of samples had two distinctly different appearances as shown in Figure 34. Four of the samples exhibited the bright gray, almost etched, appearance, while the remaining seven samples had an overall black, sooty appearance. Representative samples from each of these two groups were sectioned and mounted. The microhardness depth profiles did not reveal any nitride layer on either sample, however visual examination did reveal a 12 micron thick layer on the sooty sample. No layer could be discerned on the gray sample. These microstructure are shown in Figure 35.

7.3.4 AISI 4150

As mentioned previously, one of these samples was not heat treated. This anomalous sample and a normal sample were sectioned and prepared. The properly heat treated sample had a thin nitride layer, approximately 20 microns thick, which was not detected in the microhardness profile but was observed visually. The annealed sample had a nitride layer roughly seven times as thick. This difference is probably due to the fact that in the annealed sample the alloying elements which might form nitrides are tied up as large spheroidal carbides, thus they do not restrict the travel of nitrogen through the material. In the properly heat treated

samples much more of the alloy content is initially in solid solution. During the nitriding process, precipitates will form by diffusion and some of the nitrogen will be tied up, thus limiting the concentration and depth of penetration of the nitrogen.

7.4 Wear tests with AFS 50/70

The abrasion test results are tabulated in Table III, along with the respective coefficients of variation and the number of tests performed. The wear scars were examined using a JEOL JSM 35 scanning electron microscope equipped with a Kevex Microanalyst 8000 energy dispersive x-ray analysis system (EDS). Special sample holders had to be designed and manufactured to allow the wear test sample to be inserted in the scope chamber and the wear scar positioned in the beam for examination.

7.4.1 Thyssen 4122

Thyssen 4122 in the annealed state showed by far the largest wear volume loss at an average of 338.4 mm^3. Because of the large depth of the wear scars, the edges of the rubber wheel were rounded, with a concurrent deposition of rubber debris at the edges of the scar. This material was removed with acetone prior to the normal cleaning and weighing procedure. The damage to the wheel edges means that the wear

loss, large as it is, is probably lower than it should be. The damage to the wheel edges did not seem to be progressive, but rather reached a certain point and then stabilized. This rounding of the wheel edges required frequent, and severe, truing of the wheel. The wheel face was trued after every second test. Truing the wheel did not influence the test results, which indicates that the equilibrium corner roundness was reached early in the first test after truing or else has little effect on the total volume of these deep scars. Complete removal of the rounded corners requires cutting approximately 2.3 millimeters (0.090 inch) off the wheel diameter. Visual examination of the wear scars show light scratches parallel to the abrasion direction and several low transverse ridges extending across the wear scar. Since these ridges extend along the axis of the original bar from which the test samples were cut, it is thought that they represent segregation in the microstructure, possibly regions of high chrome content associated with stringer type inclusions.

Scanning electron microscopy of the wear scar confirms the presence of long linear scratches, and reveals regions of smeared metal as shown in Figure 36. This indicates that the wear mechanisms are microcutting, plowing, and possibly adhesion of metal to the sand grains. Examination of the wear debris revealed numerous shaving type of particles

formed by microcutting as shown in Figure 37. Some long needle-like particles were observed which may result from plowing, Figure 38. In addition, fragments of sand grains with a sheet-like layer of smeared metal on the surface were observed, Figure 39. The arrow indicates the region of metal. EDS confirmed the presence of iron and chromium in each particle, indicating that these are wear particles.

7.4.2 D-2 tool steel

Wear volume loss for D-2 tool steel, which contains a relatively large volume fraction of chrome carbides, is intermediate between the Thyssen 4122 and the steel-carbide composite materials. The wear loss averaged 37 mm^3, slightly higher than the 36 mm^3 specified by ASTM G65, but well within the allowable tolerance of +- 3 mm^3. The coefficient of variation, at 4.5%, is also well within the allowable 7% maximum. This indicates that the wear test apparatus and procedure are capable of producing valid results.

Visual examination of the wear scars show light scratches parallel to the abrasion direction and scattered low mounds. These mounds may represent regions protected by large carbides.

The scanning electron microscope again confirmed the presence of linear scratch-like features. These scratches often bend to one side, with a debris accumulation at the

turn. EDS shows silicon as well as iron and chromium in the debris, which may indicate fracture of a sand grain, see Figure 40. The other features noted were large gouge-like depressions associated with a ridge of material with transverse cracks in a thin surface layer of the ridge, as shown in Figure 41. It is thought that the cracks are in a ridge of material which has been plowed out of the surface but not detached, or else reattached.

The low mounds noted in the visual examination were of such low relief that they are difficult to locate precisely in the SEM. By attaching an indicator to the sample it was possible to look at a mound, however nothing was detected. EDS did show somewhat higher chromium than at other locations, however the difference was not large. This may result from the volume of material being sampled or because the carbides are subsurface.

Examination of the wear debris revealed short microchip type of particles and cigar shaped particles which look like accumulations of silica fragments, but which EDS indicates contain iron. The microchips, Figure 42, indicate that microcutting is occurring. The cigar shaped particles may result from deformation of microchips prior to their escape from the wear scar. Two possible mechanisms could result in the formation of this shape particle. The debris may roll between the wheel surface and the sample, as shown in Figure

43a, or it may become trapped between two sand grains and either the wheel or the sample, as shown in Figure 43b. This latter mechanism would also account for the silica fragments, since little pieces knocked off the sand grains would be embedded into the wear particle.

7.4.3 FerroTiC CM45

This material had the largest wear volume loss of the composite materials containing a high volume fraction of hard carbides, averaging 21.5 mm^3.

Visual examination did not reveal any indication of the linear scratching observed in Thyssen 4122 and D-2.

Scanning electron microscopy revealed an entirely different wear scar morphology. The worn surface consists of a large number of exposed particles, which EDS confirmed as high in titanium. Many of the particles have a crescent shaped void on the entry side, indicating that the carbides have shifted in the direction of wheel rotation, shown in Figure 44. Careful examination showed only a few carbide particles to have been fractured. However, occasional features which look like sheets of material detaching form the surface, as shown in Figure 45, and ragged transverse ridges which may indicate where a sheet has recently detached, were seen. Examination of the wear debris revealed flat plate-like particles which EDS confirmed to be wear

particles, Figure 46. Small particles, which may be microchips, shown in Figure 47, were occasionally observed. Cigar shaped particles similar to those found in D-2 debris were observed, Figure 48, as well as what appears to be a wear flake in the process of being rounded into a cigar shaped particle, Figures 49.

5.4.4 FerroTiC CM25

This material had much better wear resistance than FerroTiC CM45. This was unexpected, since it had a much lower volume percentage of titanium carbide, contained significant numbers of large pores, and had much lower Rockwell hardness. The lower hardness probably reflect the effects of fewer, larger carbide particles and the porosity rather than a difference in matrix hardness.

The wear scars exhibited a slightly grooved or striated appearance with a dull matte surface. Several deep, relatively large randomly placed pits were present in the wear scars. These pits were severely eroded by the abrasion process so that no visible signs of the original cause of the pit formation could be ascertained, even by SEM. It is thought that they may be due to large pores which became exaggerated by abrasion. This was seen to happen on one specimen of the supposed AISI 4150 which the heat treater had Rockwell tested in the wear scar region. The Rockwell

indentation widened slightly and elongated greatly because any sand grain which "fell into" the indentation would tend to gouge out the edge as it was pulled out. In essence, the indentation artificially increases the depth of abrasive penetration into the surface. This process would create a groove in the wear scar. The problems encountered with wheel truing showed that grooving tends to get worse with additional wear. This may be the process which formed the striated surface topology. The striations and pits are shown in Figure 50.

Scanning electron microscopy of the wear scar showed similarities to FerroTiC CM45. The surface contained many titanium carbide particles, as confirmed by EDS. These particles had mostly been shifted in the direction of abrasion (wheel rotation). The FerroTiC CM25 differed in that it had relatively large areas with few carbides and these regions showed linear scratches from microcutting and plowing, as shown in Figure 51. Examination of the wear debris confirmed the presence of microchips, including some classic examples shown in Figure 52. The other common type of wear debris consisted of flat sheets or plates, as shown in Figure 53. The wear debris also contained cigar shaped particles.

7.4.5 Ferrotitanit

This material had the lowest wear volume loss of any of the non-nitrided materials. The wear scar had slight striations near the edges and an overall dull matte appearance.

As with the two grades of FerroTiC, SEM showed a surface containing many exposed carbide particles which had been moved in the direction of wheel travel, leaving crescent shaped voids. The examination also revealed several shallow pits which may be areas where delamination wear sheets have detached recently. In addition, what appear to be cracks leading under surface layers were seen, as shown in Figure 54. One small sheet, still loosely attached, was observed and is shown in Figure 55. The wear debris consisted mostly of wear sheets or plates, as shown in Figure 56. One very small microchip containing a titanium carbide was observed and is shown in Figure 57.

7.4.6 CPM10V RC 55

This material, with the lowest hardness of the high carbide volume fraction materials, had the fourth lowest wear volume loss. This material outperformed both grades of FerroTiC which contained more hard carbide particles and had higher bulk hardness. In addition, the titanium carbide in the FerroTiC materials is slightly harder than the vanadium carbides found in CPM10V, however since both carbides are

considerably harder than silica, this should have little effect. The wear scars were very similar in appearance to those of Ferrotitanit, containing light striations along the edges with an overall dull matte finish.

As with the other materials containing large volume fractions of hard carbides, SEM showed that the wear scars contained many exposed carbides with crescent shaped voids on the entry side. In addition to these small voids, a large number of larger, deeper pits were observed, as shown in Figure 58. These appear very similar to the shallow pits seen in the Ferrotitanit wear scars, except that they are more numerous and somewhat larger. Due to a malfunction in the electromagnet, no wear debris was obtained from this series of tests.

7.4.7 CPM10V RC 59

When heat treated to the higher Rockwell hardness, this material exhibited better wear resistance. Thus CPM10V at the higher hardness had the second lowest volume wear loss, behind Ferrotitanit.

The wear scars had a uniform matte finish, but without the striations present in the wear scars of Ferrotitanit and the softer heat treatment of CPM10V.

Scanning electron microscopy again showed that the surface contained numerous exposed carbide particles, with

accompanying crescent shaped voids. The wear scars also contained several pits with an "L" shape, as shown in Figure 59. Careful examination showed that many of these pits had cracks in the deepest region running approximately parallel to the abrasion direction, as indicated by the arrow in Figure 60.

One unusual, but interesting, feature present in the wear scars are is shown in Figure 61. This consists of a short, relatively large gouge. There is a feature along one edge of this gouge which looks like a crack extending into the material. It is thought that these large gouges occur when a sand grain, rather than an asperity on the sand grain, is the abrasive. In most cases the width of the scratches or gouges in the wear scar indicate that asperities on the sand grains, such as the crystal terminations illustrated in Figure 10, or sharp protrusions resulting from fracture or chipping of the sand grains, form the contact regions which result in plowing and microcutting. This is to be expected because, as discussed previously, these regions concentrate the force into much smaller areas, resulting in higher stresses which can cause penetration into the surface and result in linear grooves. However, the wide gouge shown here indicates that at least occasionally conditions are such that even the large radius of the rounded sand can penetrate the surface. This may indicate some occurrence which temporarily

caused a much higher stress. Possibly one sand grain encountered a group of grains and rolled between them and the sample surface. In this case the one grain would temporarily carry the load for all of them, resulting in higher stress. By whatever mechanism, it appears that a single occurrence may serve to initiate a crack. If this is true then there are two possible mechanisms of crack initiation. One is fatigue, where the materials accumulates damage from repeated loading cycles from passing sand grains, either rolling or sliding. The other is this large stress single event. This one event mechanism avoids the crack initiation phase of fatigue crack initiation and growth. In brittle materials time to initiate a critical crack may represent most of the life of the part, or in this case most of the time to create a wear particle.

The wear debris consisted mostly of flat sheets or plates, shown in Figure 62. However, as indicated by the arrow in Figure 62, microchips were occasionally present. The particle shown in Figure 63 has the appearance of a chip formed by the wedge mechanism proposed by Hokkirigawa and Kato [43].

7.5 ION NITRIDED SAMPLES

As discussed previously, these samples all were supposed to receive the same nitriding treatment. However, as shown

by optical microscopy, either they did not all receive the prescribed treatment or the effect on different materials was radically different. This was true of the effect on the wear resistance of the various materials as well. Comparison of the wear volume loss for non ion nitrided and ion nitrided samples of the same material showed changes ranging from a 45% decrease in wear loss to an 86% increase in wear loss.

7.5.1 CPM10V RC 55 ion nitrided

Ion nitriding significantly improved the wear resistance of this material. The mean wear volume loss decreased from 16.06 to 11.86 mm^3 as a result of nitriding. This was the lowest wear volume loss of any material tested.

The wear scar had much the same appearance as the non ion nitrided samples, except that there wear no visible striations, just an overall matte finish.

Scanning electron microscopy showed that the wear scars were similar to those of the non ion nitrided samples, consisting of large numbers of exposed carbides. However, only some of these carbides had crescent shaped voids associated with them. This differs from non nitrided samples in which virtually all of the carbides had crescent voids. This may indicate that the strength of the interface increased as a result of nitriding, but a more likely cause is a increase in matrix hardness which would decrease the

matrix ductility and make void formation by carbide motion more difficult.

Although it is difficult to see in the scanning electron micrographs, many of the particles with crescent voids have small cracks extending from the opposite side. The arrow in Figure 64 indicates cracks emanating from a carbide particle. On a larger scale, there were pits which appear to the result of loss of wear particles by fracture as would occur during delamination. These are shown in Figure 65, a lower magnification view of Figure 64. Figure 66 shows a small wear sheet very close to complete detachment from the sample surface.

The wear debris consisted primarily of flat sheets like the one shown in Figure 67. The microchip attached to a silica fragment, shown in Figure 68, indicates that some microcutting is occurring. Unfortunately there is no way to determine if the microchip formed before or after the silica fragment was broken from a sand grain. The other interesting particle found in the wear debris is shown in Figures 69 and 70. Figure 69 shows a relatively intact sand grain with crystal terminations on one end. Figure 70 shows the end of these terminations at higher magnification. The arrows point to two tiny microchips. EDS indicated iron in these particles suggesting that they are matrix material from the sample. The EDS analysis of the other fragments in this view

are showed only silica. Also visible in Figure 69 is a cigar shaped wear particle, located on the end of the sand grain opposite the crystal terminations. EDS confirmed the presence of iron in this particle.

7.5.2 CPM10V RC 59 ion nitrided

The wear volume loss was greater for the ion nitrided samples than for the same material without nitriding. In addition, the wear test results fell into two groups corresponding to the two surface colors. The gray samples had higher wear volume loss than did the black samples. This correlates with the presence of a thin nitride layer on the black samples but no layer on the gray samples, as observed by optical microscopy.

Scanning electron microscopy of wear scars on the gray samples showed the large numbers of exposed carbides typical of the high carbide fraction materials, as shown in Figure 71. The wear scars showed a relatively large number of loosely attached wear sheets, compared to the other CPM 10V samples. This would be anticipated from the higher wear volume loss.

The unworn surface of these samples had a very irregular, chipped or fractured appearance, as can be seen in Figure 72. Cracks can be seen in the surface which may have contributed to the high wear volume loss. No machining marks

were visible either optically or in the scanning electron microscope on these samples, unlike the other CPM10V samples. Although this surface must have originated in the nitriding process, the mechanism is not known.

The black samples showed a fractured layer at the extreme entry and exit regions of the wear scars. Progressive examination from the extreme ends of the wear scar toward the center showed that the layer became more fractured, with sections obviously spalled off. The percentage of spalled area increased until all of the underlying surface was exposed. This layer appeared to be nearly continuous outside the wear scars, with only a few cracks visible. The central region of the wear scar, where wear had occurred on the underlying material, showed the typical exposed carbide morphology of other CPM10V wear scars. The surface layer, with several spalled areas, is shown in Figure 73. The surface of the central region is shown in Figure 74.

Wear debris from the two groups of samples showed little difference. Both showed flat plate-like particles and microchips. The lack of larger numbers of plates in the black samples may represent an artifact of the magnetic collection technique used. If the surface layer is not magnetic, it would not be collected. Thus the similarity of wear debris may simply indicate that the wear mechanism of

the core material of the black samples is the same as the gray samples.

7.5.3 Thyssen 4122 ion nitrided

This material showed significant improvement in wear performance as a result of nitriding. However, the wear volume losses showed a large variation, with the results of the six tests falling into three pairs of results. To determine the cause of the variability of the wear tests results, sections were cut from a sample in each of the groups. As reported in the optical microscopy section, there was a variation in nitride layer thickness which correlated with the wear volume loss results. Samples that had the thicker nitride layer had lower wear volume loss. This indicates that the nitride layer is functioning as a barrier coating. The wear rate would be expected to be low until the nitride layer is penetrated, then it would increase and eventually reach the wear rate of the non-nitrided material.

Visual examination of the wear scars shows a sharp step in the depth of the scar at each end. It is thought that this represents the end of the nitride layer. This step was not present in either of the groups of nitrided CPM 10V samples. This may be because the much smaller volume wear loss does not allow development of the step, in which case a

test of much longer duration might show the step. The other possibility is that the step forms because of the large difference in hardness between the core and the nitride layer. One might expect that the effect on wear would be larger in the case of a hard layer over a soft core than in the case of a hard layer over a hard core.

Scanning electron microscopy showed a sharp transitions in the appearance of the wear scar near both ends of the scar, shown in Figure 75. The region at each end of the wear scar, corresponding to the region on top of the step, contained many sharply defined linear scratches, as can be seen in Figure 76. The region in between these scratched regions showed linear scratches, but also exhibited smeared metal in sheets which in some cases are becoming detached, shown in Figure 77. The center region is nearly identical to the appearance of the wear scar of the non-nitrided samples. This tends to confirm that the step in the wear scar represents the limits of the nitride layer. The difference in appearance between the two regions indicate that different wear mechanisms may be predominant. The linear scratches on the end regions indicate that microcutting is probably the controlling mechanism, while the smeared metal in the central region indicates that substantial plowing is occurring. The presence of loosely attached sheets of metal shows that the plowing is causing wear. The wear debris showed both wear

sheets and microchips. The wear sheets often have scratches on the surface, as seen in Figure 78, although this is not always the case. Two possible explanations for the scratches are that the wear sheets with scratches are part of the nitride layer or that the plowed sheets become work hardened before detaching and acquire sharply defined scratches. If they are part of the nitride layer it would indicate that in addition to microcutting of the surface, the layer is spalling off. If spalling is occurring it may be both a cause and an effect of the steps in the wear scar. Spalling would tend to cause a sharp transition, or step. At the same time, the presence of the step introduces a bending moment on the edge of the surface layer as sand grains slide over the step, which would tend to break pieces off the edge. The wear sheets without scratches may result from plowing, or may simply be upside down. An oddly shaped microchip is shown in Figure 79. The width of this chip changes from narrow to wide and back to narrow. It is possible that this particular chip formed soon after the nitride layer was first penetrated, so that the narrow regions are from the nitride layer while the wider center area is from the core material. Because the core is much softer than the nitrided layer, one would expect that an asperity would penetrate much more deeply into the core material, resulting in a larger chip.

7.5.5 AISI 4150 ion nitrided

As mentioned previously, the non-nitrided samples of this material were defective so that no comparison of the effect of nitriding can be made. Comparisons with the Thyssen 4122 samples do reveal some interesting points. The very sharp steps in the Thyssen wear scars are present in the wear scars of nitrided 4150, but the steps are not as sharp and are much less obvious. This would indicate that the step is due to the difference in hardness between the core and the surface layer, thus it is most apparent in the Thyssen 4122 which has the lowest core hardness.

As in the Thyssen material, SEM revealed different wear surface morphologies for the regions on top of the step and below the step. In the nitrided 4150 scars the transition was much less obvious, as was the difference in surface morphology. However, as can be seen in Figure 80 and 81, there is a change in the character of the scratches from predominantly cleanly defined microcutting type grooves to a more random, smeared and dented form. Many of these scratches probably originated by microcutting, but are altered by subsequent plowing. It is thought that the small pits in Figure 81 may result from indentation of the surface by asperities on rolling particles. These pits are missing from Figure 80. This is not to indicate that fewer particles

are rolling, but rather that the harder surface resists penetration.

The debris from ion nitrided AISI 4150 consists almost entirely of microchips.

7.6 Interrupted testing

It was not intended to do interrupted testing, however several tests were terminated before completion for various reasons. The results of these tests were analyzed and some additional tests were conducted when extra samples were available. A number of these short duration tests occurred on D-2 samples during the initial setup of the wear test apparatus. In addition to these fortuitous results, tests were run in which the test was stopped after prescribed intervals and the sample was removed and weighed. The same sample was then reinserted into the test machine, taking care that the wheel reentered the same scar, and the test was completed. The raw data showed enough sample to sample variation to mask real differences, however when the data were plotted as a ratio of the volume loss after an interval to the total volume loss for that sample the wear rate became linear, as shown in Figure 82. This linear relationship indicates that there is no significant run-in, either of the sample or of the wheel, for this material.

The other interesting data come from two tests on

Thyssen 4122 ion nitrided samples which were terminated before completion due to interruption of the sand flow. These samples indicate that the wear rate is increasing during testing, and approaching the wear rate of plain Thyssen 4122. The data are presented graphically in Figure 83. Care should be taken in examining this plot, since the points are single individual tests. Since the data points come from different samples, and this material exhibited the highest sample to sample variability due to different nitride layer thicknesses, these points cannot be interpreted as a strict progression. Also, since these are separate tests, each point is the total wear volume loss for the duration of that test. Thus the slope of a line from the origin to the data point is the average wear rate for a test of that duration. The plot clearly shows that the average wear rate is increasing with test duration. Because the points are from different samples, plotting lines from one point to the next and taking the slope over the revolution (sliding distance) interval gives only a rough indication of the average wear rate. However, the fact that the wear rate approaches the untreated wear rate shows that the function of the nitride layer is to delay the onset of severe wear.

The other characteristic noted on the wear scars from short duration tests was that the site at which the nitride layer was first broached was not at the center of the wear

scar. The two factors which change over the length of the wear scar are the stress normal to the sample surface and the abrasive size and angularity. Scanning electron microscopy has shown that there is no observable difference in the sand grains when comparisons are made with used and new sand. Also, it is reasonable to expect that what degradation does occur is most likely to occur at the region of highest stress. Therefore, the fact that the area in which the wear scar first penetrates the nitride layer is offset toward the entry end of the wear scar indicates that the greatest normal stress occurs before the center of the contact region rather than at the center as would be expected from the static stress distribution. As discussed previously, this is thought to be a result of elastic deformation in the rubber wheel.

7.7 Low Speed Tests

As mentioned previously, one set of low speed tests were run using D-2 samples. The purpose of the tests was to evaluate the effect of sliding velocity on the wear volume loss and the wear mechanisms. For these tests the wear test wheel ran at 83 RPM, while sand flow rate and total sliding distance remained constant.

These low speed tests had a mean wear volume loss of 28.1 cubic millimeters with a coefficient of variance of

7.7%. Thus a 58.5% decrease of sliding velocity, from 143.6 to 59.6 meters per second, caused a 24.1% decrease in the mean wear volume loss, from 37.02 to 28.1 cubic millimeters.

Since the sand flow rate remained constant, the number of grains per square millimeter of wheel surface increased from 2.95 to 7.11, assuming the elongated grain shape discussed previously. This greater particle density decreases the load per particle but increases the number of particles abrading the surface. The slower wheel speed also results in a much longer test, increasing the total number of sand particles to which the surface is exposed from 161,580,000 grains to 389,340,000 grains. The greater particle density also increases the probability of particle interactions which may influence the probability of a particle sliding rather than rolling. Thus the decrease in the severity of individual contacts due to lower per particle load and lower sliding velocity are offset by increased severity of grains sliding rather than rolling and the increased opportunity due to the total number of abrasive grains.

Scanning electron microscopy of the wear scars showed no observable change in the wear scar morphology on the slow speed tests compared to the normal speed wear scars. From this it is inferred that the wear mechanism is the same in each case. Wear debris were not collected from the low

speed tests because these tests were run before the magnetic collection apparatus was installed.

8.0 DISCUSSION

The goal of this research was to find an accelerated test which could be used to evaluate potential materials for application as extruder tooling. This goal has been partially met. The ASTM G65 dry sand rubber wheel test meets most of the criteria necessary to duplicate the wear mechanisms in an extruder. For relatively homogeneous materials, such as low to medium alloy steels, this test produces wear by microcutting and plowing. These are the mechanisms expected to cause wear in extruders. However, for composite materials containing relatively large volume fractions of hard particles the large difference in size of the abrasive particles between AFS 50/70 sand and the crushed fused silica used to make electronic molding compound results in different wear mechanisms as a result of interactions of the abrasive particles and the hard particles in the material. Whereas the small particles of the fused silica can fit between the hard particles and erode the matrix, the much larger sand grains cannot fit and so encounter the hard particles. These encounters apply large stresses to individual hard particles, leading to crack initiation and growth, which results in wear by delamination of sheets of material. The surface morphology which results from this delamination wear, consisting of large numbers of exposed

carbides which have been shifted in the matrix, is not observed in parts worn in service. Attempts to remedy this problem by using the fused silica as the abrasive were plagued with problems caused by the poor flow characteristics of this material.

8.1 Steels

Abrasion of steels by AFS 50/70 occurs by microcutting and plowing. Although both of these mechanisms occurred in all of the steels tested, plowing was much more obvious in the softer materials. However, since the softer steels are also more malleable making the removal of material by plastic deformation more difficult, it is probable that the majority of actual material loss occurs by microcutting in all cases. There is some evidence in the wear debris that wedge type wear is occurring. This mechanism is really a transition between plowing, in which no immediate removal of material occurs, and microcutting, in which little ridge formation by plastic deformation occurs. Therefore it is not surprising to find this mechanism occurring where the other two are both present.

8.2 Composites

The materials which contain large volume percentages of hard carbide particles all have very similar wear scar

surface morphologies, consisting of numerous exposed carbides which have crescent shaped crevices on the "upstream" side relative to abrasive travel direction. They also all exhibit "comet tailing", in which the matrix material immediately "downstream" from the carbide has been protected by the carbide particle.

These characteristics reveal several things about the wear of these materials. First, plowing and microcutting are not the major wear mechanisms even though they are occurring on two scales. On a small scale, plowing and microcutting are occurring, and are responsible for the comet tailing seen in the scanning electron micrographs of the wear scars. However, interaction with the carbide particles severely limits the depth of penetration, so that the chip size is very small and the resulting wear rate is low. Since the carbides are much harder than the silica abrasive, cutting or plowing of the carbides is a very rare occurrence. The size and shape of the asperities on the abrasive places a limit on the amount of material which can be removed. Since the carbide particles in general are larger than the space between them and the silica can only plow or cut the matrix, wear would soon stop if this were the major mechanism. If this mechanism were capable of removing the carbide particles, one would not expect the wear scar surface to consist of numerous carbides. On a larger scale, where the

whole sand grain rather than small asperities is interacting with the abraded surface, there is no evidence of plowing but microcutting is occurring by an occasional grain. This is evidenced by the occasional short, wide gouges seen in the wear scars. However, the fact that these relatively rare features are conspicuously different from the rest of the wear scar shows that this is not the primary wear mechanism. Thus plowing and microcutting are occurring on two scales, one which is very prevalent but which can remove only a small quantity of material and one which could possibly remove large amounts of material but which occurs only rarely.

Delamination is a wear mechanism originally proposed to explain wear in sliding metal contact and is similar to fatigue spalling of rolling contact bearings. It is not usually associated with abrasion, however rolling and sliding are the two ways in which abrasive particles transit the wear contact region in three body wear. Delamination is a fatigue process in which cumulative plastic deformation leads to the initiation of subsurface cracks which grow parallel to the surface but eventually come to the surface and cause the loss of a wear sheet. Particulate reinforced composites are ideally suited to be susceptible to this wear mechanism since the cracks often initiate at second phase particles. Because the carbides are much stronger than the matrix materials, the carbide particles can be considered rigid. Since the

carbides are smaller in diameter than the sand grains they will act to concentrate any force applied to them into a small region of matrix below the carbide particle. Thus even nominally elastic encounters may result in the plastic compression of subsurface regions of the matrix. This would result in tensile residual stresses perpendicular to the surface which would tend to initiate subsurface cracks parallel to the surface.

As in any fatigue process, the time to initiate a crack may represent a substantial portion of the life of the part, or in this case the time to create a wear particle. Unlike the rolling and sliding situations that delamination wear is normally associated with, abrasion introduces two possible mechanisms for single event crack initiation in addition to the normal damage accumulation method. Cracks were observed in association with the gouges caused by the large scale microcutting described above. Thus the removal of a microchip may also introduce relatively large cracks into the surface of the material. It is also possible that the force applied to a carbide by an abrasive particle could drive the carbide into the surface and create a crack much as a wedge splits wood.

A potentially more damaging phenomenon is crack branching. This trait is often designed into composite materials as a method of toughening them by making crack

growth more difficult. In this situation, however, it has the effect that formation of a wear particle initiates the crack that forms the next wear particle, thus introducing a positive feedback mechanism. Examination of the wear scars often revealed either cracks or loosely attached particles in areas from which wear particles had recently been lost, and the plate shaped wear debris particles often contained cracks.

Thus the time to initiate a crack may not be a factor in the delamination wear of these composite materials, or it may be a factor in the early stage, creating an initial period of very low wear rate until sufficient secondary cracks have been created to achieve a steady state.

Any attempt to model dry sand rubber wheel abrasion would involve a very large number of variables. Consideration of the effect of the rubber would include the hardness, deformation and recovery characteristics, constraint effects from the wheel core as a function of rubber thickness, and the effects of temperature variations on these characteristics. From the sample would come initial and ultimate hardness, work hardening rate, fracture toughness, crack propagation rate, fatigue strength, and shear strength. Composite materials would have multiple sets of the above mentioned parameters plus factors such as interparticulate spacing, particle size, and interface

strength. Abrasive particle size, shape, angularity, fracture toughness, hardness, and compressive strength would all need to be considered, as well as environmental factors such as applied load, sliding speed, temperature and chemical activity. The large number of variables results from the possibility that several wear mechanisms are operating at one time and may either compete or complement each other.

9.0 CONCLUSIONS

As discussed above, this research was partially successful in meeting the goal of determining a test method

of evaluating materials for extruder tooling. In the case of steels, testing with AFS 50/70 gave the same wear scar morphology as the limited testing with Glasgrain fused silica. This similarity of wear surface morphology indicates that the ASTM G65 test may be a valid method of evaluating the potential performance of these materials. In the case of the high carbide volume fraction materials, however there were significant differences in the wear surface morphologies which resulted from the two abrasives. The similarity of the "galled" portion of the Glasgrain wear scar to the wear surface of parts returned from actual service shows that the size of the abrasive grains plays an important role the wear of these materials. Thus the lack of success was related to the inability to feed the fine crushed fused silica abrasive to the wheel-sample interface in an even and consistent fashion. The coarser AFS 50/70 abrasive failed to duplicate the abrasive matrix erosion observed in the use worn parts due to abrasive particle size effects which limited the abrasive-matrix interactions and introduced additional wear mechanisms.

Several conclusions can be drawn from this research:

a) Wear of the steels occurred by microcutting and plowing, hence increased hardness reduces wear by decreasing the depth of penetration of the abrasive into the surface which reduces the amount of material removed at one time.

b) Wear of the composite materials occurred primarily by delamination, with some microcutting. Delamination may initiate by fatigue or by the single event processes of large scale microcutting or splitting.

c) Crack branching acts as a source of additional cracks. Thus the formation of one wear particle leads to the formation of more.

d) Ion nitriding improves the abrasive wear resistance of both steels and composites when it is successful. The wear test results on these samples were highly variable due to large variations in the effectiveness of the nitriding process.

e) The nitride layer acts as a barrier coating, providing a period of much reduced wear rate. After penetration of this layer the wear rate approaches the wear rate of the same material without nitriding.

f) Microgeometry of the sand grain surface is important because most of the microcutting on both steels and composites is done by asperities on the grains. This was especially true for secondary growth crystal terminations on the sand grains which acted as cutting tools in some cases.

g) Although degradation of sand is limited, that which occurs is important as a source of small particles and because it increases the angularity of the abrasive particles.

h) Wear rate is constant for non-nitrided steels.

i) The friction force alters the distribution of normal force on the contact region, resulting in a shift of the location of maximum stress and possibly altering the magnitude of the maximum stress.

10.0 RECOMMENDATIONS FOR FUTURE WORK

It should be possible to utilize the Glasgrain type of crushed fused silica as the abrasive in a rubber wheel abrasion test. One possible approach would be to restrict the particle size range to minimize packing density and particle interlocking. Otherwise it would probably be necessary to mix the silica with some liquid to create a slurry.

Three other interesting areas of investigation suggested by this research are:

1) examine the effect of the abrasive particle shape by using both a spherical and an elongated particle shape in some abrasive where these shapes are available with all other factors the same.
2) examine and analyze the effect of deformation of the rubber by the friction force on the stress magnitude and distribution.
3) use single asperity simulated abrasion to examine and verify the single event crack initiation mechanisms.

References:

1. Webster's New Universal Unabridged Dictionary, Deluxe second edition, Simon and Schuster, (1983)

2. Haworth, R. D. Jr., Transactions of the American Society for Metals, 41, p. 819-869, ASM, Cleveland, (1949)

3. Avery, H. S., Wear. 4, No. 6, p. 427-449, Elsevier Sequoia, Lucerne, (1961)

4. Glossary of Terms and Definitions in the Field of Friction, Wear and Lubrication, Organization for Economic Co-operation and Development, p.13, O.E.C.D. Publications, Paris, (1969)

5. Babichev, M. A., "Investigation of the Abrasive Wear of Metals by the Brinell Method", Friction and Wear in Machinery, Vol. 14, p.1-29, (1960)

6. Khruschov, M. M., "Principles of Abrasive Wear", Wear, Vol. 28, p 69-88, 1974

7. Richardson, R. C. D., "The Wear of Metals by Relatively Soft Abrasives", Wear, Vol. 11, p. 245-275, (1968)

8. Tadmor, Z. and I. Klein, Engineering Principles of Plasticating Extrusion, p. 1-10, Robert E. Krieger Publishing Company, Huntington, New York, (1978)

9. Martelli, F. G., Twin-Screw Extruders: A Basic Understanding, p. 7, Van Nostrand Reinhold Company Inc., New York, (1983)

10. Matthews, G., Polymer Mixing Technology, p. 160-190, Applied Science Publishers, London, (1982)

11. Cogswell, F. N., Polymer Melt Rheology, George Godwin Limited, London, (1981)

12. ASM International, Electronic Materials Handbook, 1, p. 803, Metals Park, Ohio, (1989)

13. Czichos, H., Tribology, Elsevier Science Publishing Co., New York, p. 14-33, (1978)

14. Soane, D. S., and Z. Martynenko, Polymers in Microelectronics Fundamentals and Applications, p. 249-259, Elsevier, Amsterdam, (1989)

15. Electronic Materials Handbook, ASM International, Materials Park, Ohio, p. 729-821, (1989)

16. El-Raghy, S. M., H. Abd-El-Kader,and M. E. Abou-El-Hassan, "Electrochemistry of Abrasion Corrosion of Low Alloy Steel in 1% NaCl Solution", Corrosion, Vol. 40, p. 60-61, (1984)

17. Abd-El-Kader, H., and S. M. El-Raghy, "Wear-Corrosion Mechanism of Stainless Steel in Chloride Media", Corrosion Science, Vol. 26 No.8, p. 647-653, (1986)

18. Madsen, B. W., "Measurement of Erosion-Corrosion Synergism with a Slurry Wear Test Apparatus", Wear. Vol. 123, p. 127-142, (1988)

19. Bailey, J. A., Abdel-Moez Bayoumi and J. S. Stewart, "Wear of Some Cemented Tungsten Carbide Tools in Machining Oak", Wear, Vol. 85, p. 69-79,(1983)

20. Ward, M. J., "Corrosion of Tool Steels in Liquid Polymers", Senior Design Project in Materials Engineering, Prof. R. E. Swanson, advisor, VPI&SU, Blacksburg, VA (1989)

21. Luken, R. C. Jr., Effect of Heat Treatment of Mechanical Behavior of CPM10V Tool Steel, MS Thesis, Department of Materials Engineering, VPI&SU, Blacksburg, VA, 1987

22. Thomas, E.W., "The Physics of Ion Implantation", Ion Plating and Implantation - Applications to Materials, ASM International, p. 7-14, Materials Park, Ohio, (1986)

23. G. Dearnaley, Goode, P.D., Hartley, N.E.W., Proctor, G.W., Turner, J.F., and Watkins, R.E.J., "The Ion Implantation of Steel and Cemented Carbides", IPAT 79 - Proceedings of International Conference Ion Plating & Allied Techniques, p. 243-254, Spectrum Printing Company, Edinburgh, (1979)

24. B.G. Delves, and Dearnaley, G., "The Use of Ion Implantation for the Improvement of Abrasive Wear", IPAT 79 - Proceedings of International Conference Ion Plating & Allied Techniques, p. 264-271, Spectrum Printing Company, Edinburgh, (1979)

25. Spalvins, T., "Plasma Assisted Surface Coating/Modification Processes: an Emerging Technology", Ion Nitriding, ASM International, Materials Park, Ohio, p. 1-8, (1987)

26. Kovacs, W., and W. Russell, "An Introduction to Ion Nitriding: What is it? Why is it used? Where is it used?", Ion Nitriding, ASM International, Materials Park, Ohio, p. 9-17, (1987)

27. Thorton, J.A., "Fundamental Considerations in Plasma Surface Treatments", Ion Nitriding, ASM International, Materials Park, Ohio, p. 19-22, (1987)

28. Rabinowicz, E., L. A. Dunn and P. G. Russell, "A Study of Abrasive Wear Under Three-Body Conditions", Wear, Vol.4, p. 345-355, (1961)

29. Larsen-Badse, J., "The Abrasion Resistance of Some Hardened and Tempered Carbon Steels", Transactions of the Metals Society of AIME, Vol. 236, p. 1461-1466, (1966)

30. Quinn, A. C., and D. W. Hall, "The Effect of Carbon Content and Heat Treatment on the Rate of Abrasive Wear of Plain Carbon Steels", SAE paper 700688, SAE, Inc., New York, (1970)

31. Richardson, R. C. D., "The Maximum Hardness of Strained Surfaces and the Abrasive Wear of Metals and Alloys", Wear, Vol. 10, p. 353-382, (1967)

32. Avery, H. S., "An Analysis of the Rubber Wheel Abrasion Test", Wear of Materials, ASME, New York, p. 367-378, (1981)

33. Muscara, J., and M. J. Sinnott, "Construction and Evaluation of a Versatile Abrasive Wear Testing Apparatus", Metals Engineering Quarterly, Vol. 12, p. 21-32, (1972)

34. Rabinowicz, E., and A. Mutis, "Effect of Abrasive Particle Size on Wear", Wear, Vol. 8, p. 381-390, (1965)

35. Nathan, G. K. and W. J. D. Jones, "The Empirical Relationship Between Abrasive Wear and the Applied Conditions", Wear, Vol. 9, p. 300-309, (1966)

36. Sin, H., N. Saka, and N. P. Suh, "Abrasive Wear Mechanisms and the Grit Size Effect", Wear, Vol. 55, p. 163-190, (1979)

37. Zum-Gahr, K. H., Metallurgical Aspects of Wear, p. 73-104, Deutshe Gesellschaft fur Metallkunde, Oberursel, Germany, (1981)

38. Kulic, T., T. H. Kosel, and Y. Xu, "Effect of Depth of Cut on Second Phase Particle Fracture in Abrasion of Two Phase

Alloys", Wear of Materials, Vol.1, p. 23-33, ASME, New York, (1989)

39. Swanson P. A., and R. W. Klann, "Abrasive Wear Studies Using the Wet Sand and Dry Sand Rubber Wheel Tests", Wear of Materials, ASME, New York, p.379-389, (1981)

40. Blau, P. J., Friction and Wear Transitions of Materials, Noyes Publications, Park Ridge, New Jersey, p. 72, (1989)

41. Mulhearn, T. O., and L. E. Samuels, "The Abrasion of Metals: a Model of the Process", Wear, Vol. 5, P 478-498, (1962)

42. Murray, M. J., P. J. Mutton, and J. D. Watson, "Abrasive Wear Mechanisms in Steels", Wear of Materials, ASME, New York, P.254-265, (1979)

43. Hokkirigawa, K., and K. Kato, "Theoretical Estimation of Abrasive Wear Resistance Based on Microscopic Wear Mechanisms", Wear of Materials, Vol. 1, ASME, New York, p.1-8, (1989)

44. Bowden F. P., and D. Tabor, The Friction and Lubrication of Solids, Oxford University Press, London, Part I, p. 10-22 (1964)

45. Suh, N., Tribophysics, Prentice-Hall, Englewood Cliffs, New Jersey, p. 199-209, (1986)

46. Suh, N. P., "An Overview of the Delamination Theory of Wear", Wear, Vol. 44, P. 1-16, (1977)

47. Zum-Gahr, K. H., "Relation between Abrasive Wear Rate and the Microstructure of Metals", Wear of Materials, ASME, New York, P.266-274, (1979)

48. Fiore, N. F., J. P. Coyle, S. P. Udvardy, T. H. Kosel, and W. A. Konkel, "Abrasive Wear-Microstructure Interactions in a Ni-Cr White Iron", Wear, Vol. 62, P.387-404, (1980)

49. Borik, F., "Rubber Wheel Abrasion Test", SAE publication 700687, SAE, New York, (1970)

50. Xuan, J. L., I. T. Hong, and E. C. Fitch, "Hardness Effect on Three-Body Abrasive Wear Under Fluid Film Lubrication", Journal of Tribology, Vol. 111, p.35-40

51. Tsuji, E., and Y. Ando, "Effect of Air Temperature and Relative Humidity on Wear of Carbon Steels and Cast Irons", Wear of Materials, ASME, New York, p. 94-99, (1977)

Table I NOMINAL COMPOSITION (weight percent)

MATERIAL	C	Mn	Si	Cr	Ni	Mo	V	Al	TiC	Cu
AISI 4150	0.50	0.9	0.2	0.95	--	0.2	--	--	--	--
THYSSEN 4122	0.40	--	--	16.5	1.0	1.1	--	--	--	--
D-2	1.50	0.6	0.6	12.0	--	1.0	1.00	--	--	--
FERROTIC C45	0.85	--	--	10.0	--	3.0	--	--	33.0	--
FERROTIC C25	0.85	--	--	10.0	--	3.0	--	--	17.0	--
FERROTITANIT	0.65	--	--	14.0	0.4	3.0	0.50	1.0	33.0	0.9
CPM10V	2.45	0.5	0.9	5.25	--	1.3	9.75	--	--	--

Balance Iron for all materials

Table II HEAT TREATMENT (DEGREES C)

MATERIAL	ANNEAL	AUSTINITIZE	TEMPER 1	TEMPER 2	TEMPER 3
D-2	AS REC.	1010-1HR	205-1HR	-------	-------
FERROTIC C45	AS REC.	1065-1.5HR	524-.5HR	524-.5HR	510-.5HR
FERROTITANIT	595-2HR	1095-1.5HR	520-1HR	510-1HR	
CPM10V RC 55	845-1HR	955-.75HR	540-2HR	524-2HR	510-2HR
CPM10V RC 59	845-1HR	1010-.5HR	540-2HR	524-2HR	510-2HR

All samples were air cooled to room temperature between temper cycles.

Table III WEAR VOLUME LOSS (MM^3)

	MEAN (mm^3)	STD. DEV.	COEF. VAR.	# TESTS	DENSITY (g/cm^3)
D-2	37.03	1.675	4.5%	7	7.6698
FERRO-TIC	21.51	1.171	5.4%	6	6.462
THYSSEN 4122	349.26	11.28	3.2%	6	7.7
THYSSEN FERROTITANIT	13.59	0.995	7.3%	6	6.5
CPM10V RC55	16.07	0.274	1.7%	6	7.416
CPM10V RC59	14.44	0.930	6.4%	8	7.416
CPM10V RC55 +ION	11.86	0.550	4.6%	6	7.416
CPM10V RC59 +ION (all)	23.73	3.452	14.5%	6	7.416
GRAY	26.83	2.091	7.8%	3	7.416
BLACK	20.63	0.479	2.3%	3	7.416
FERRO-TIC CM25	16.02	0.756	4.7%	5	7.025
4122 ANNEALED +ION	235.30	33.50	14.2%	6	7.7
AISI 4150 + ION	141.68	0.867	0.6%	5	7.67

Table IV ROCKWELL HARDNESS VALUES

ALL SAMPLES

	# TESTS	AVG	STD DEV	COEF VAR
D-2	1170	63.38	1.390	2.2%
FERRO-TIC HT-VPI	181	67.97	4.254	6.3%
THYSSEN 4122	216	20.09	1.559	7.8%
THYSSEN FERROTITANIT	216	69.65	0.440	0.6%
CPM10V RC55	216	54.79	0.610	1.1%
CPM10V RC59	234	57.99	1.245	2.1%
CPM10V RC55 +ION	162	54.81	2.345	4.3%
CPM10V RC59 +ION	198	50.16	1.366	2.7%
FERRO-TIC CM25	180	60.43	3.547	5.9%
4122 ANNEALED +ION	198	22.57	1.752	7.8%
AISI 4150 + ION	30	46.23	1.796	3.9%

WEAR TESTED SAMPLES

	# TESTS	AVG	STD DEV	COEF VAR
D-2	126	63.50	0.984	1.6%
FERRO-TIC HT-VPI	48	68.98	2.603	3.8%
THYSSEN 4122	108	20.21	1.298	6.4%
THYSSEN	108	69.62	0.497	0.7%
CPM10V RC55	108	54.75	0.636	1.2%
CPM10V RC59	144	58.01	1.379	2.4%
CPM10V RC55 +ION	108	54.94	1.889	3.4%
CPM10V RC59 +ION	108	50.46	1.410	2.8%
FERRO-TIC CM25	90	59.98	3.423	5.7%
4122 ANNEALED +ION	108	22.75	1.525	6.7%
AISI 4150 + ION	30	46.23	1.796	3.9%

Table V 200 GRAM KNOOP MICROHARDNESS VERSUS DEPTH PROFILES

DEPTH (MICRONS)	CPM10V RC 59 BLACK	CPM10V RC 59 GRAY	CPM10V RC 55	4150	4150 SOFT	#144	4122 #143	#146
25	550	590	852	461	919	1081	-*-	1068
50	579	645	853	565	971	1178	1098	1111
75	557	647	897	577	969	1051	1028	1111
100	535	644	888	581	917	690	449	1052
125	561	621	837	553	874	417	386	458
150	587	645	813	578	812		333	378
175	578	661	732	576	500	347		
200	568	642	671	520	342		311	324
225	575	626	626	528		307		
250	582	625	606	492	302		303	313
275	576	634	592	503		310		
300	569	633	581	488	301			
325	570	645	585	499		309		
350	571		589	475	297			
375	579		587	474		310		
400	587	615	590	453	295			
425	585	591	580			308		
450	582	619	600	434	292			
475	580	615	593			306		
500	577	609	579	404	285			
525	573	591	584			306		
550	568	598	582	404	291			
575	565	593	574			308		
600	561	607	584	397	285			
625	573	601						
650	584	603		386	287			
675	579	615				305		
700	574	608	572	380	280			
725	581							
750	587			362	285			
775	583					311		
800	579	579	570	341	283			
825	580							
850	581			326	284			
875	583					303		
900	586	586	565	326	284			
925	578							
950	571			320	290			
975	584					302		
1000	598	583	579	312	281			

-*- Sample cracked

All results are averages of three series except Thyssen 4122 #143 and #146 which are single series.

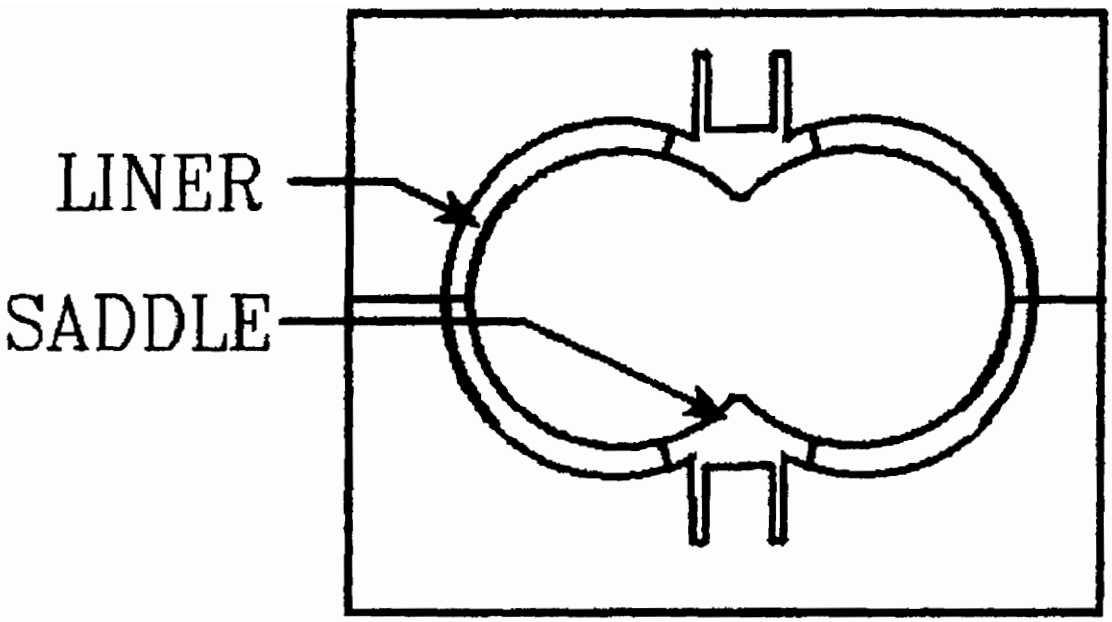

Figure 1: Schematic of an extruder barrel showing liners and saddles

Figure 2: Worn saddle returned from service

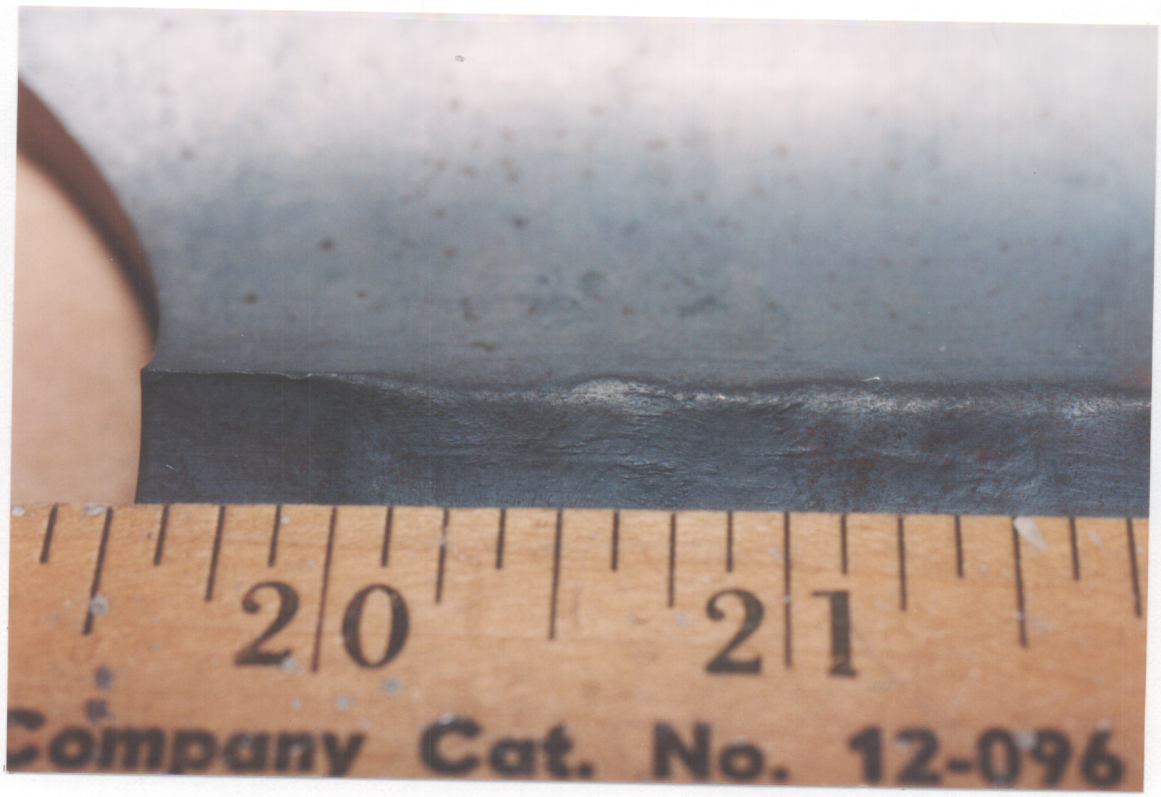

Figure 3: Worn saddle region of a linerless barrel

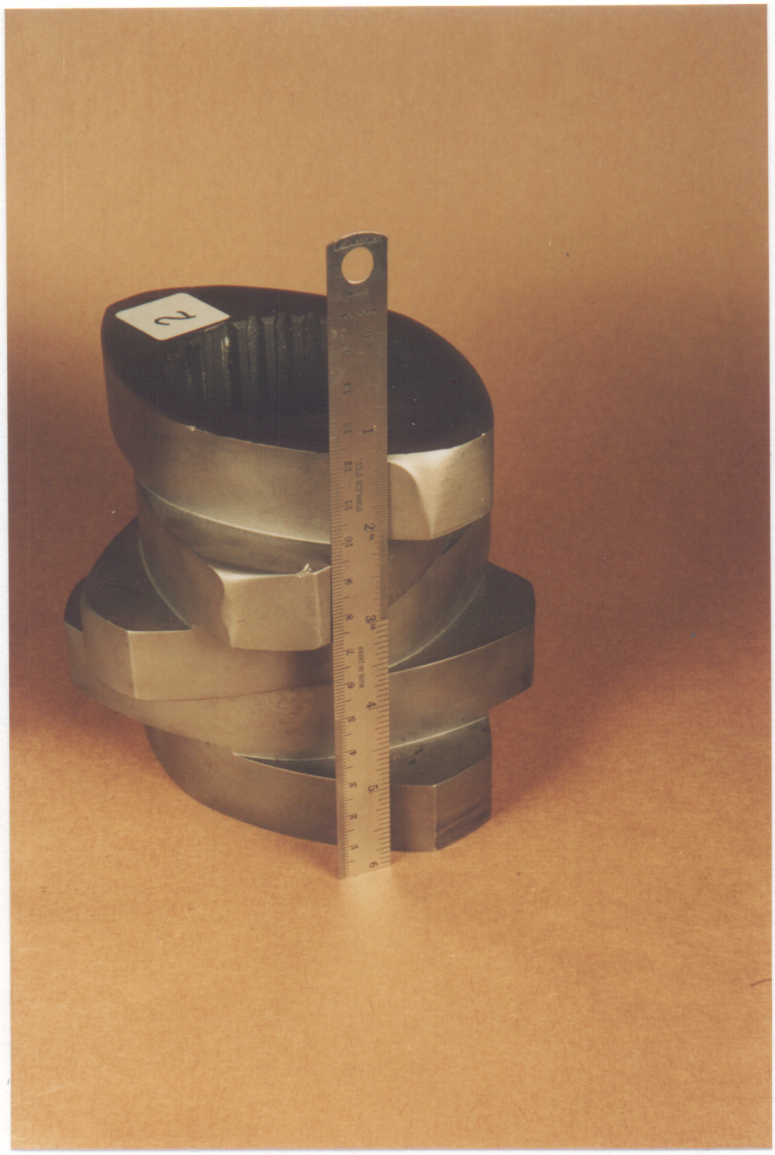

Figure 4: Worn mixing element removed from service

Figure 5: Surface morphology of high wear region of saddle

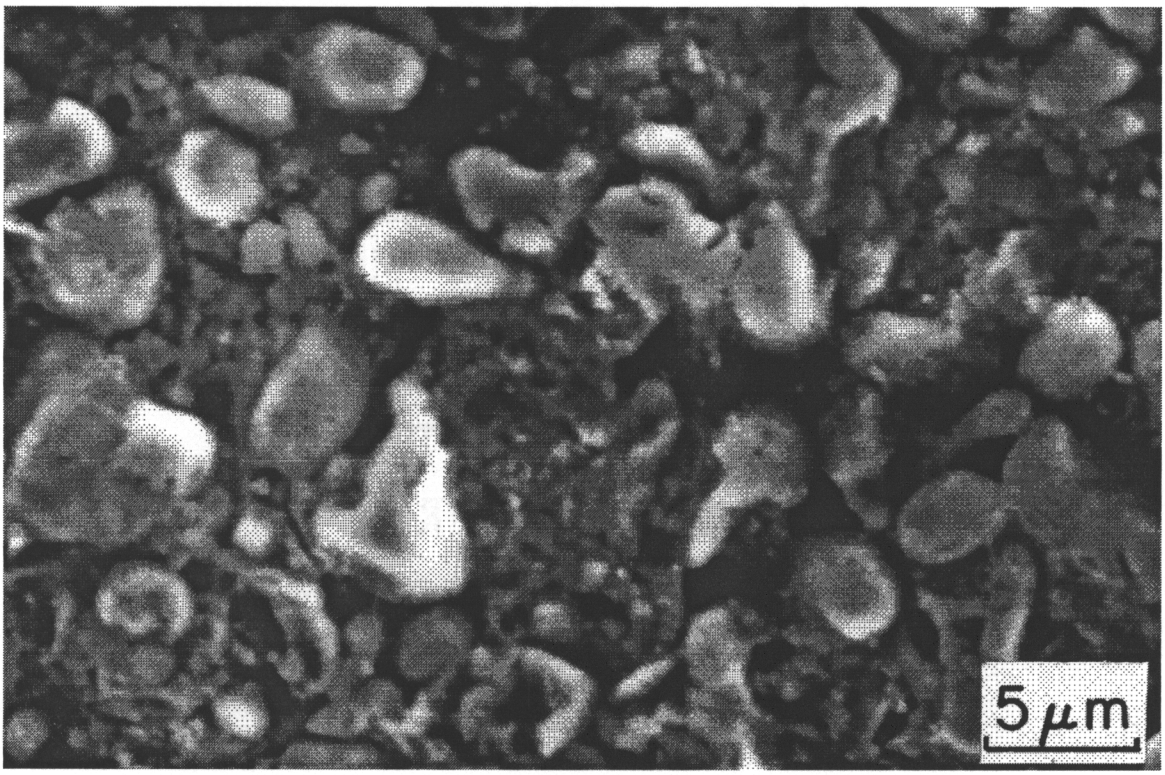

Figure 6: Surface morphology of low wear region of a saddle

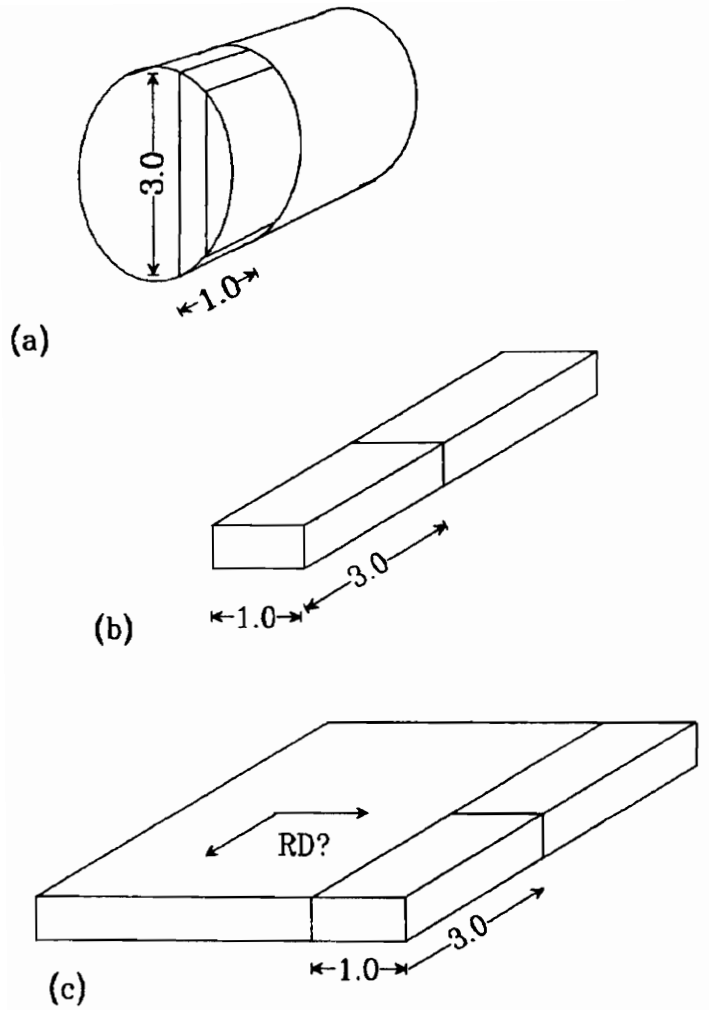

Figure 7: Sample configuration and orientation

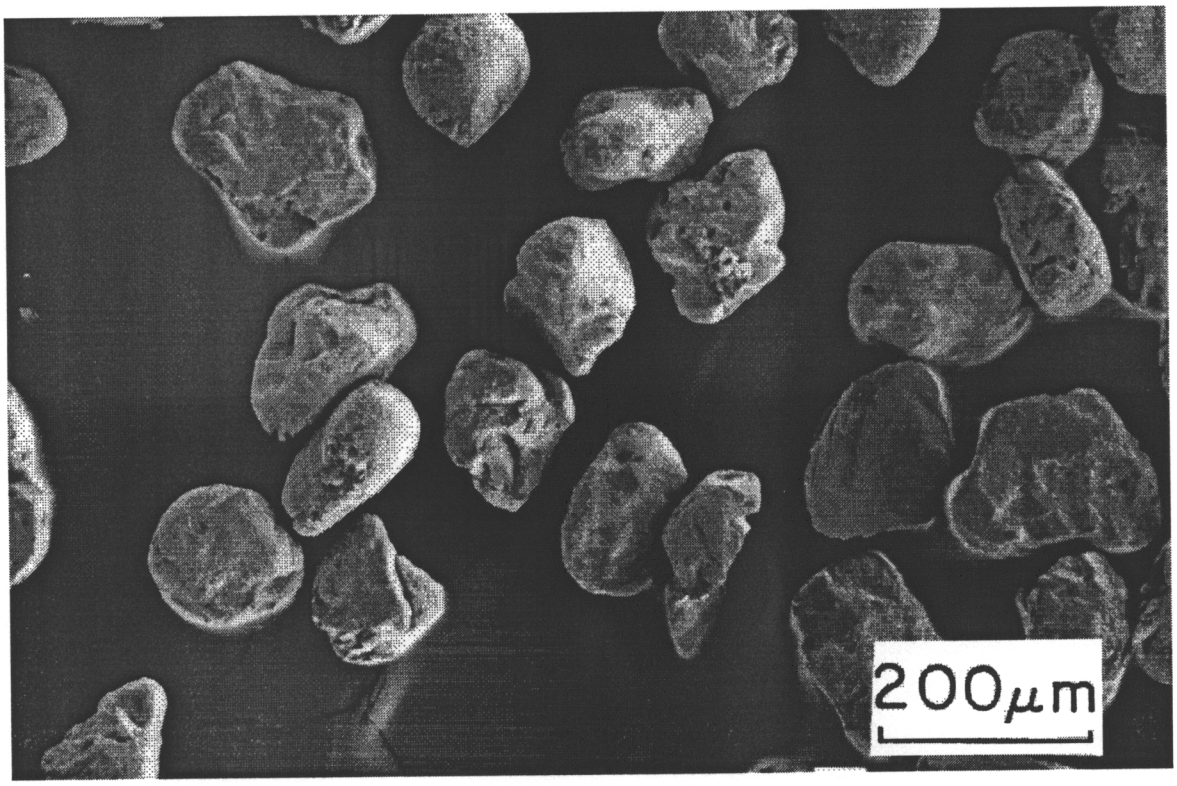

Figure 8: Typical AFS 50/70 sand grains

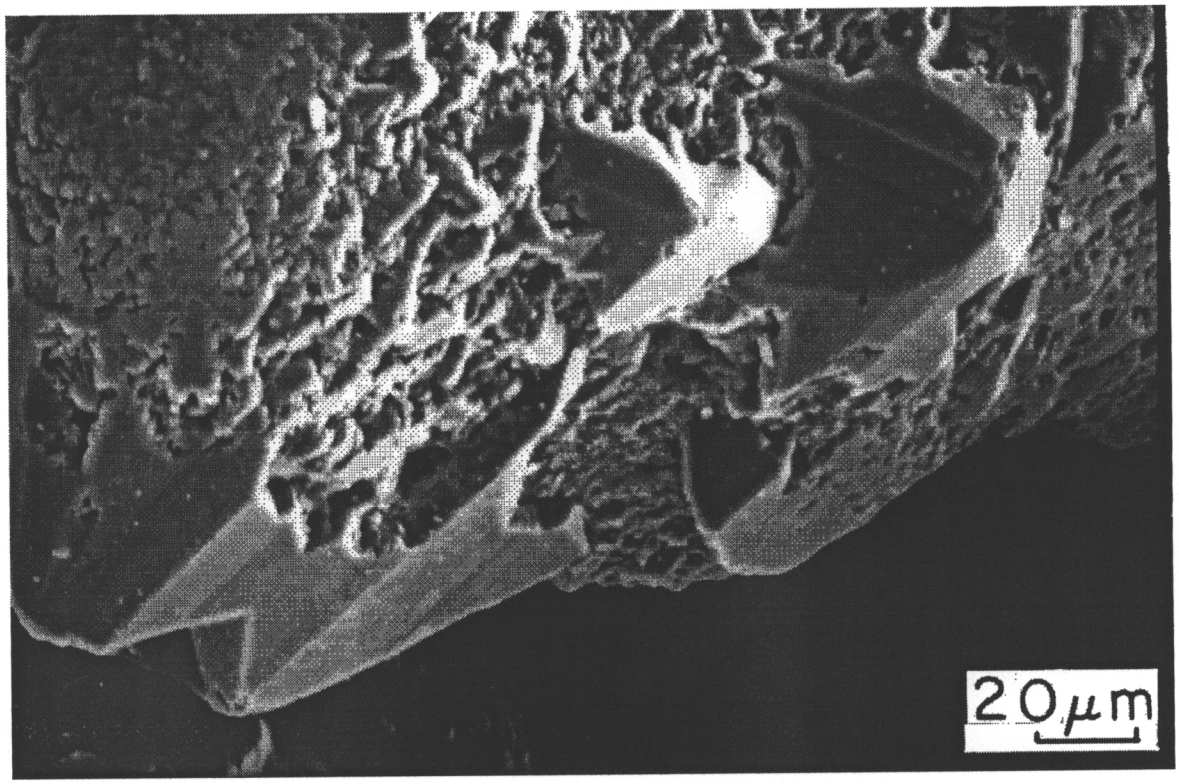

Figure 9: AFS 50/70 sand grain showing crystal terminations

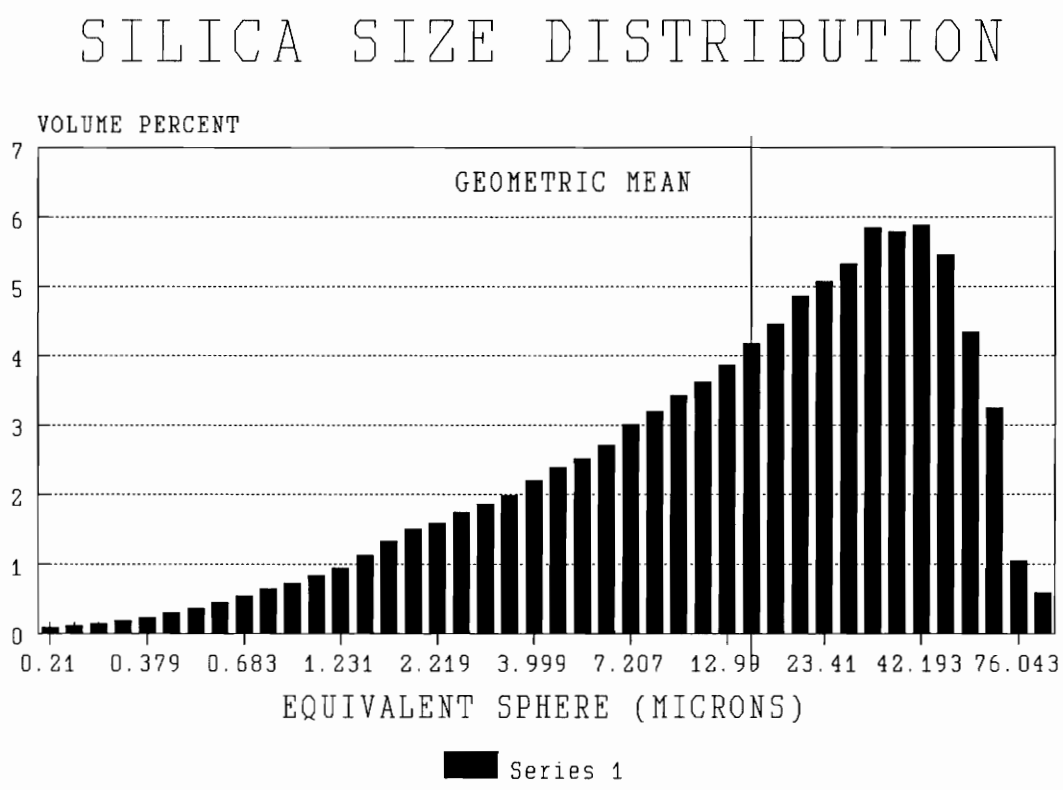

Figure 10: Size distribution Glasgrain fused silica (equivalent spheres)

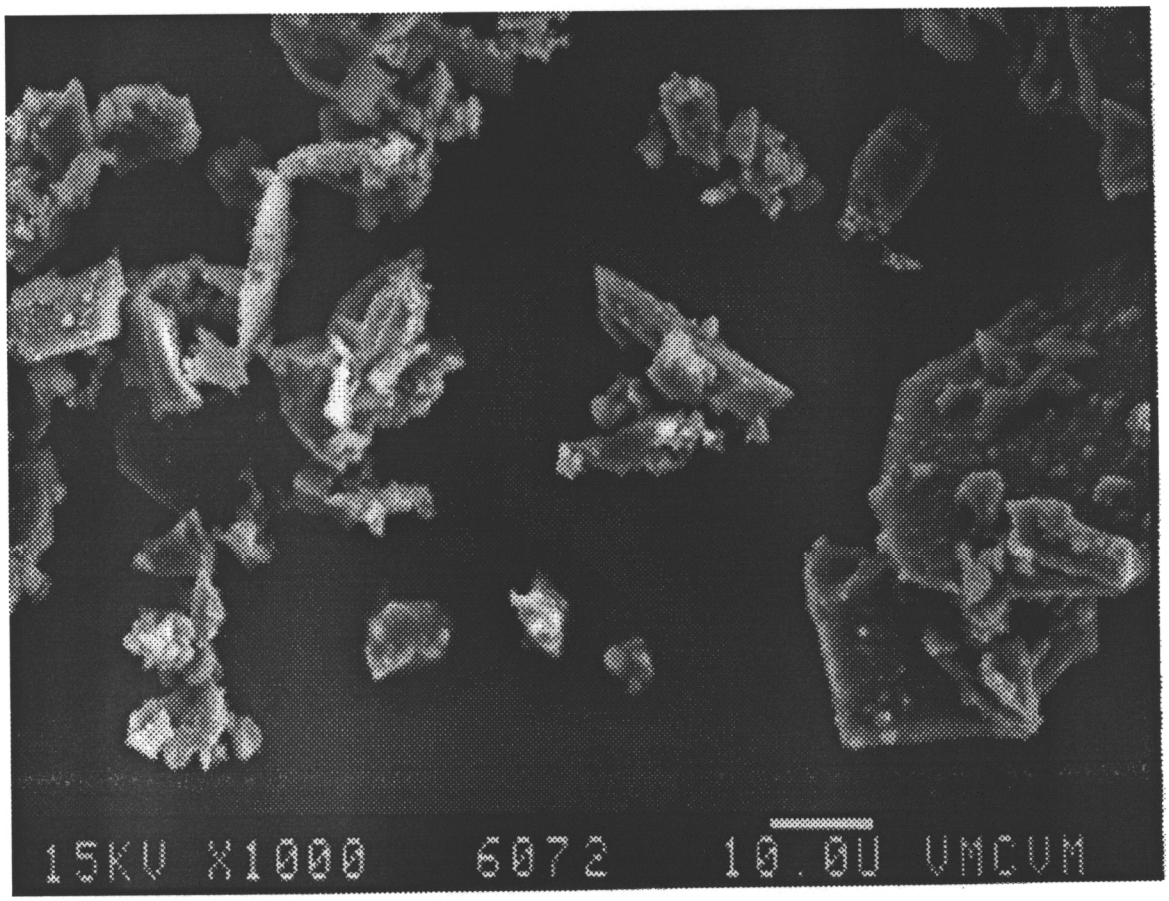

Figure 11: Typical particles of Glasgrain fused silica

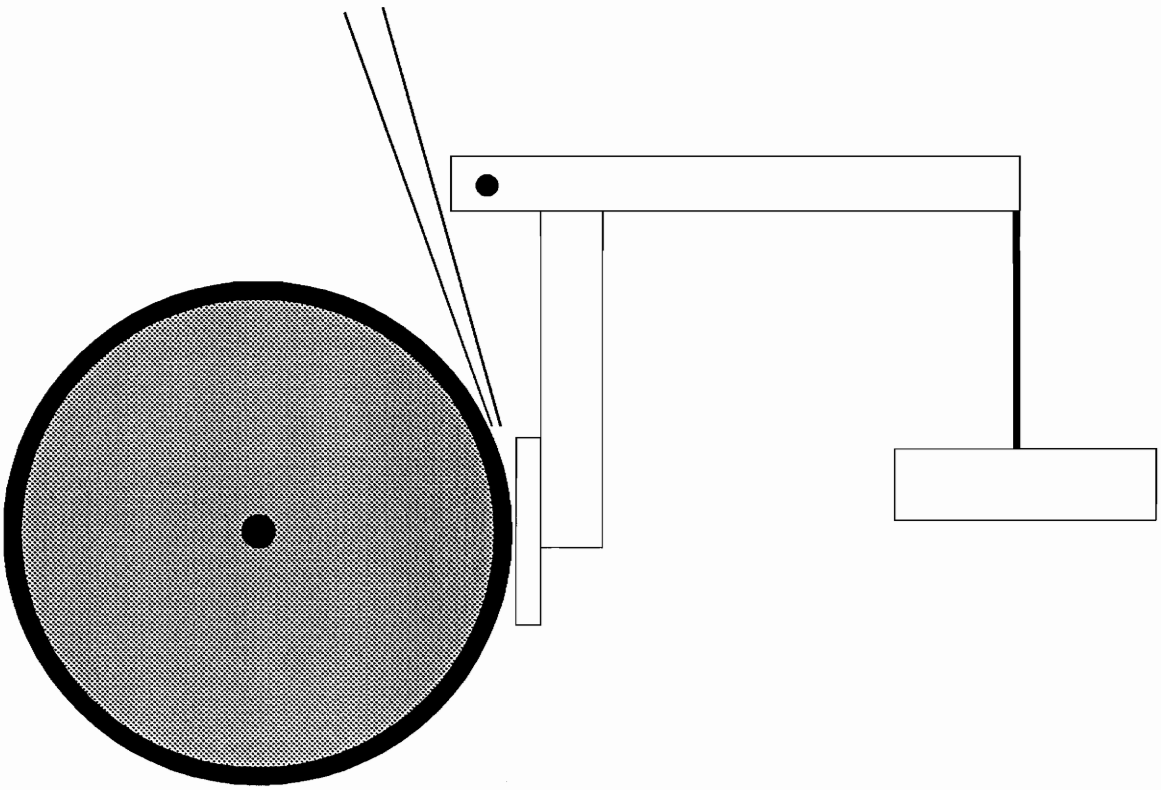

Figure 12: Schematic of the dry sand rubber wheel test apparatus

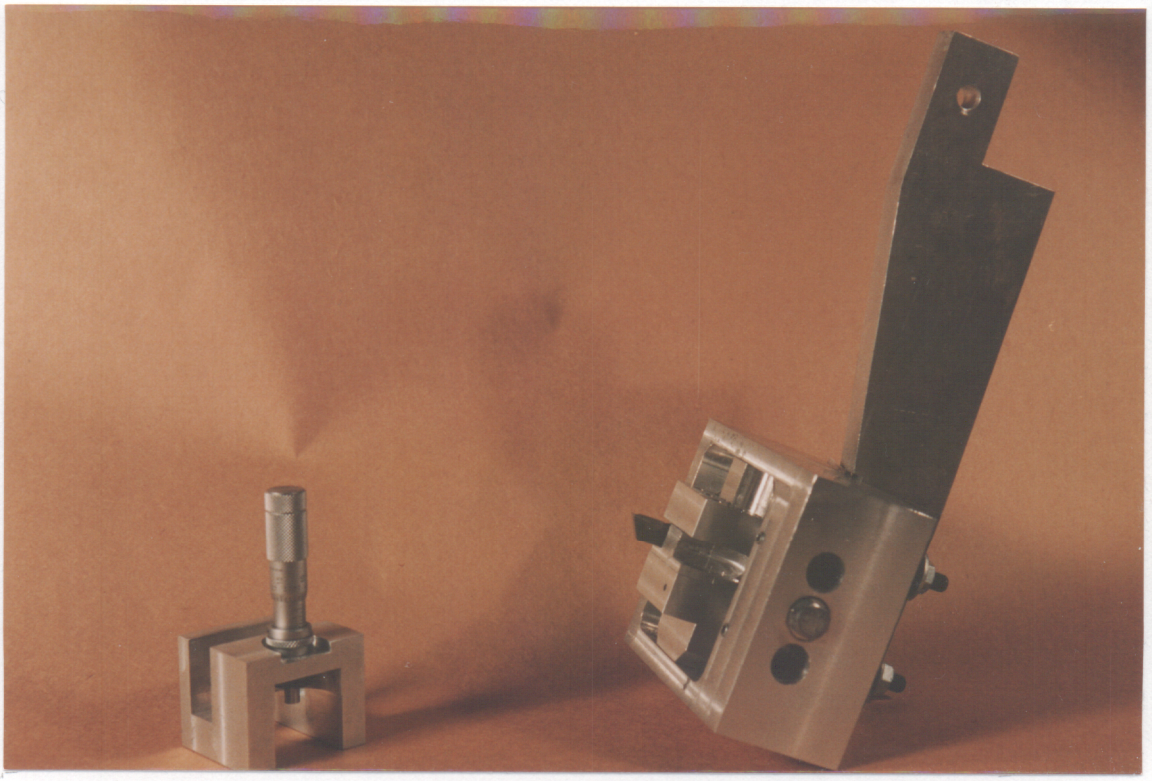

Figure 13: Tool bit holder and micrometer feed for truing wheel

Figure 14: Grinding attachment for truing test wheels

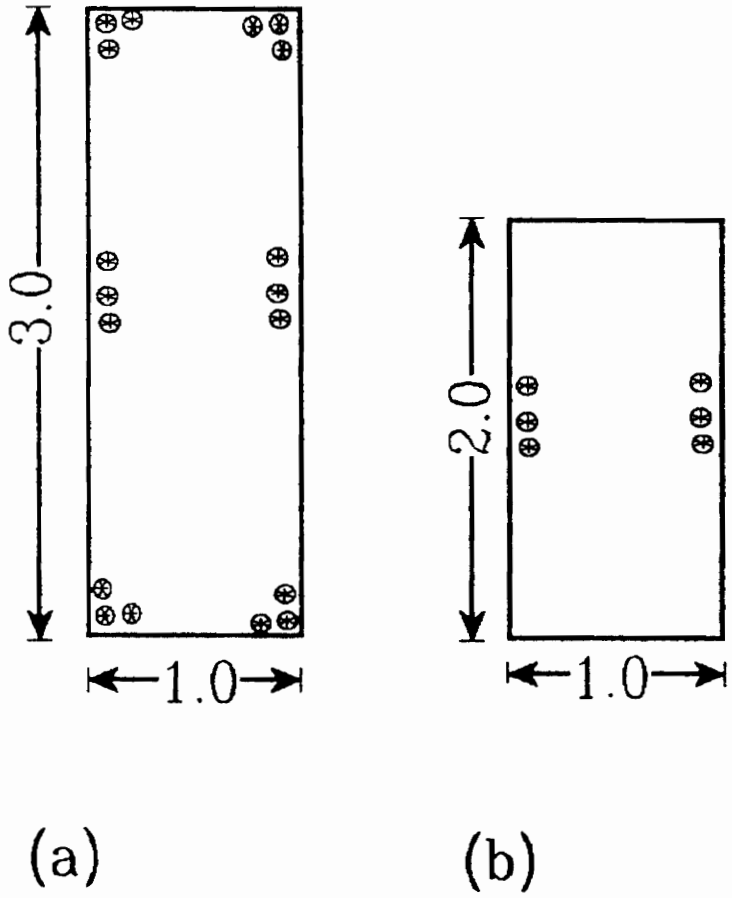

Figure 15: Rockwell test locations

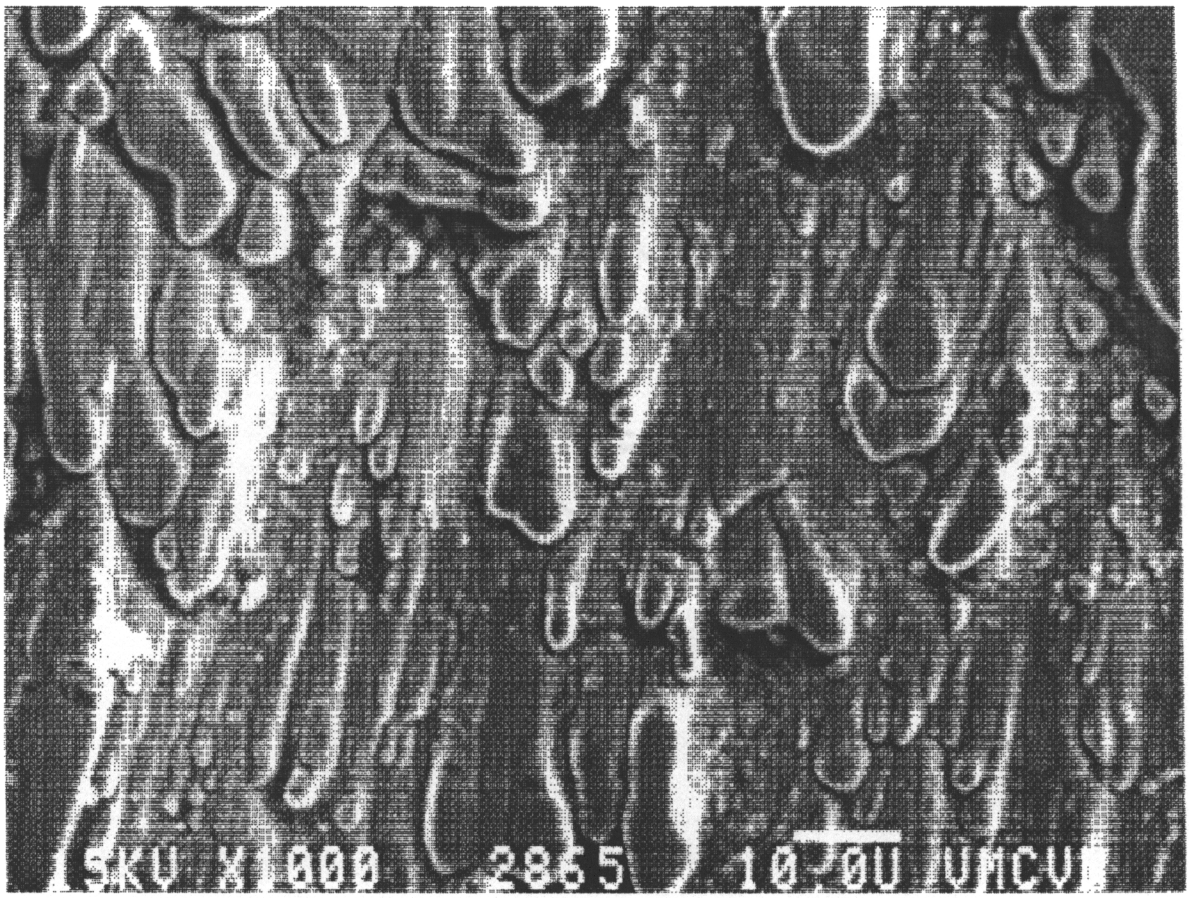

Figure 16: "Galled" region of D-2 steel wear scar abraded by Glasgrain fused silica showing exposed carbides

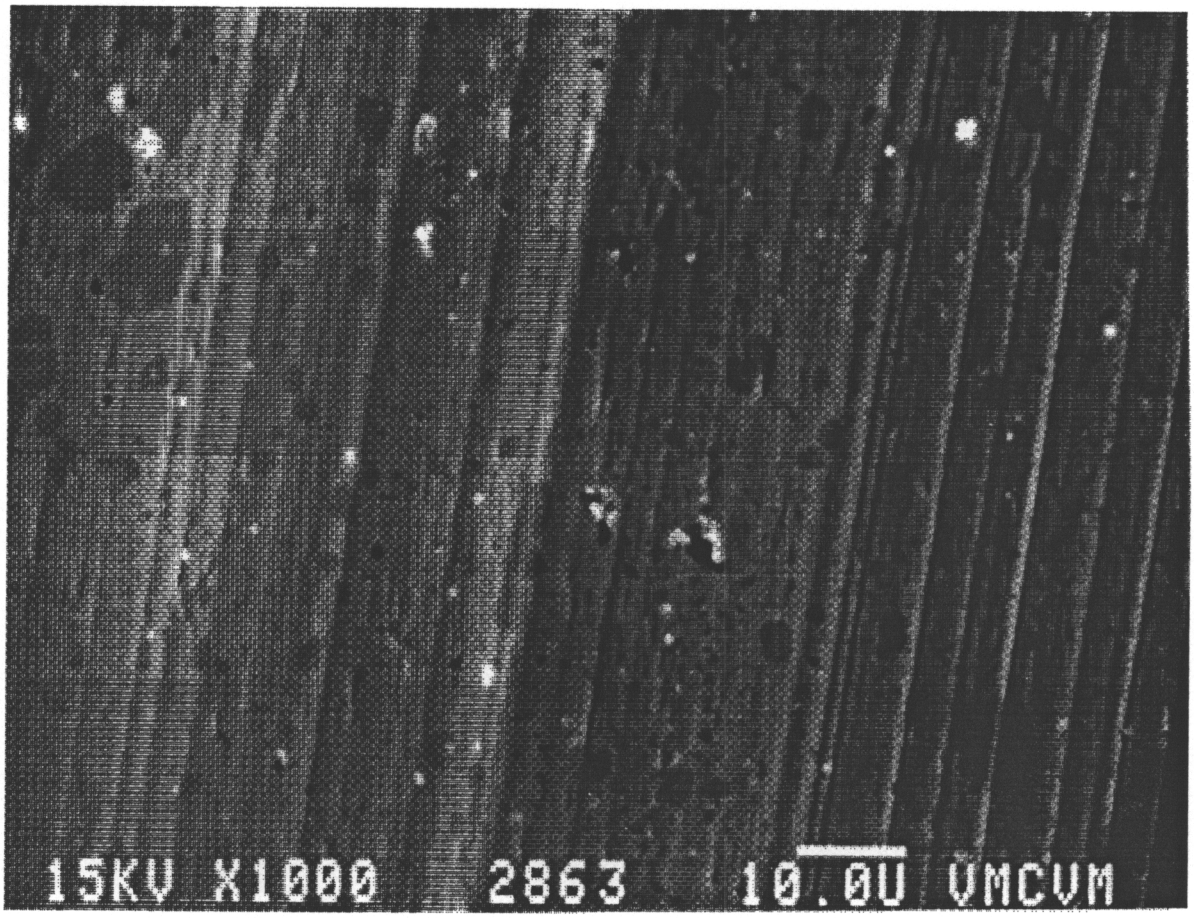

Figure 17: "Polished" region of D-2 wear scar abraded by Glasgrain showing linear scratches .

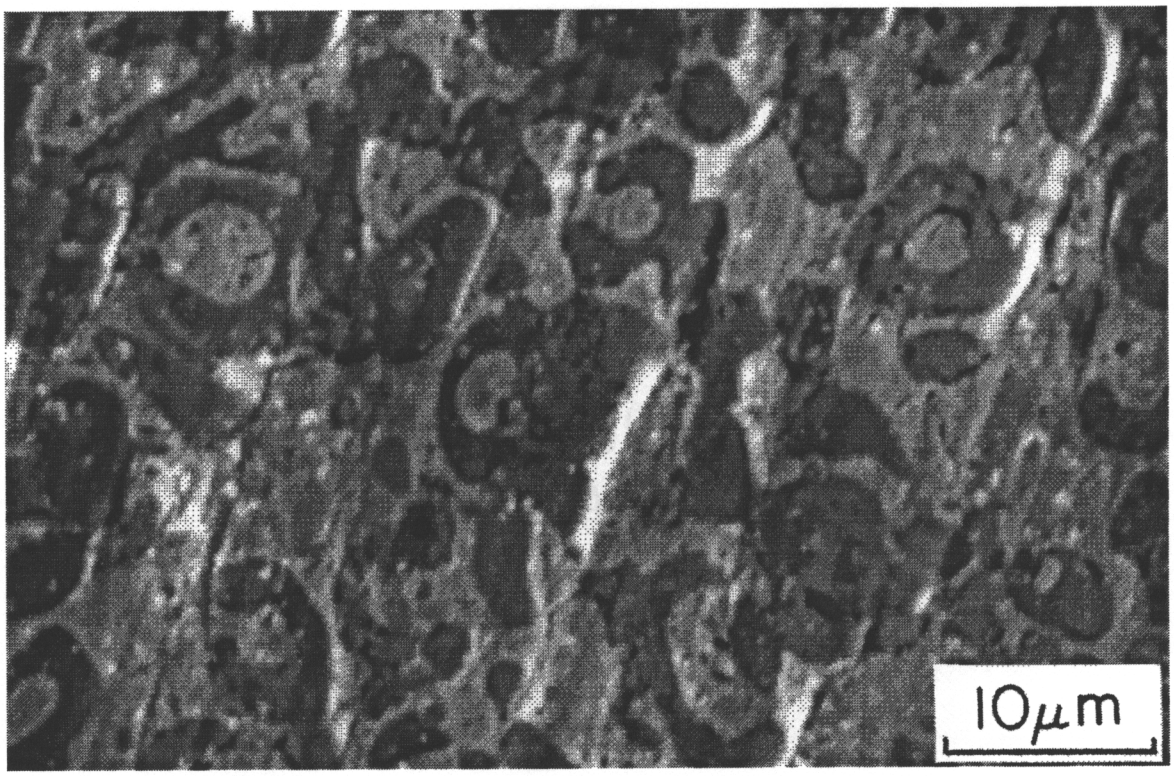

Figure 18: Wear scar surface of FerroTiC abraded by Glasgrain fused silica

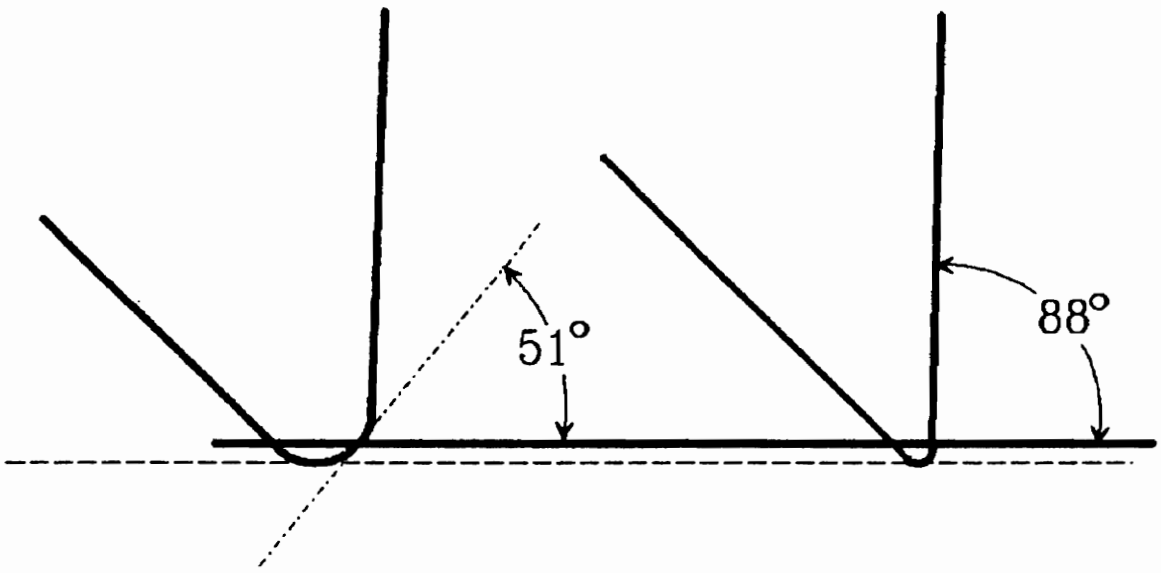

Figure 19: Effect of asperity tip radius on critical angle

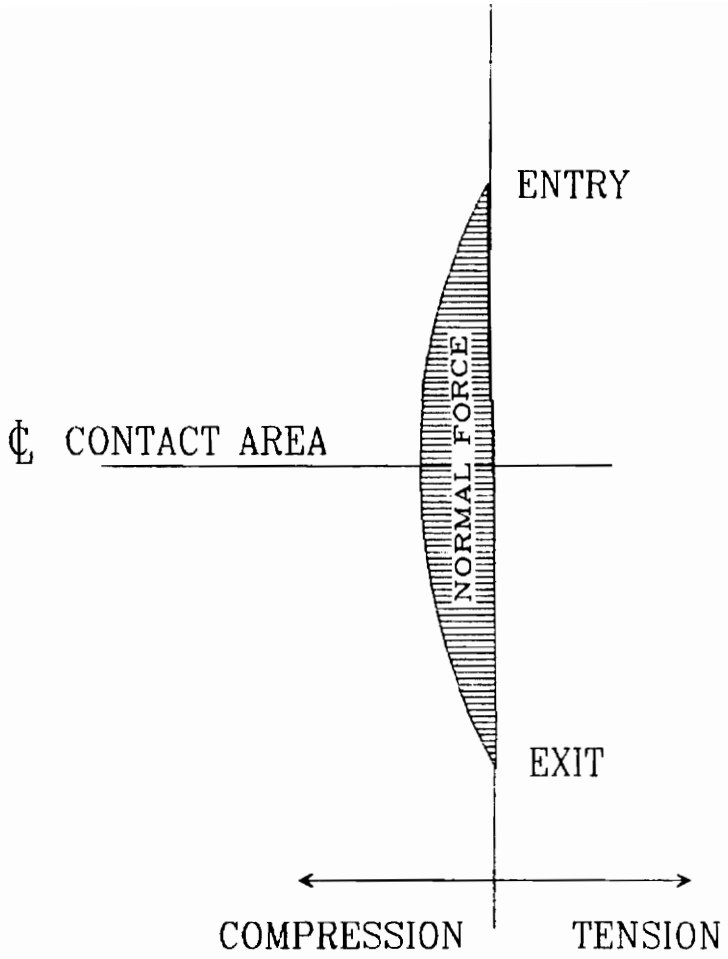

Figure 20: Static normal force distribution along contact region.

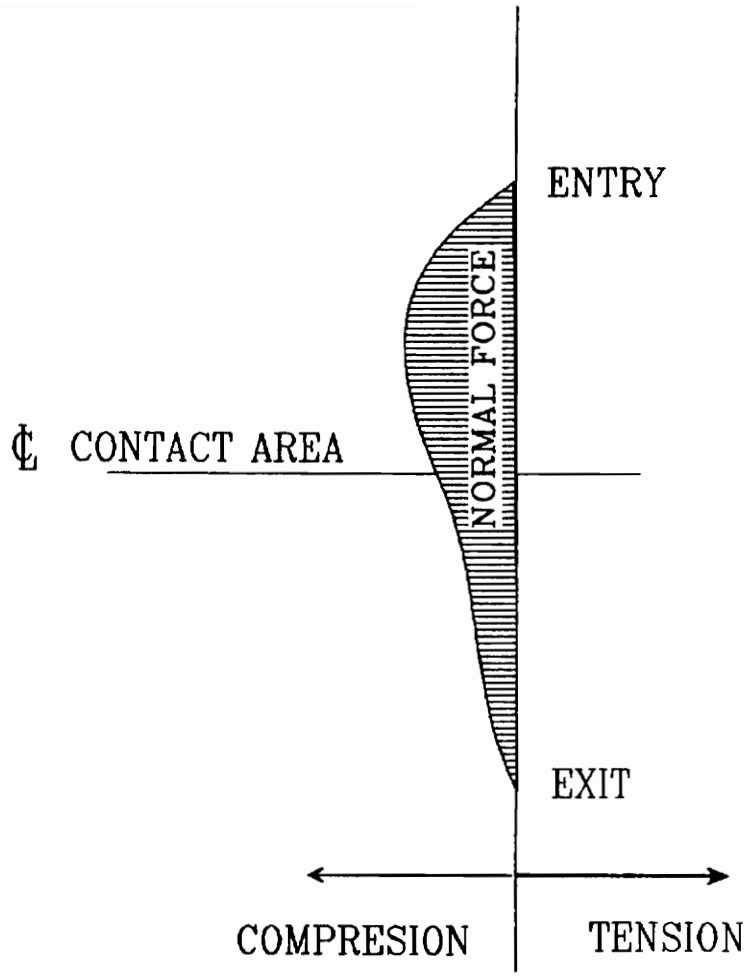

Figure 21: Dynamic normal force distribution along contact region.

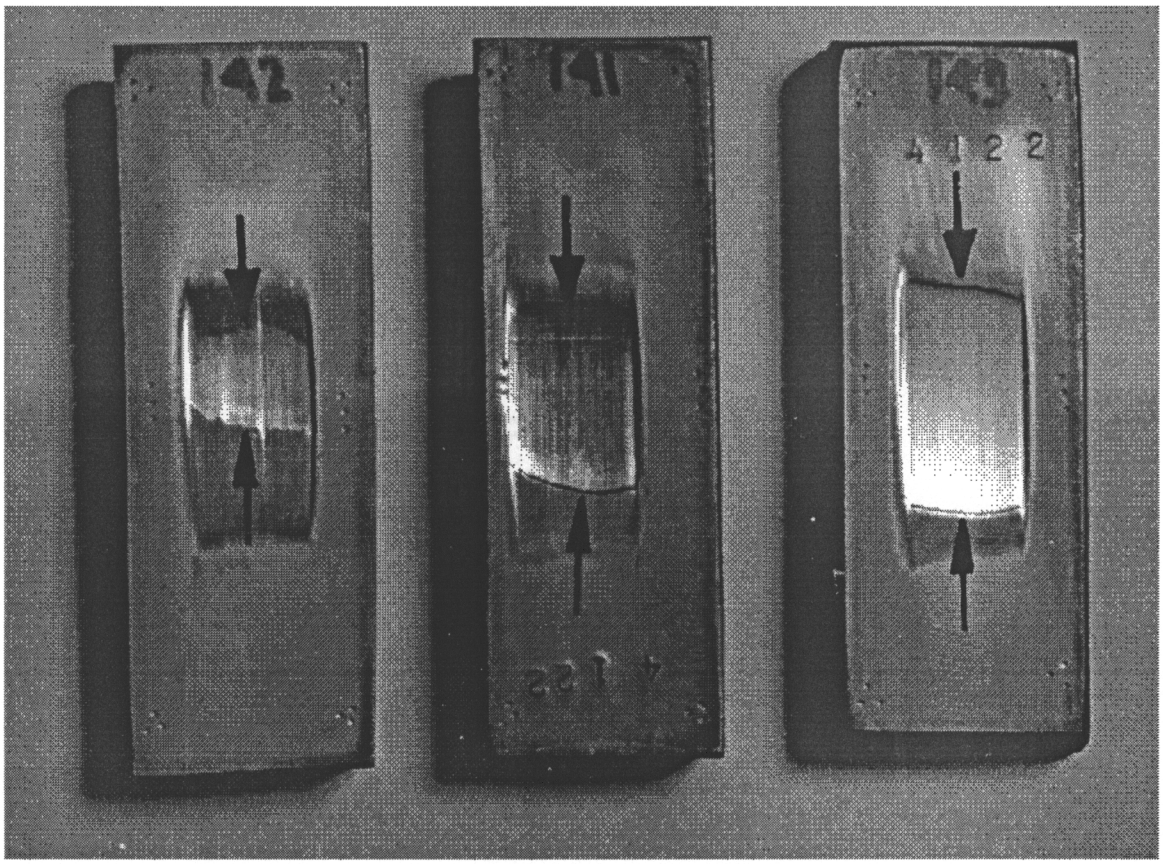

Figure 22: Interrupted test samples showing movement of the wear scar with test duration.

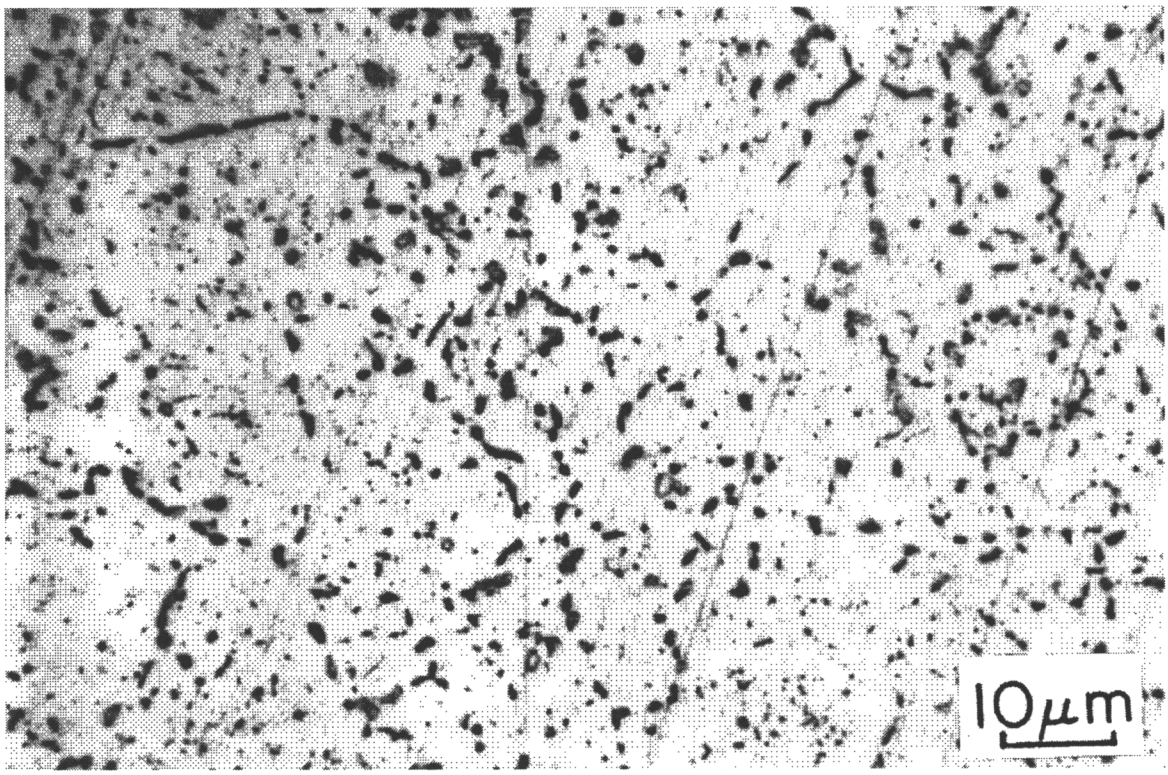

Figure 23: Microstructure of Thyssen 4122.

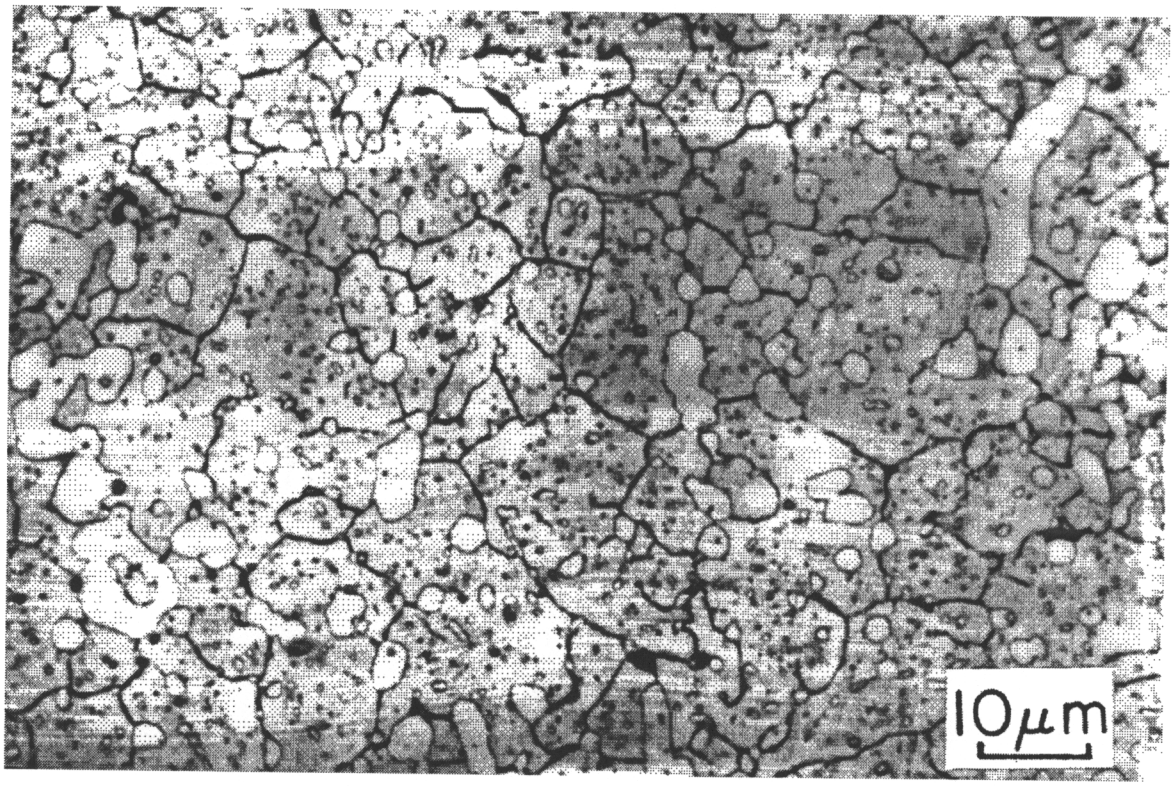

Figure 24: Microstructure of D-2 tool steel.

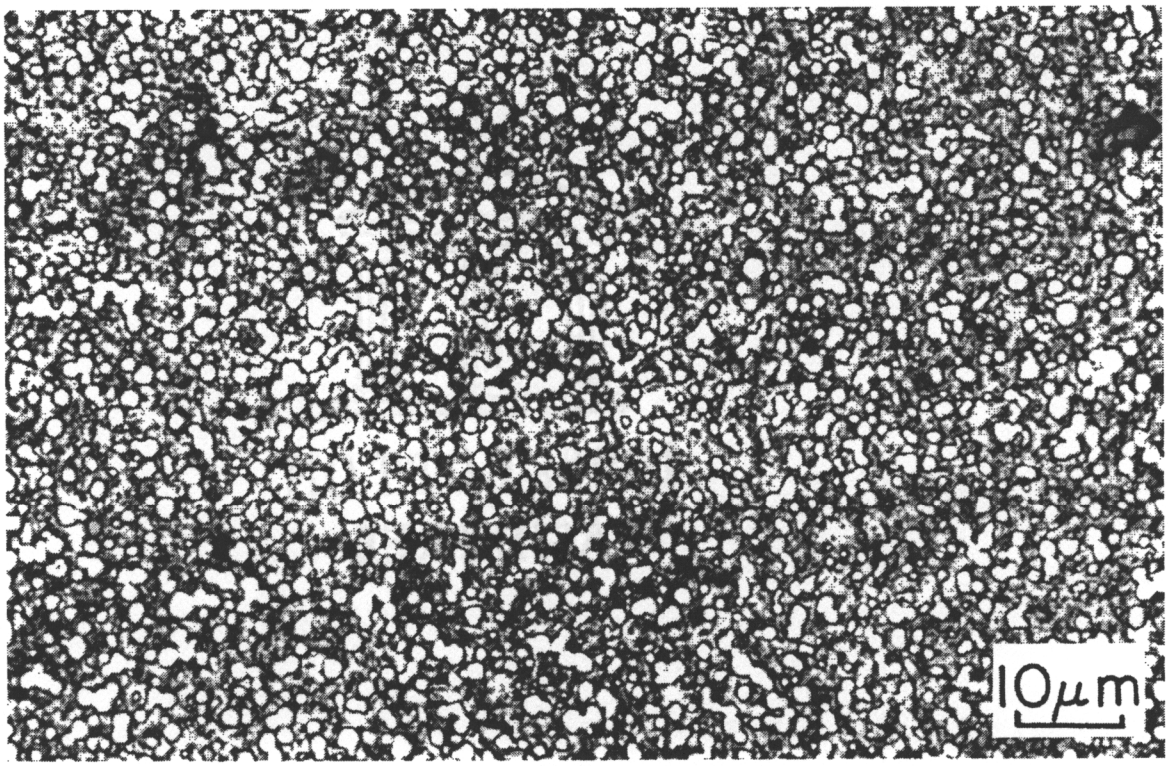

Figure 25: Microstructure of CPM10V.

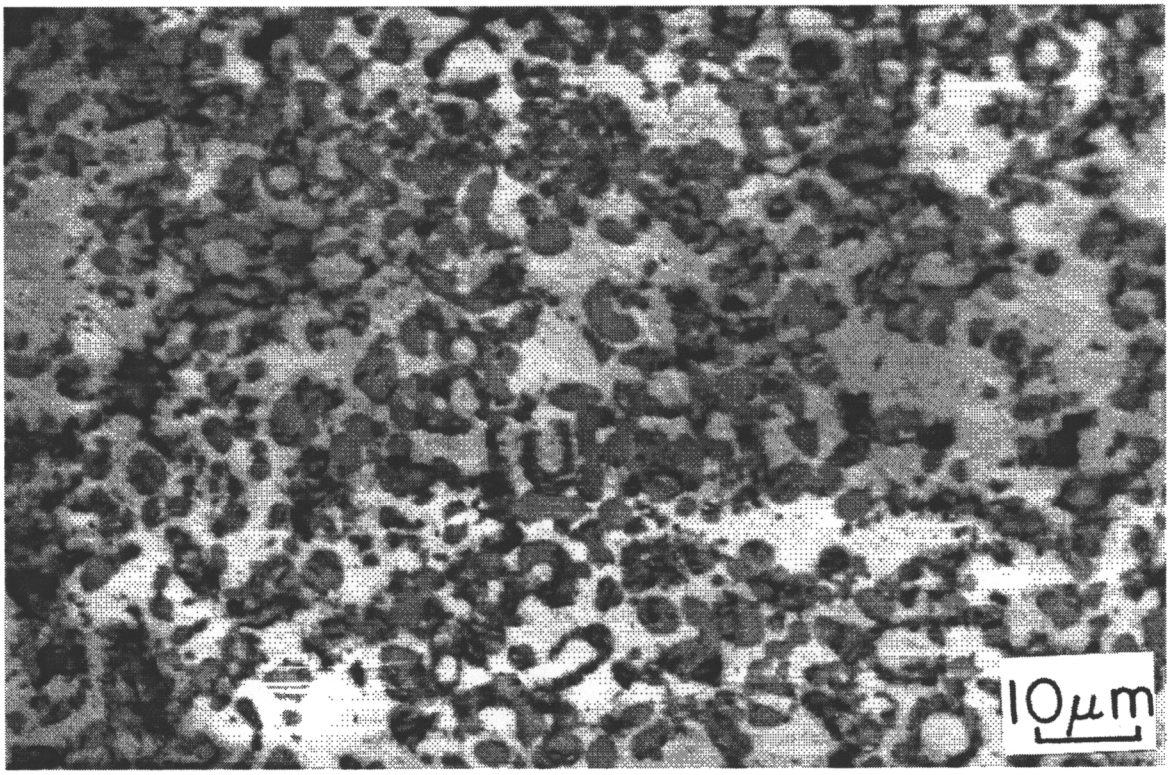

Figure 26: Microstructure of FerroTiC CM45.

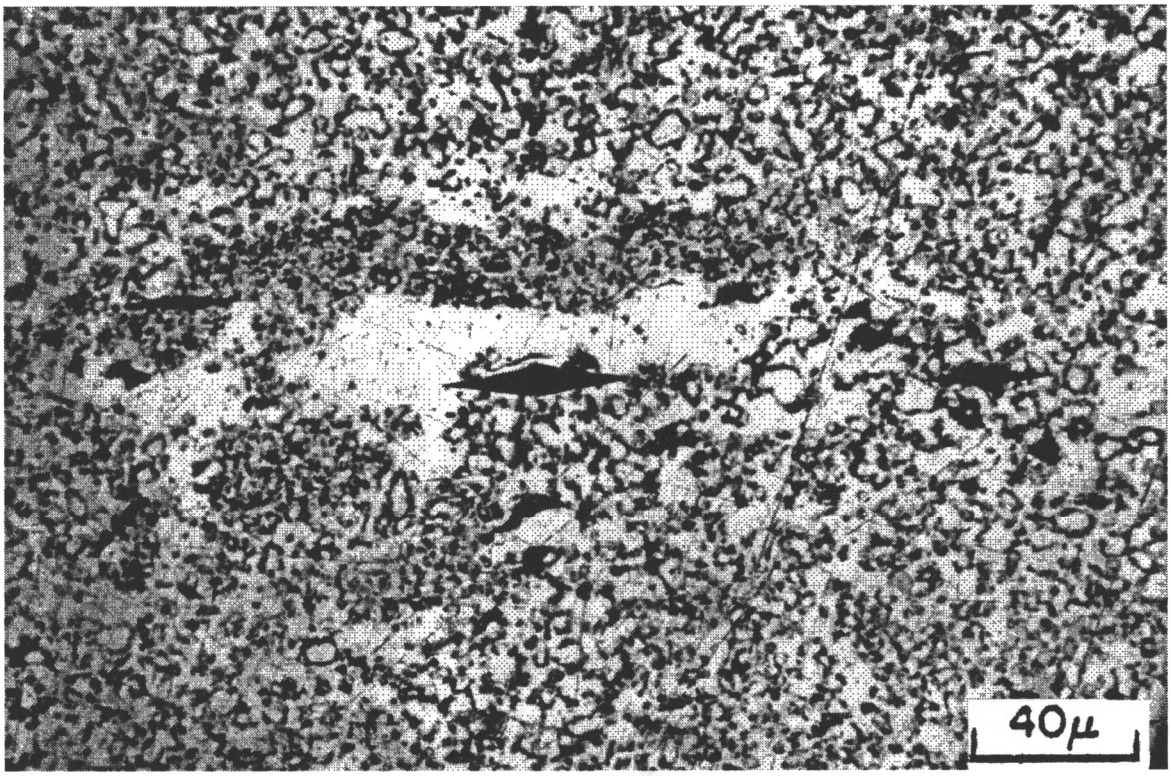

Figure 27: Nonuniform distribution of titanium carbides in FerroTiC CM45.

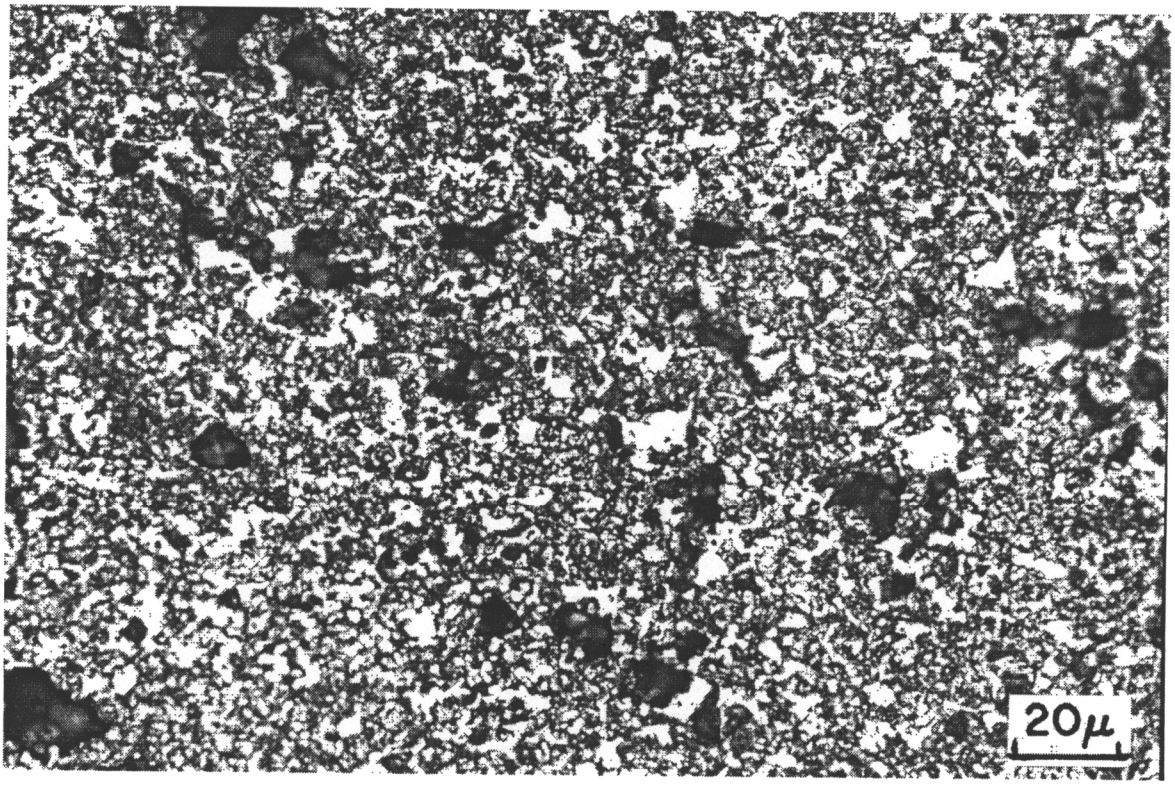

Figure 28: Microstructure of FerroTiC CM25.

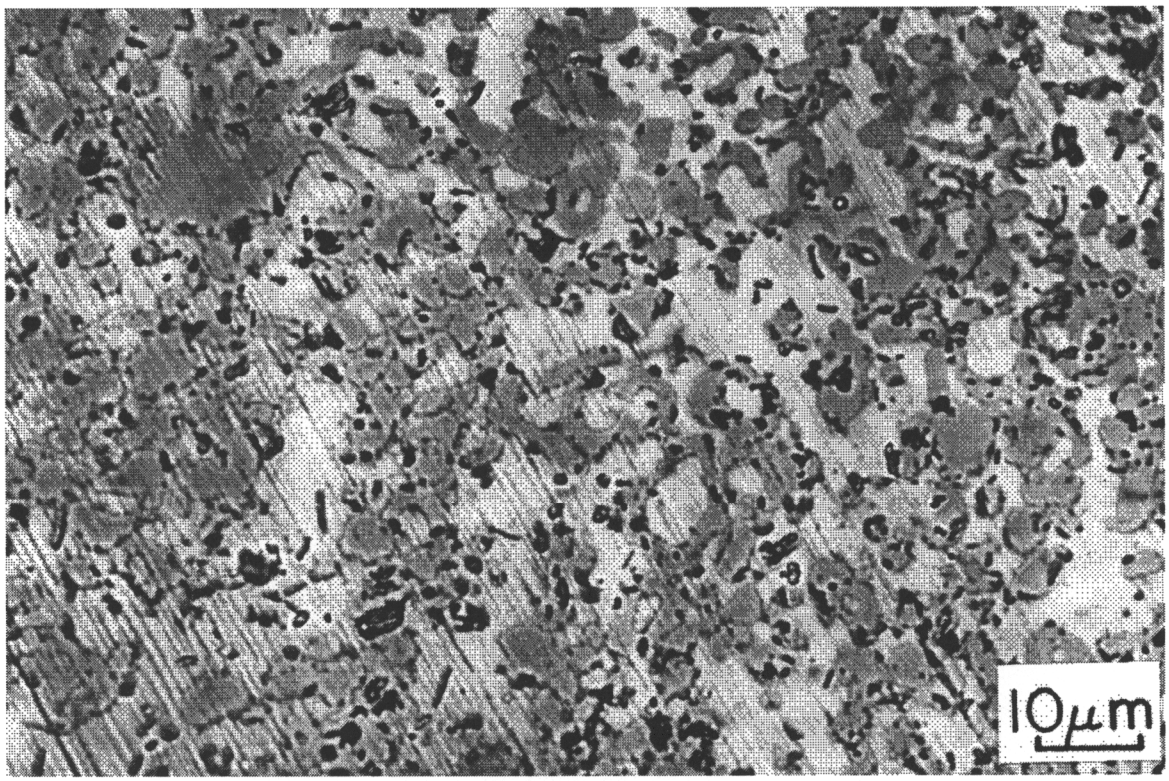

Figure 29: Microstructure of Ferrotitanit.

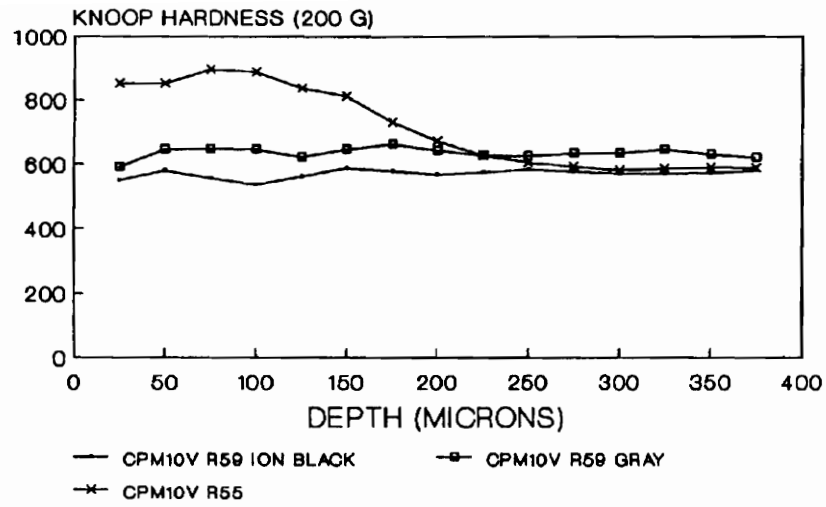

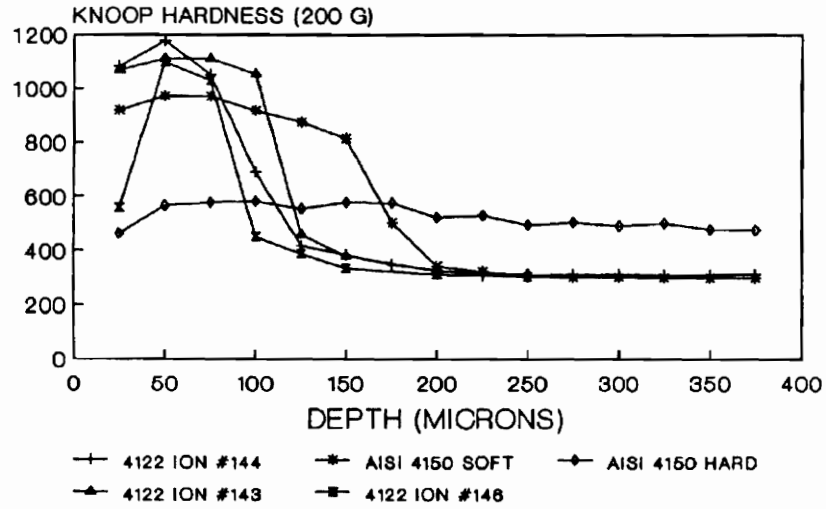

Figure 30: Microhardness versus depth profiles for ion nitrided samples.

Figure 31: Typical surface appearance of Thyssen 4122 ion nitrided samples.

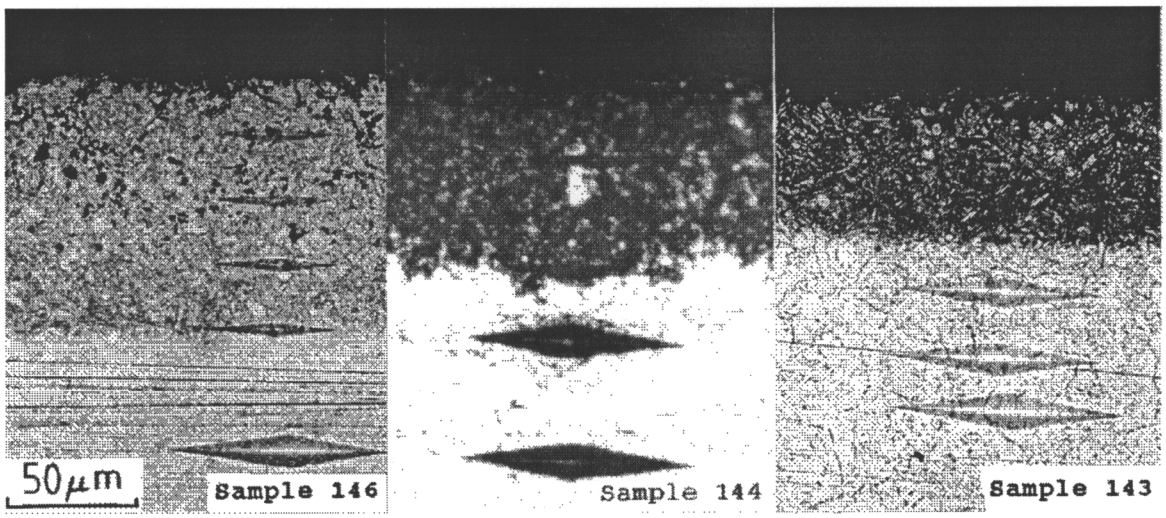

Figure 32: Variations in nitride layer thickness on Thyssen 4122.

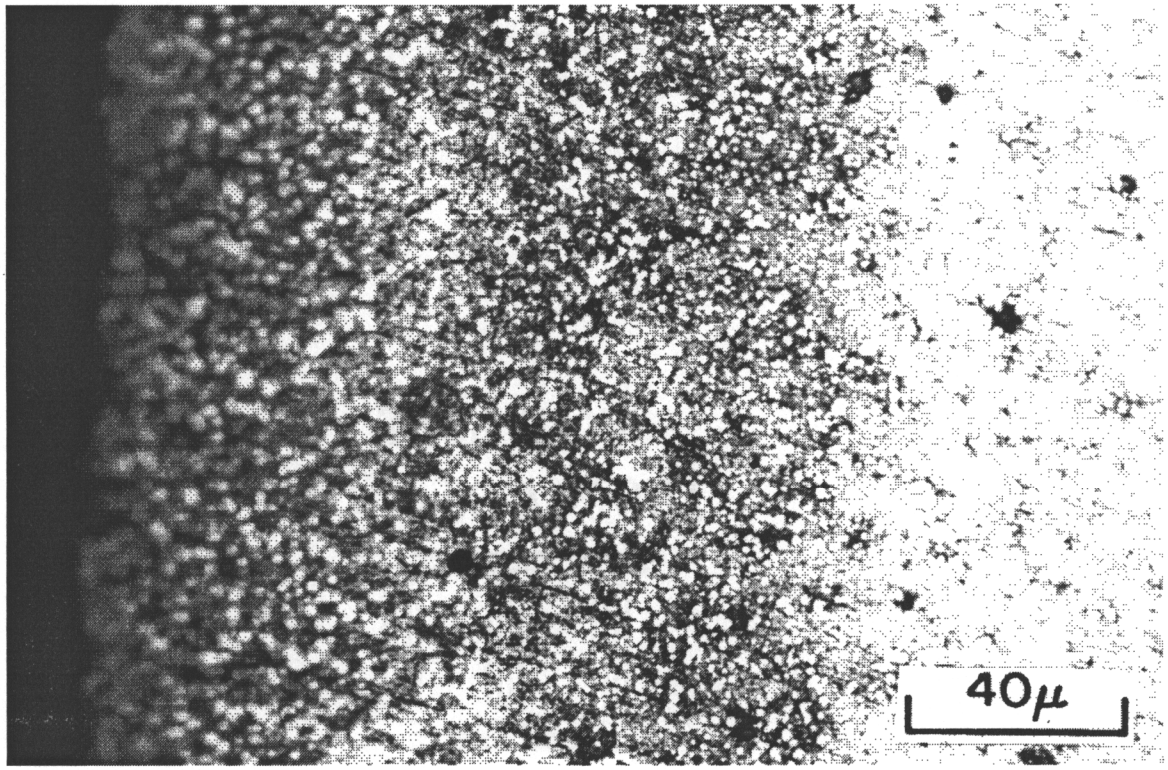

Figure 33: Ion nitride layer on CPM10V RC 55 samples.

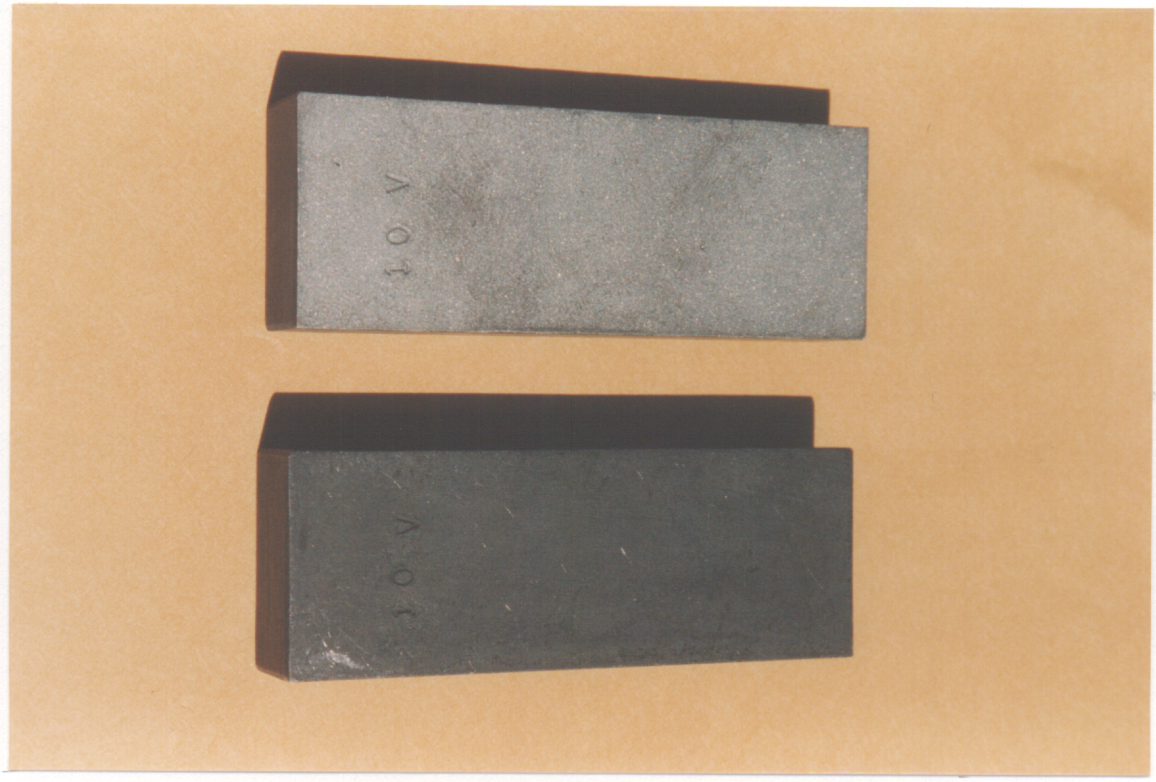

Figure 34: Two different surface appearances of the ion nitrided CPM10V RC 59 samples.

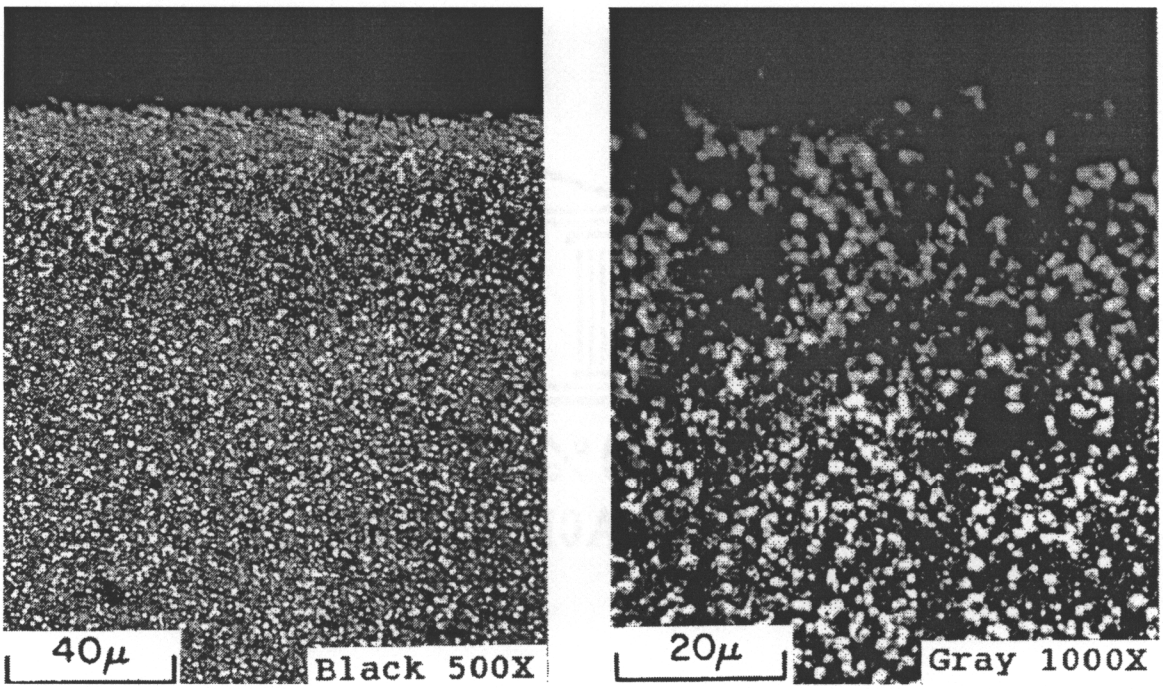

Figure 35: Microstructures of the gray and black ion nitrided CPM10V RC 59 samples showing lack of nitride layer on the gray sample and thin layer on the black sample.

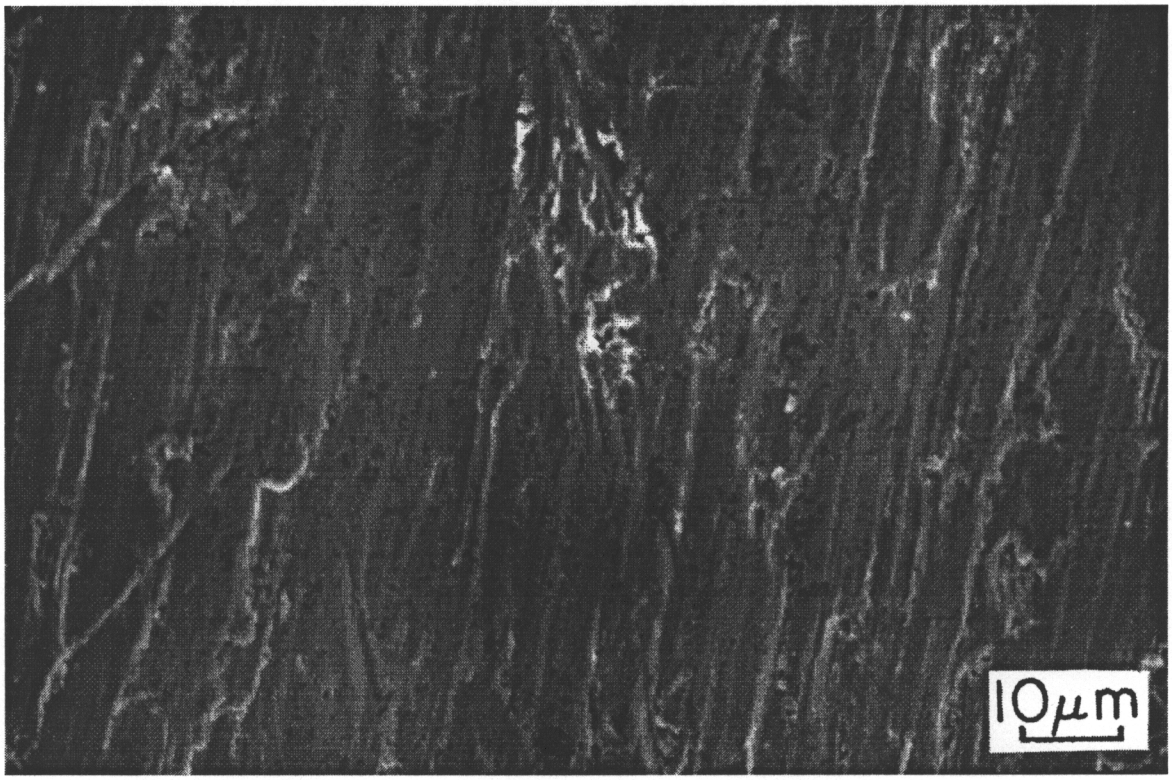

Figure 36: Wear scar on Thyssen 4122.

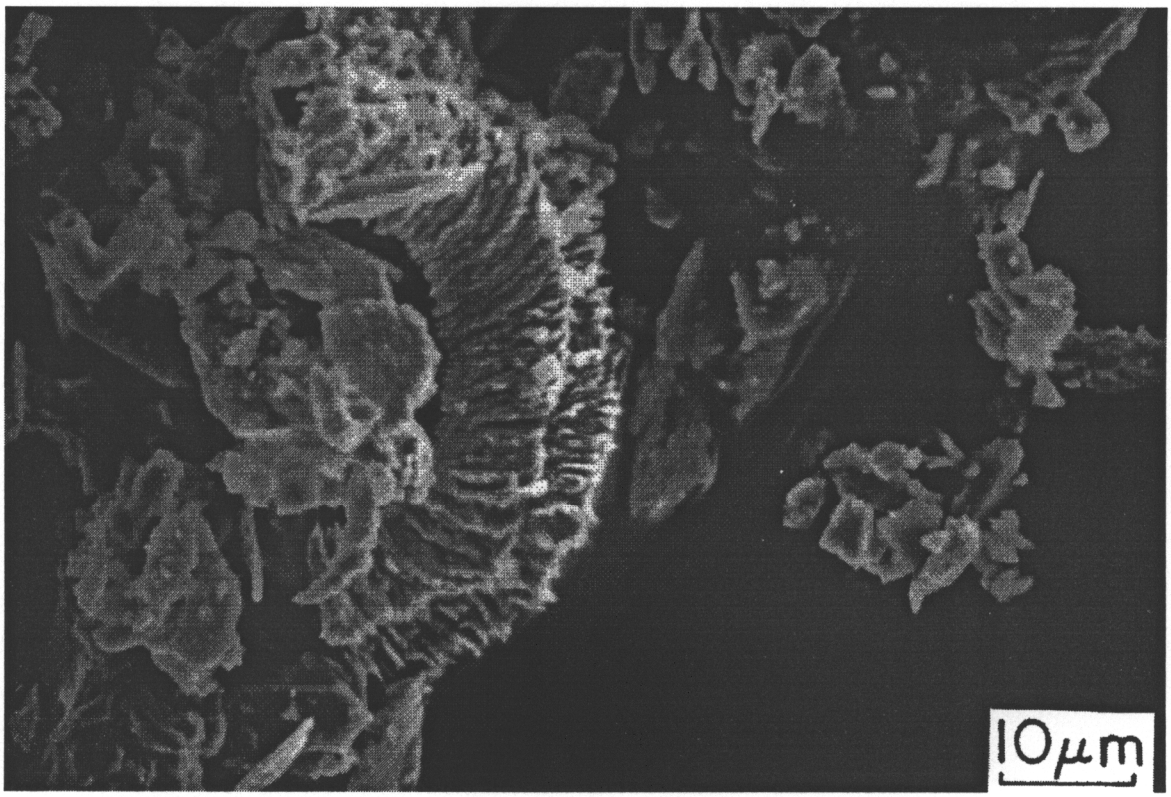

Figure 37: Microchip wear debris from Thyssen 4122.

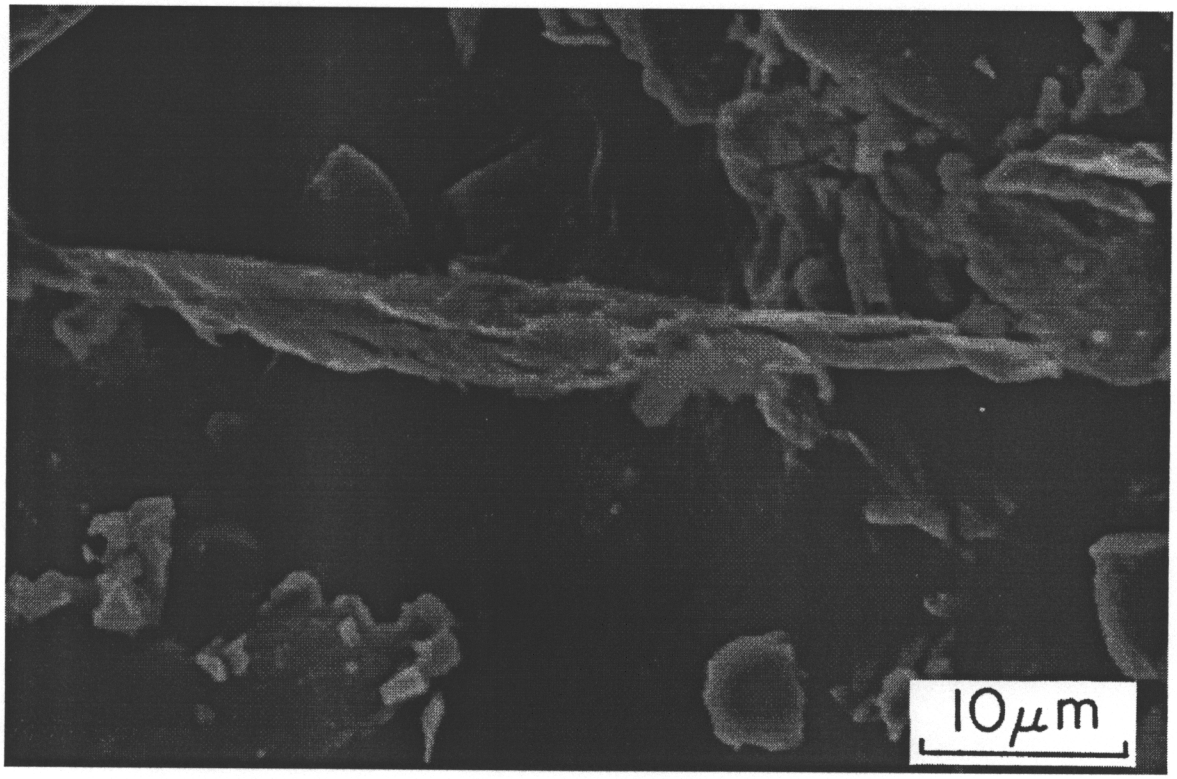

Figure 38: Acicular plowing wear debris from Thyssen 4122.

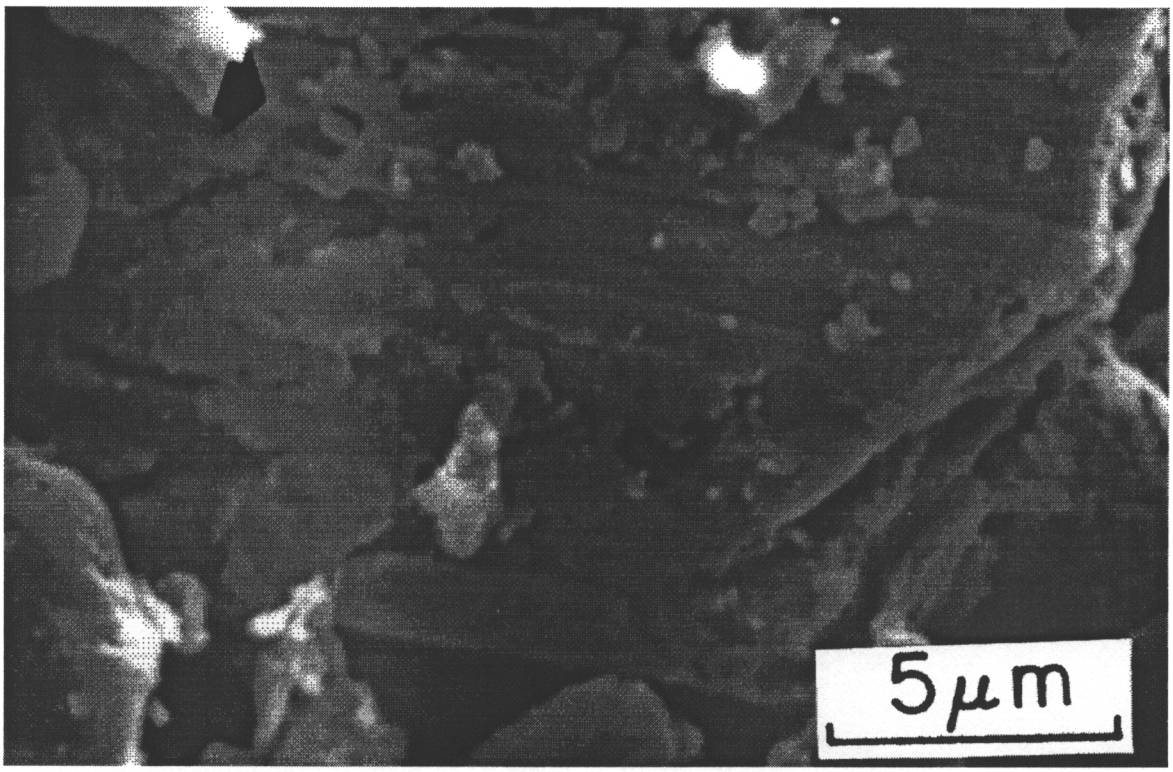

Figure 39: Sand grain fragment with transferred metal.

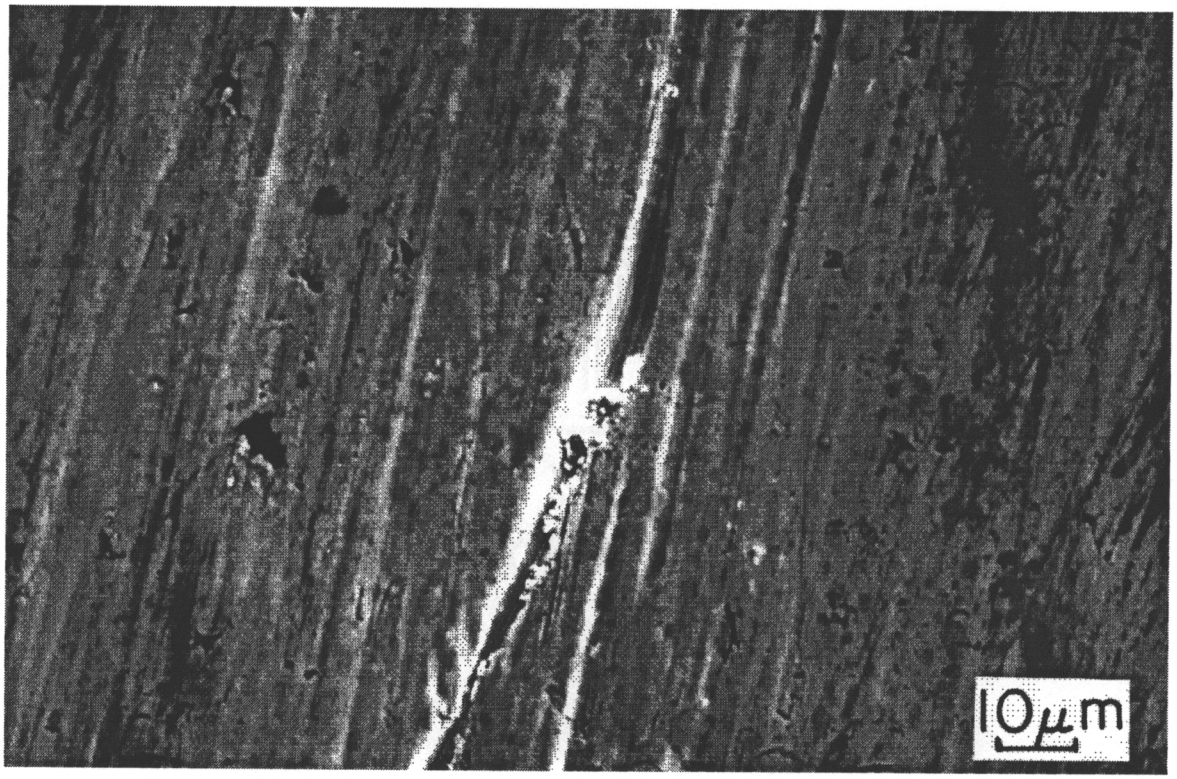

Figure 40: Wear scar on D-2 tool steel. Debris at bend in scratch contains silica and may indicate fracture of a sand grain.

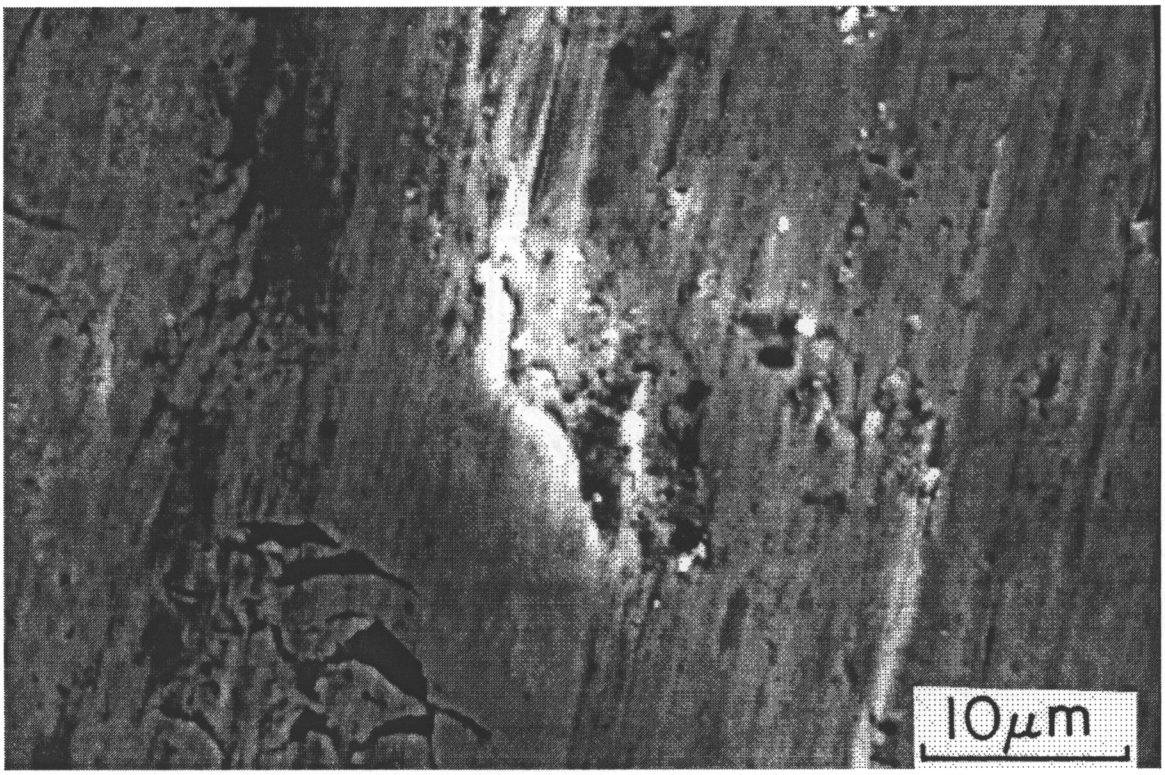

Figure 41: Ridge of plowed metal on a D-2 wear scar showing transverse cracks.

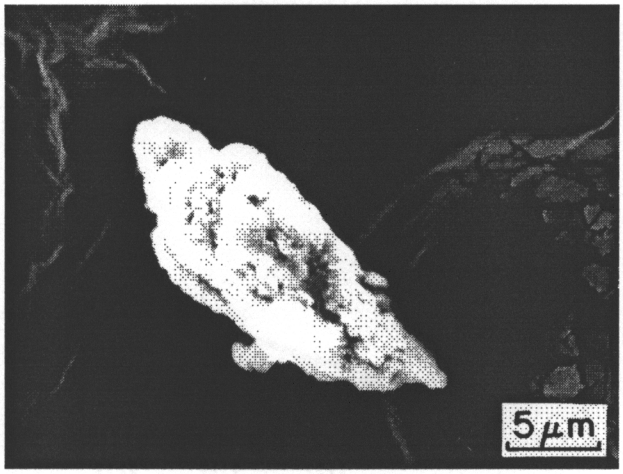

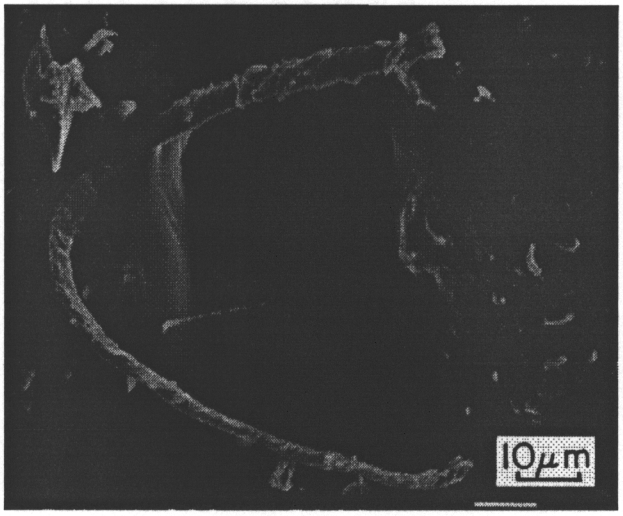

Figure 42: D-2 wear debris containing microchips and cigar shaped particles.

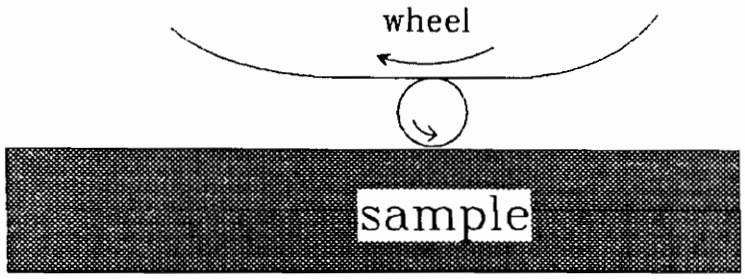

(a)

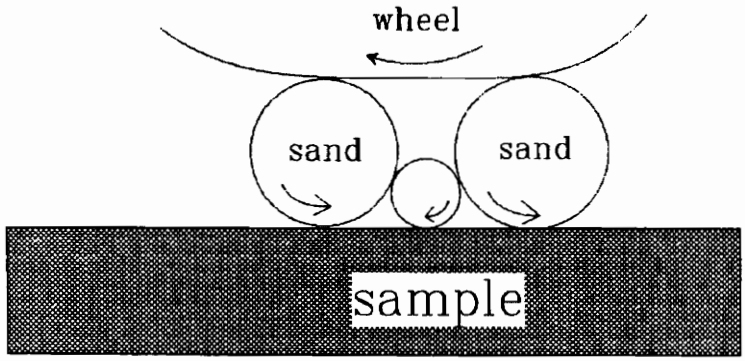

(b)

Figure 43: Mechanisms for formation of cigar shaped particles.

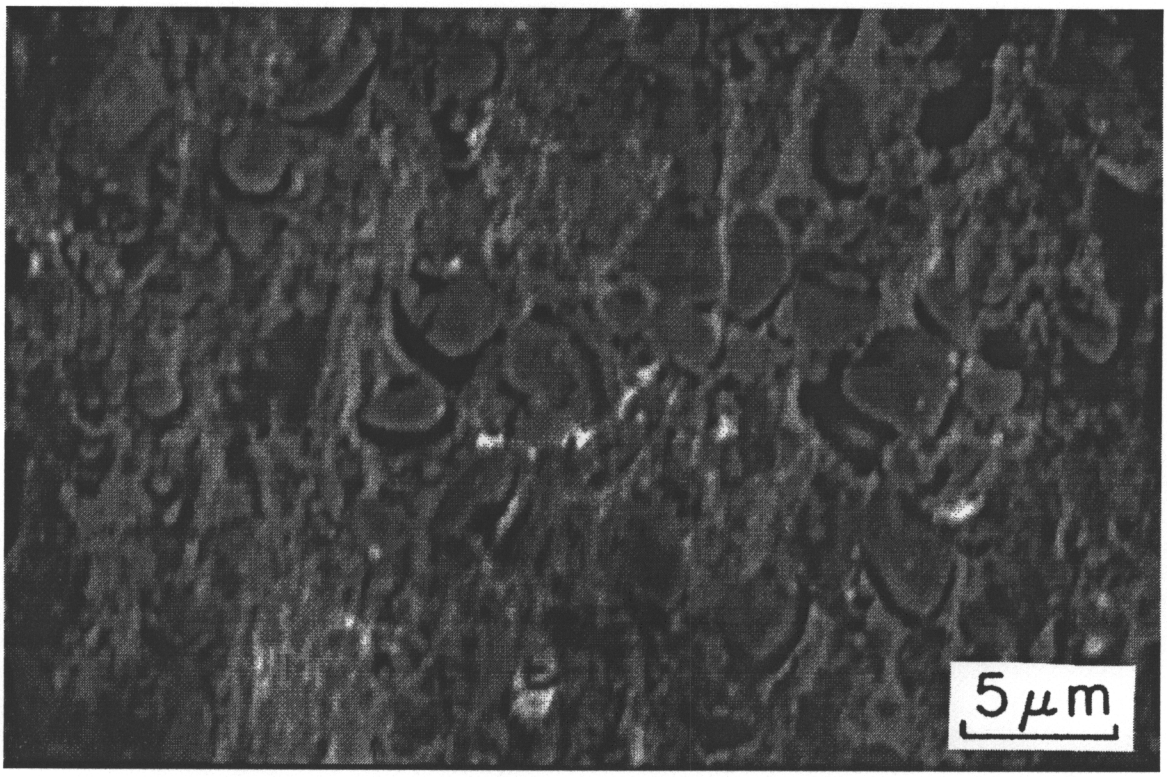

Figure 44: Wear scar on FerroTiC CM45 showing exposed titanium carbides shifted in the matrix.

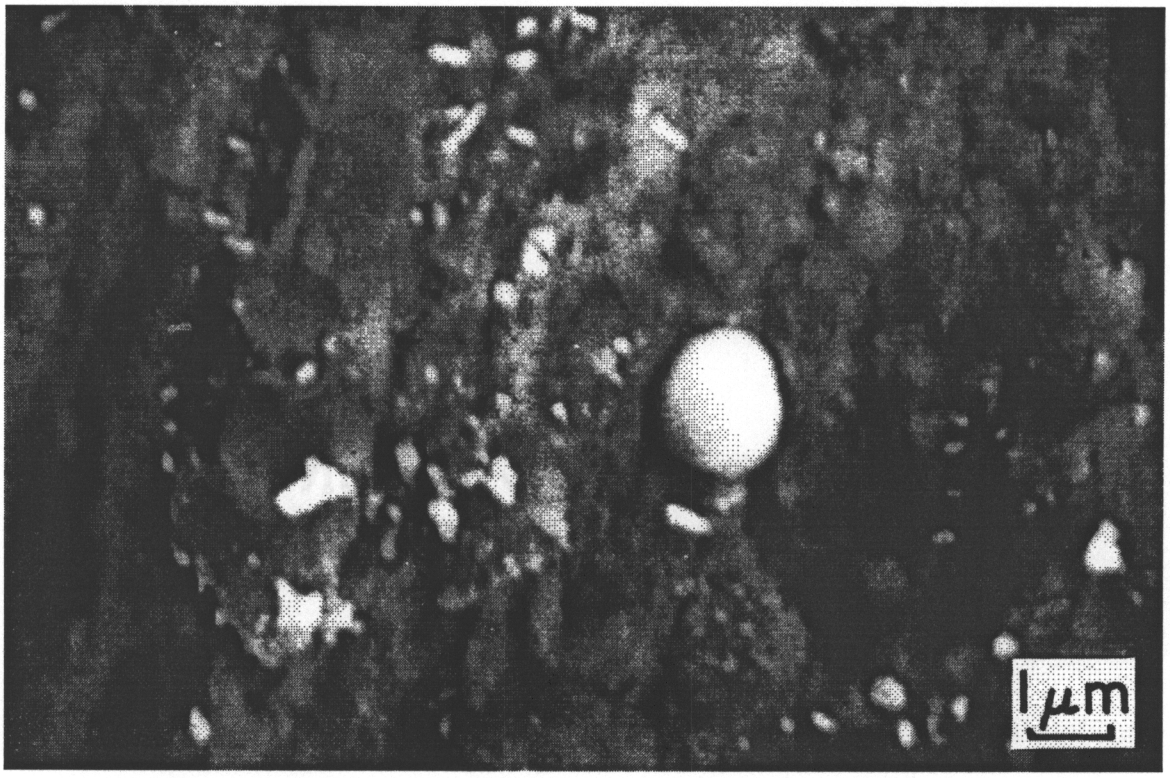

Figure 45: Wear sheet detaching from FerroTiC CM45 wear scar.

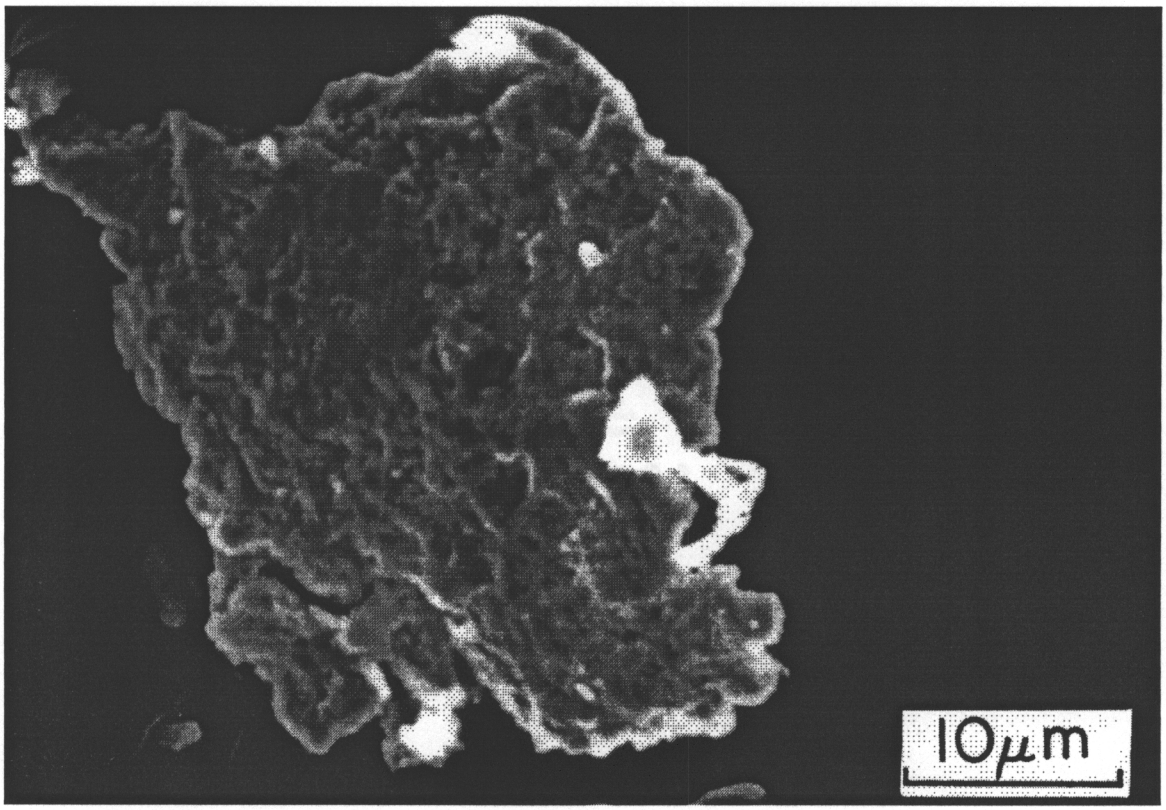

Figure 46: Plate shaped particles in wear debris from FerroTiC CM45.

Figure 47: Microchip type particles in wear debris from FerroTiC CM45.

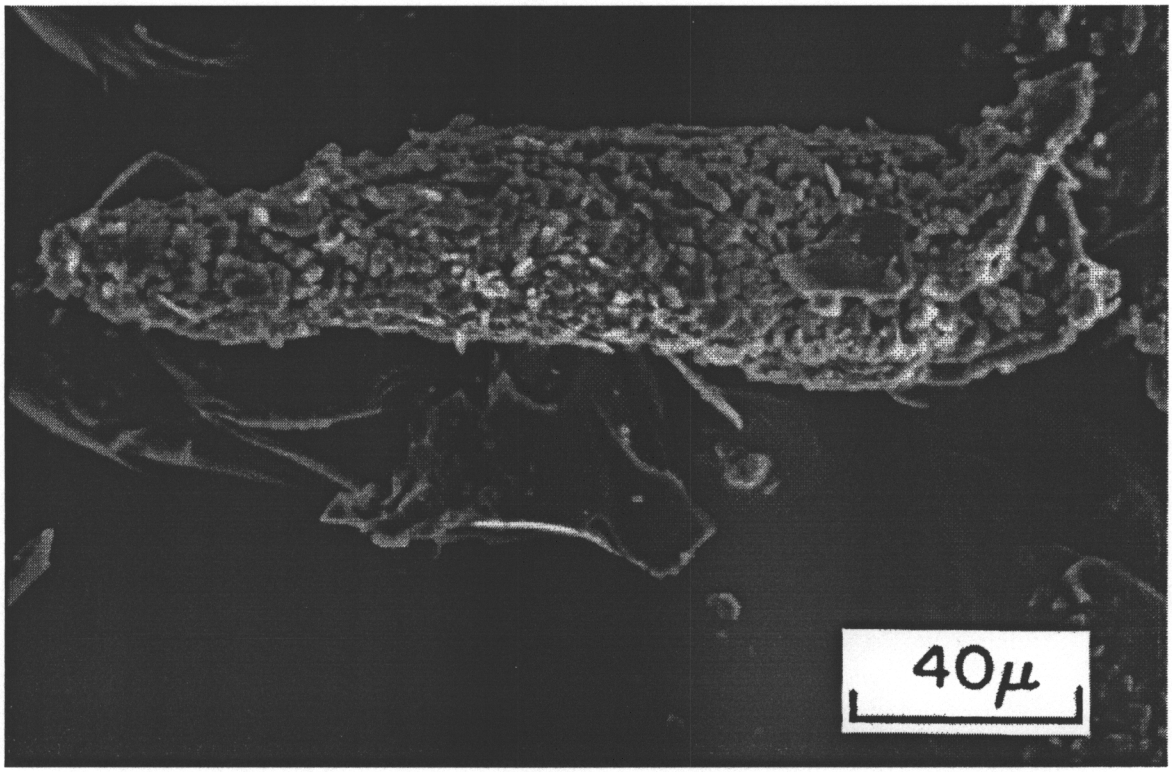

Figure 48: Cigar shaped particle in wear debris from FerroTiC CM45.

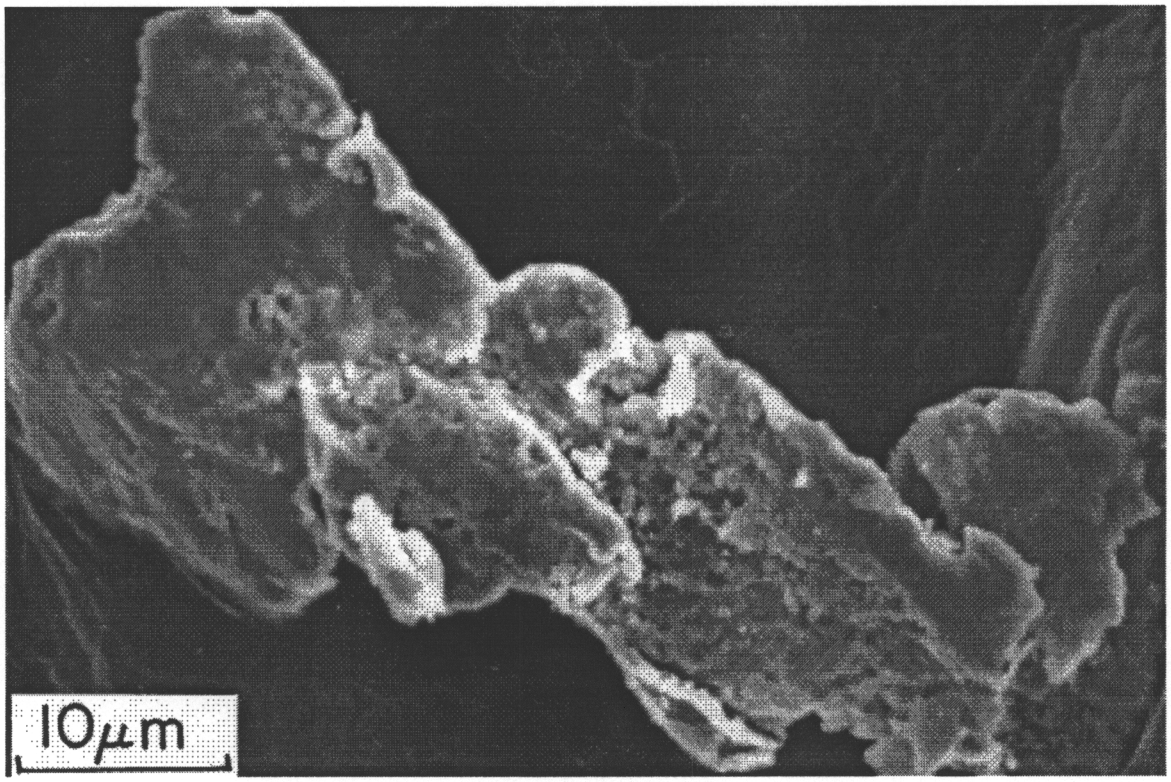

Figure 49: FerroTiC CM45 plate type wear particle becoming rounded into a cigar shaped particle.

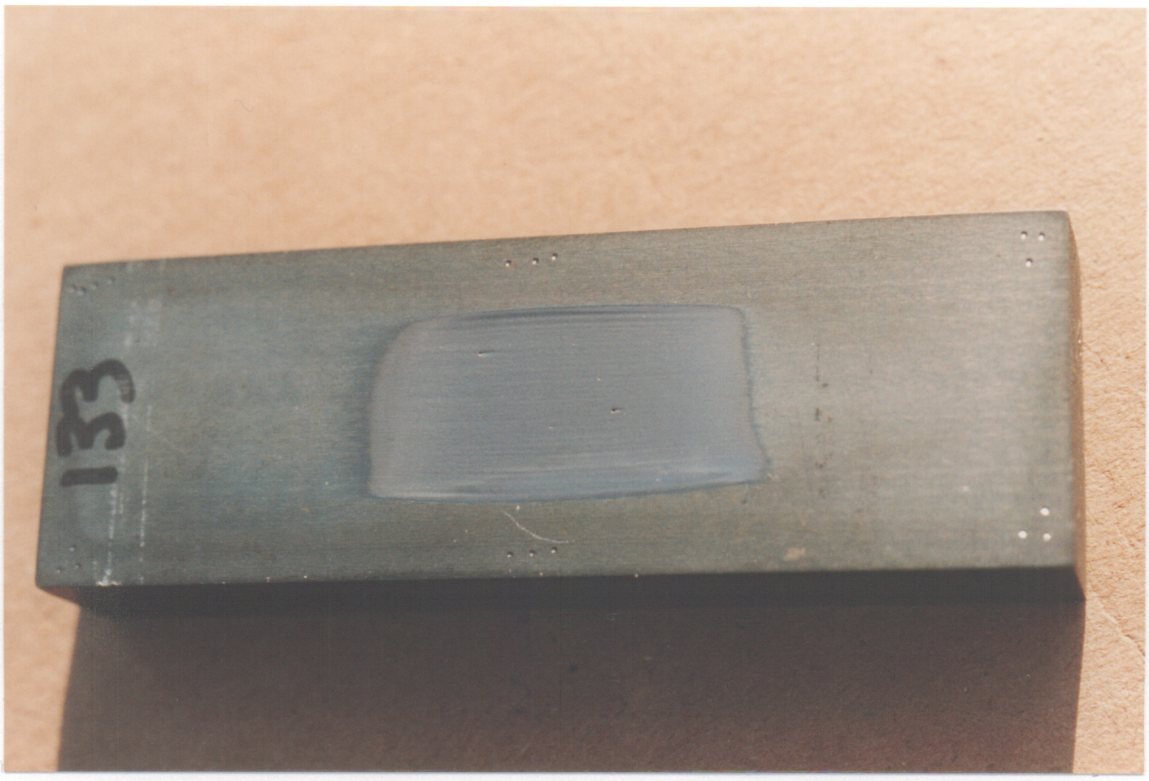

Figure 50: Macrograph of FerroTiC CM25 wear scar showing pits and striations.

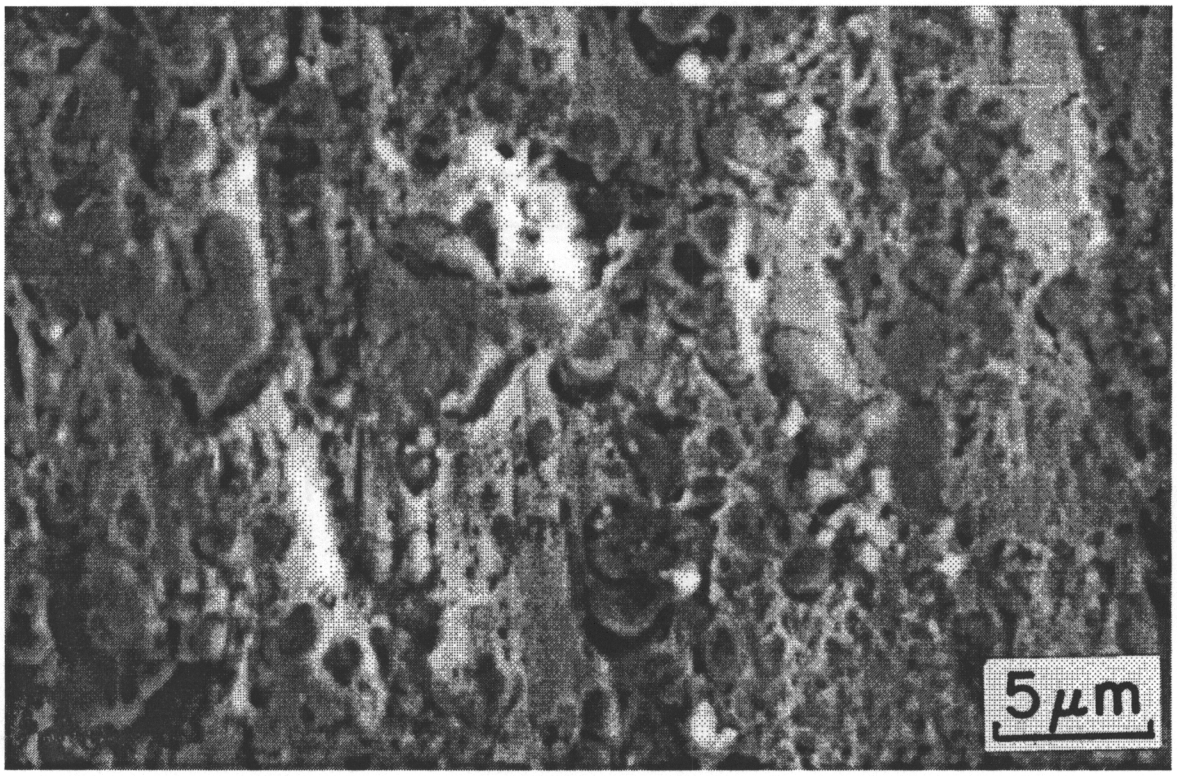

Figure 51: Wear scar on FerroTiC CM25.

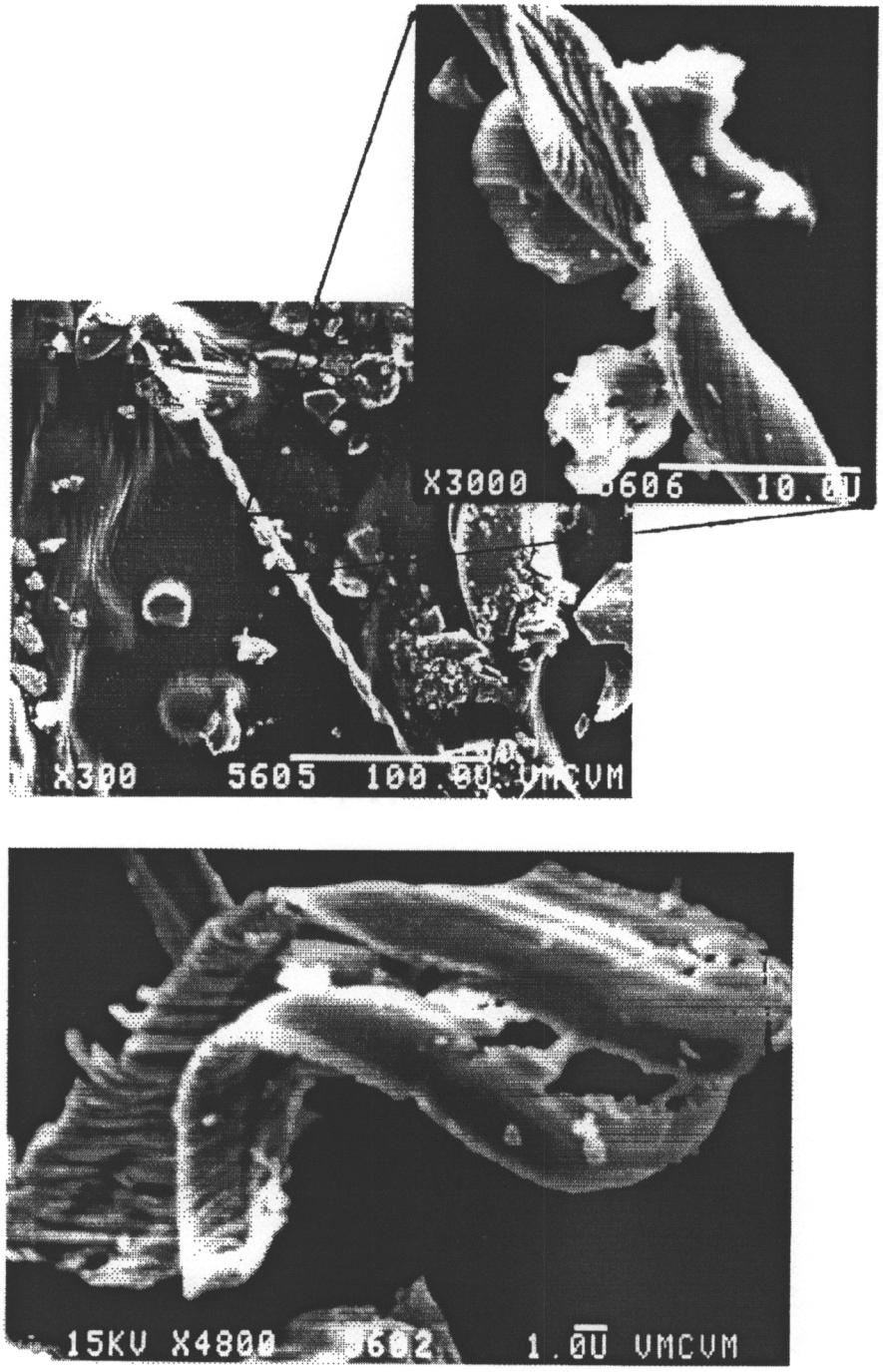

Figure 52: Microchips in wear debris from FerroTiC CM25.

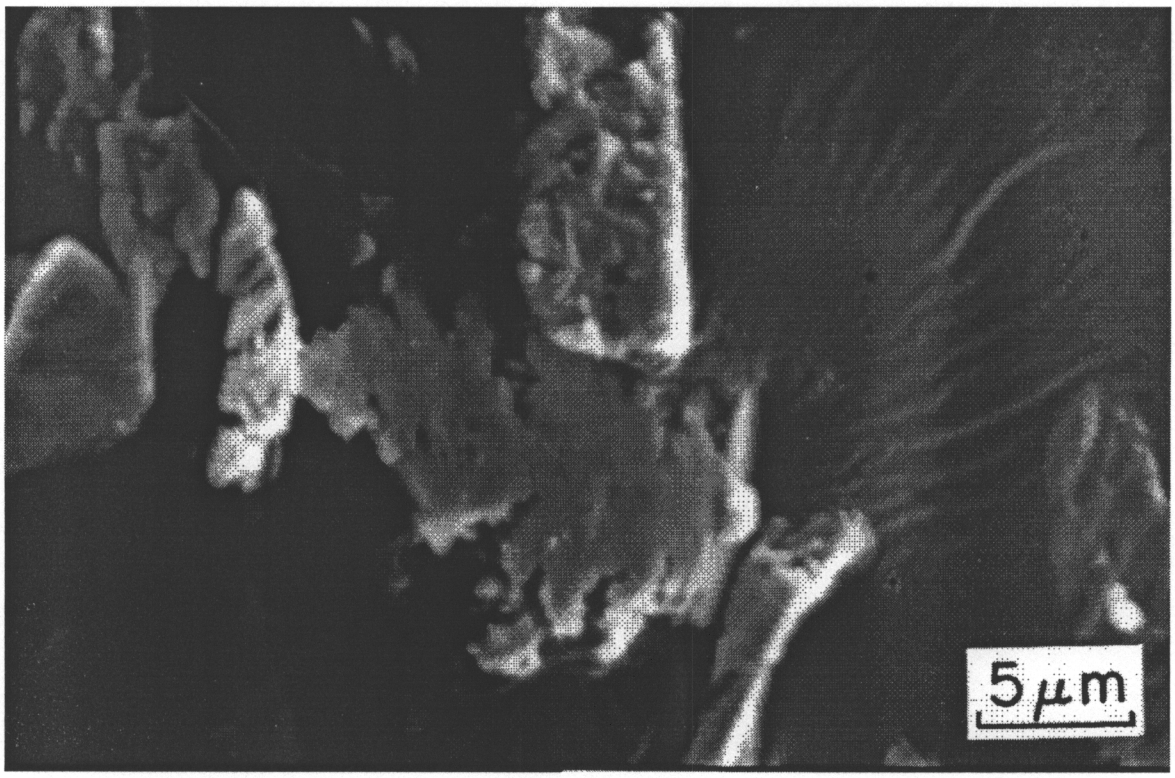

Figure 53: Plate type wear debris from FerroTiC CM25.

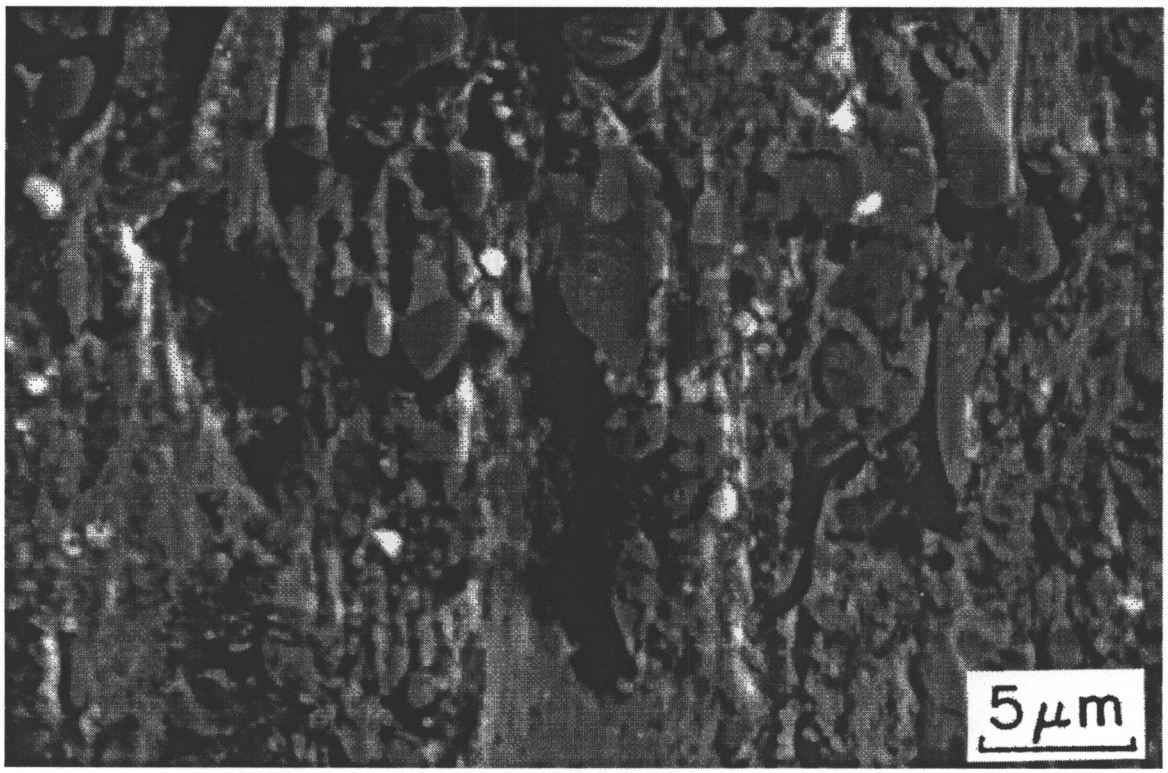

Figure 54: Wear scar on Ferrotitanit. Note cracks in surface.

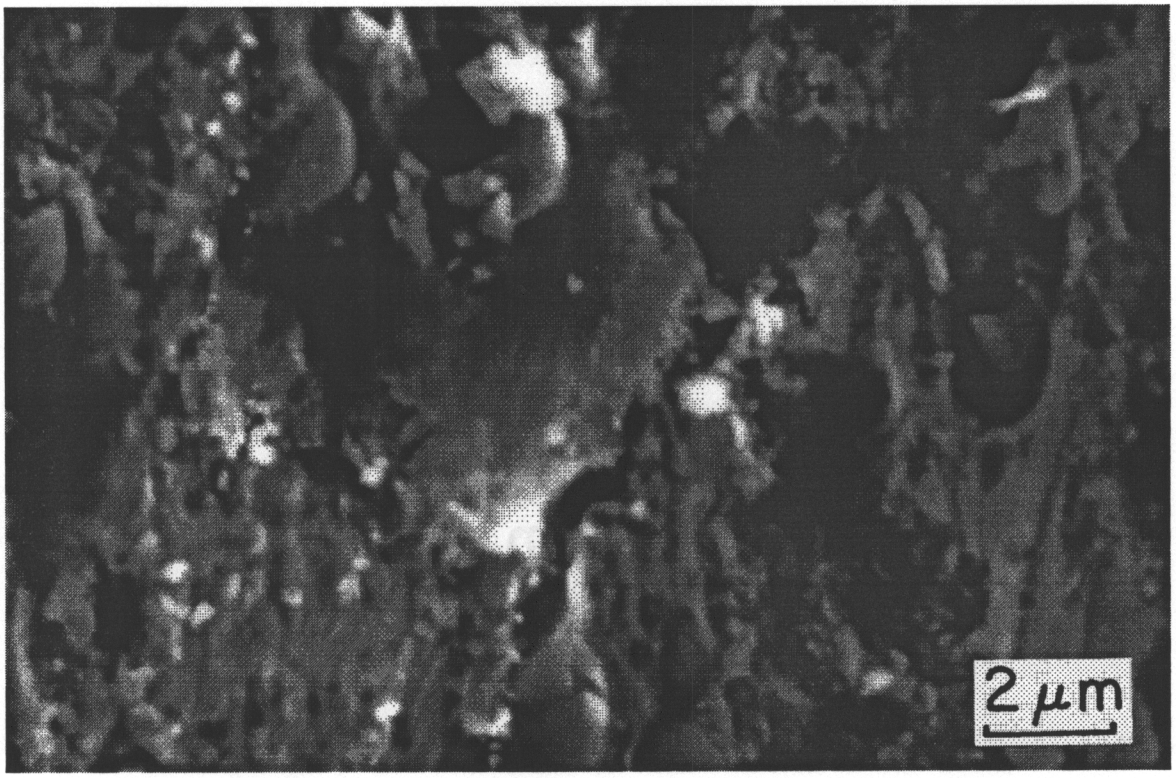

Figure 55: Loosely attached wear sheet on Ferrotitanit.

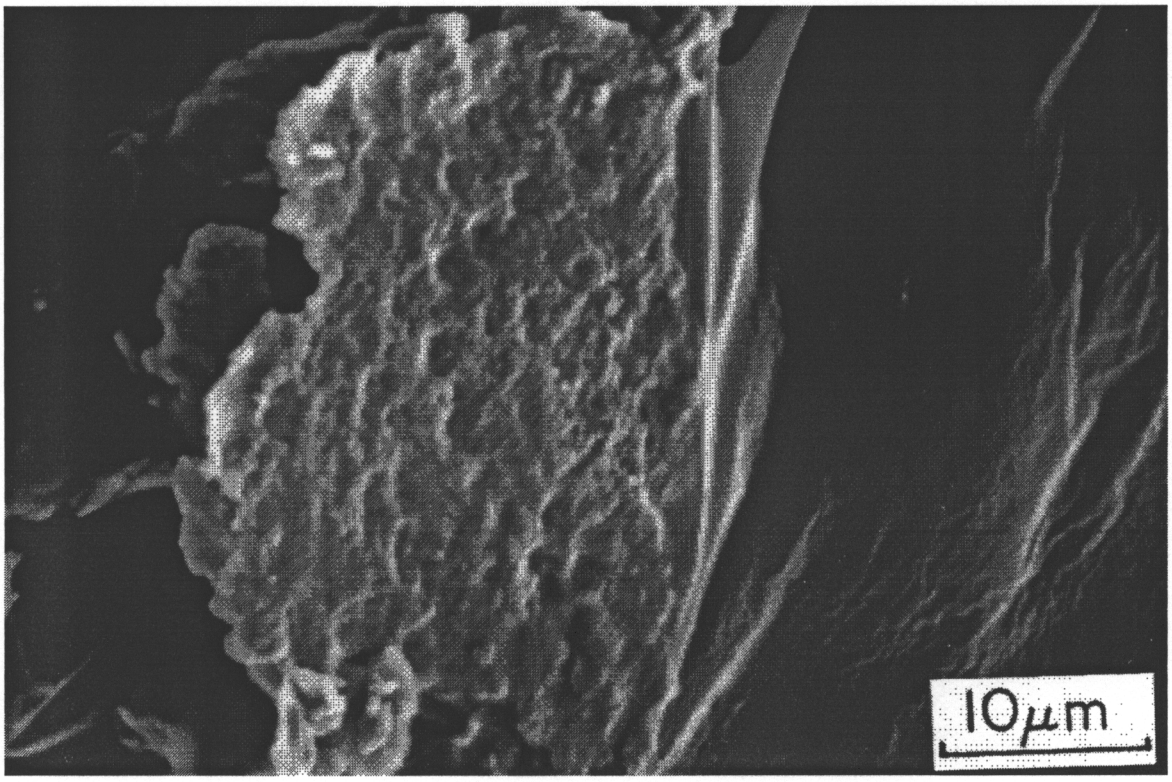

Figure 56: Sheet or plate type wear particles typical of Ferrotitanit.

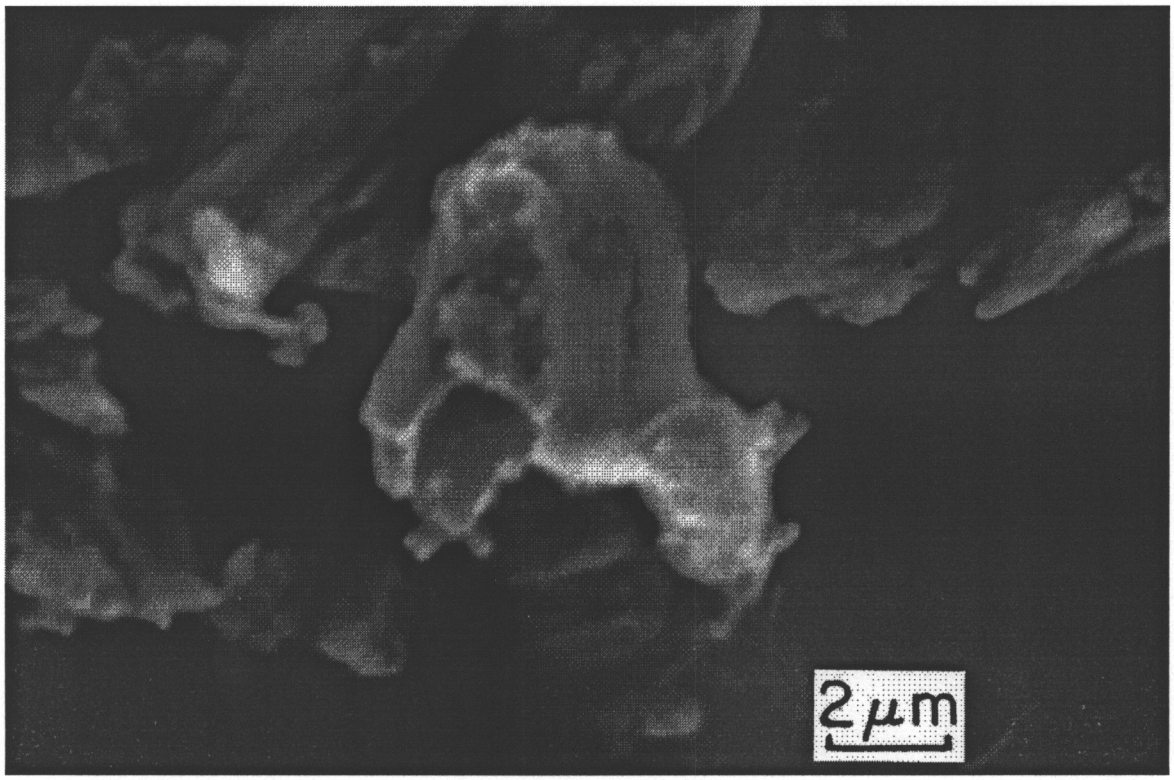

Figure 57: Small microchip containing a titanium carbide particle found in the wear debris from Ferrotitanit.

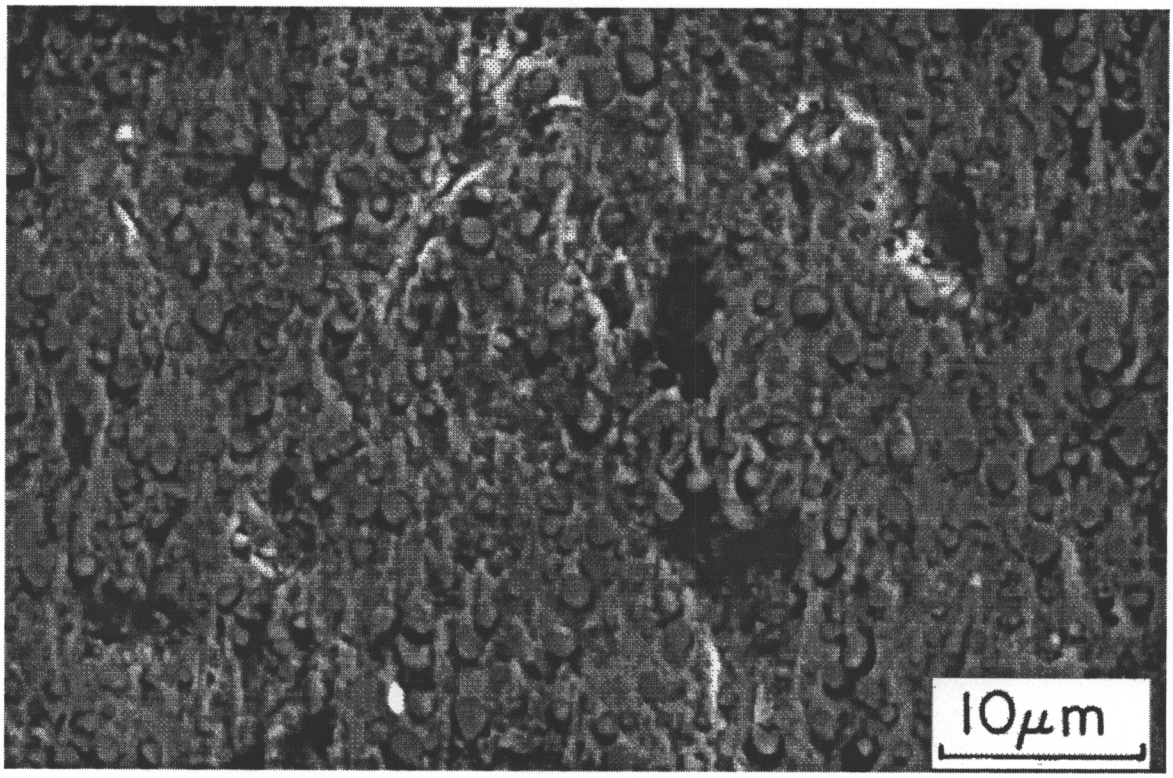

Figure 58: Pits in wear scar of CPM10V RC 55.

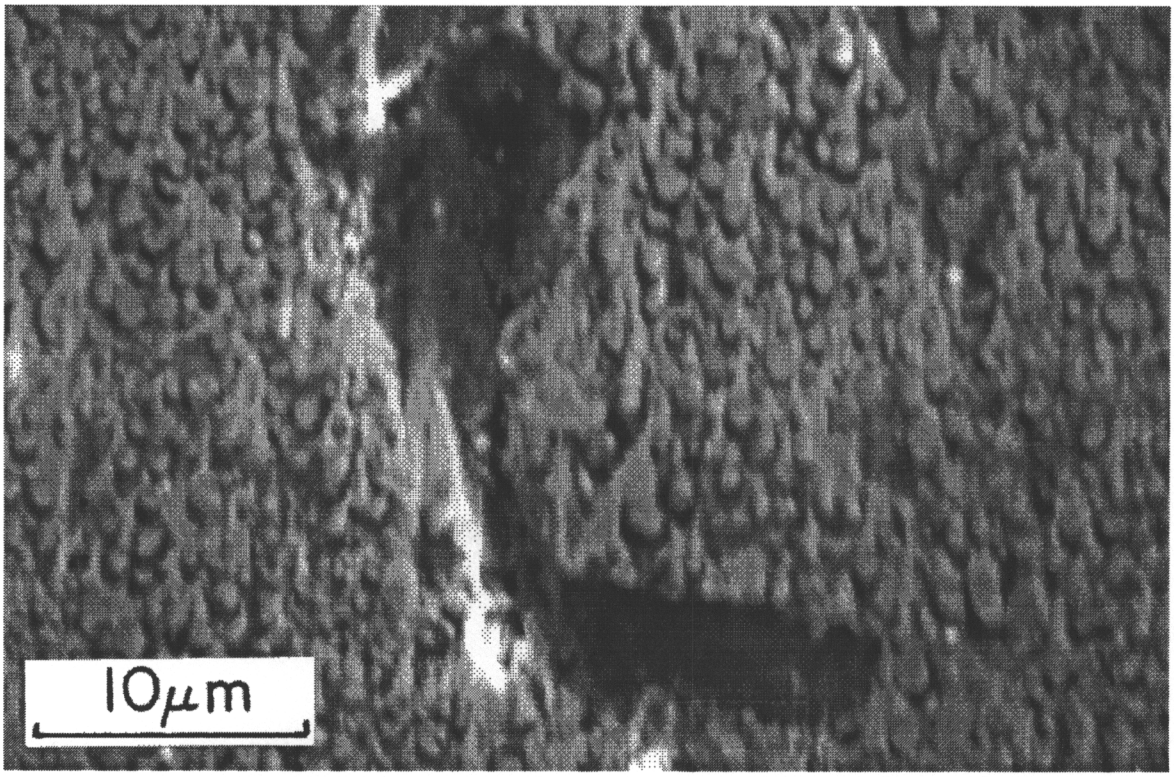

Figure 59: CPM10V RC 59 wear scar.

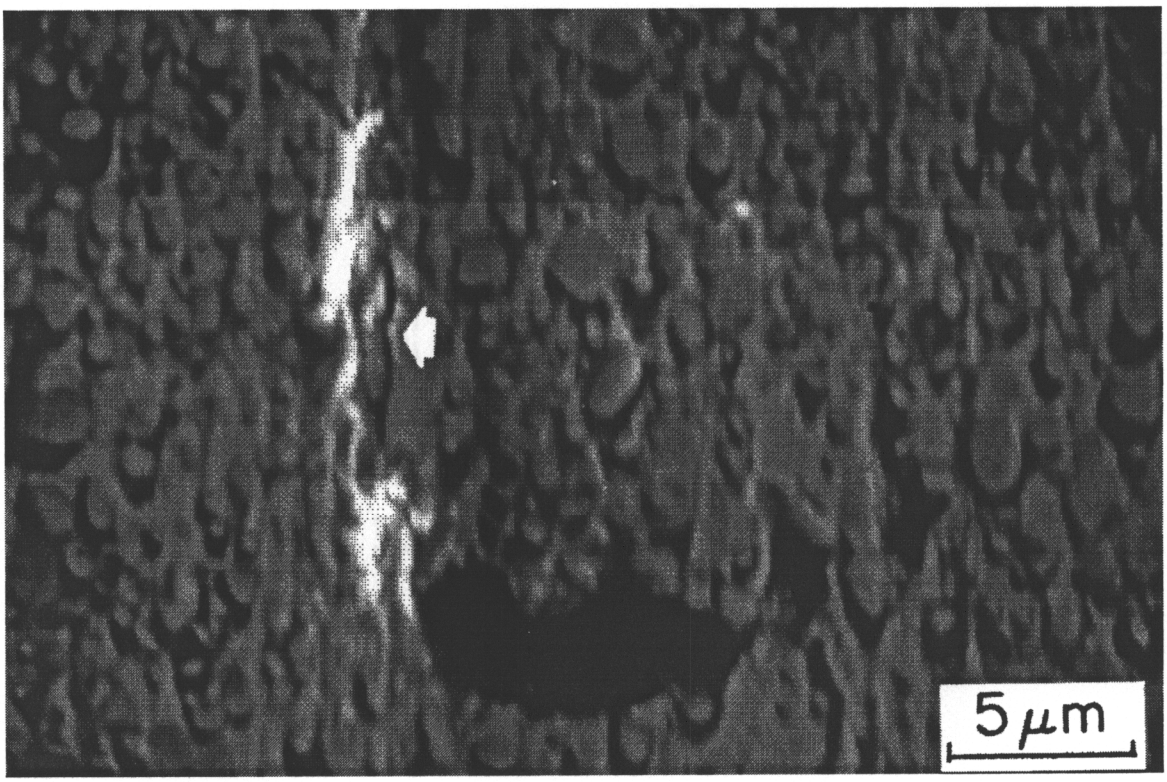

Figure 60: Crack in bottom of "L" shaped pit in CPM10V RC 59 (arrow).

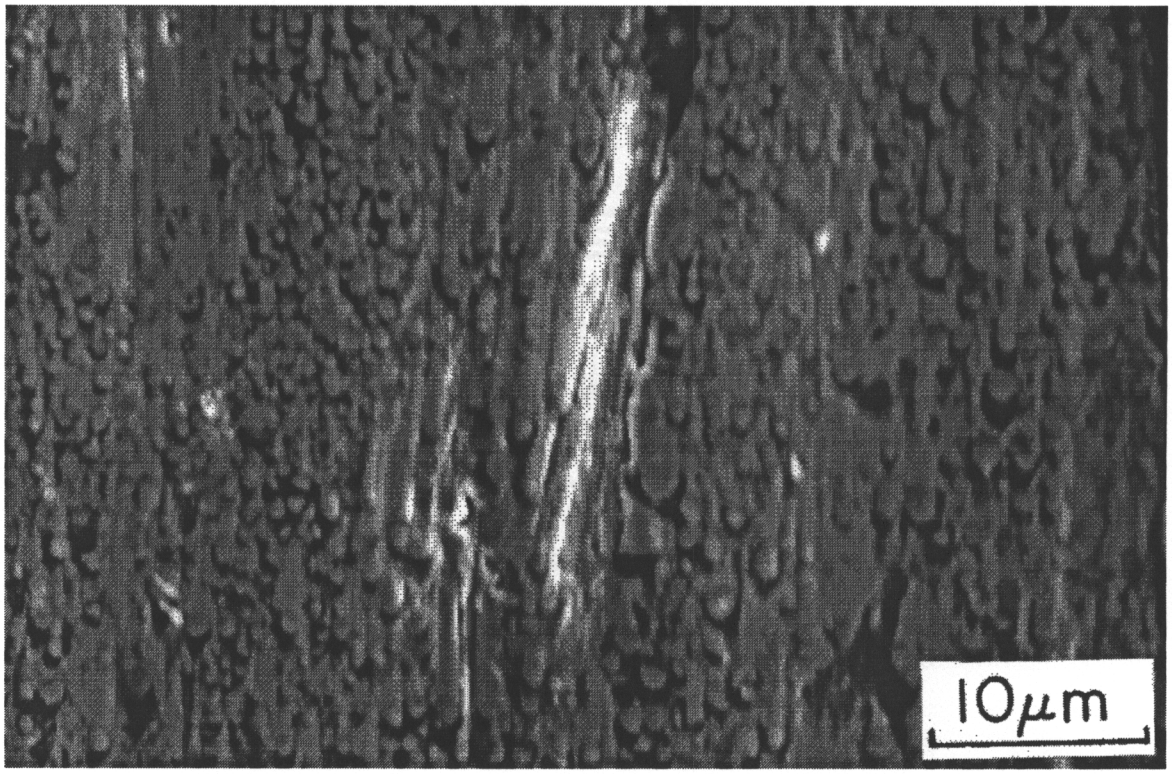

Figure 61: Large gouge in wear scar of CPM10V RC 59 with longitudinal crack at right edge.

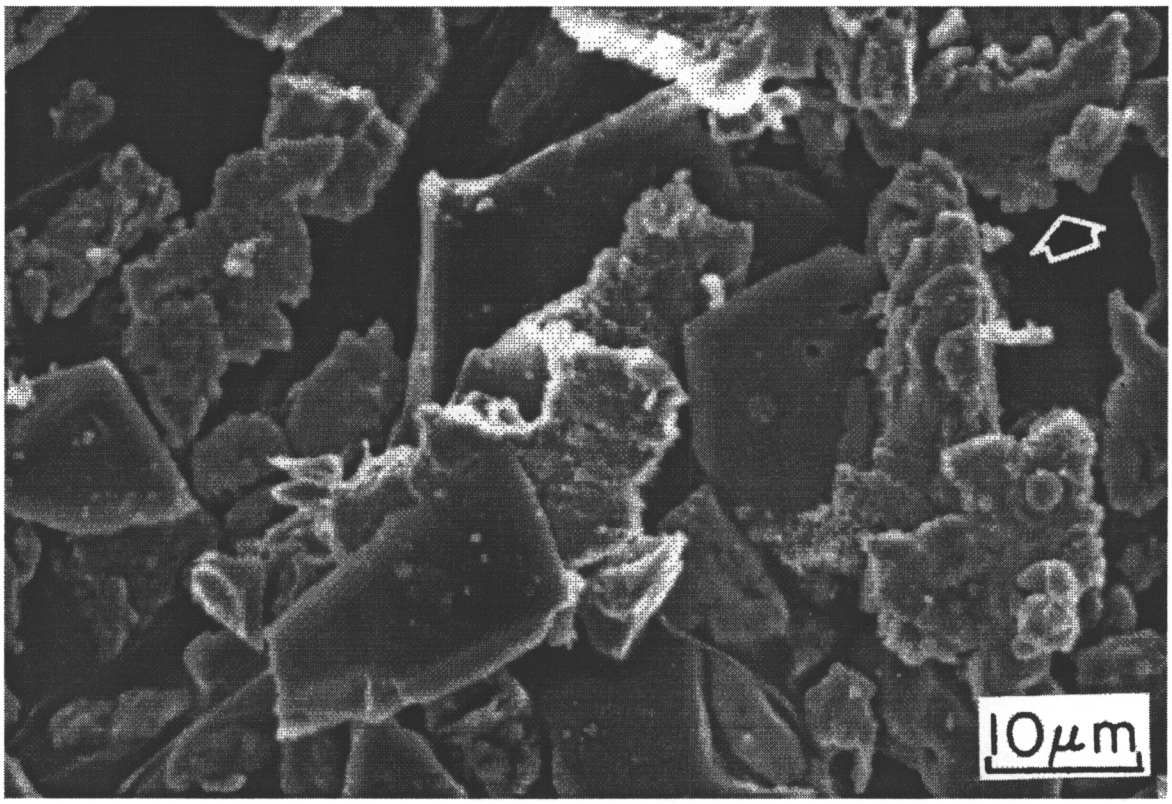

Figure 62: Wear debris from CPM10V RC 59 consisting mostly of sheet or plate type particles, with occasional microchips (arrow).

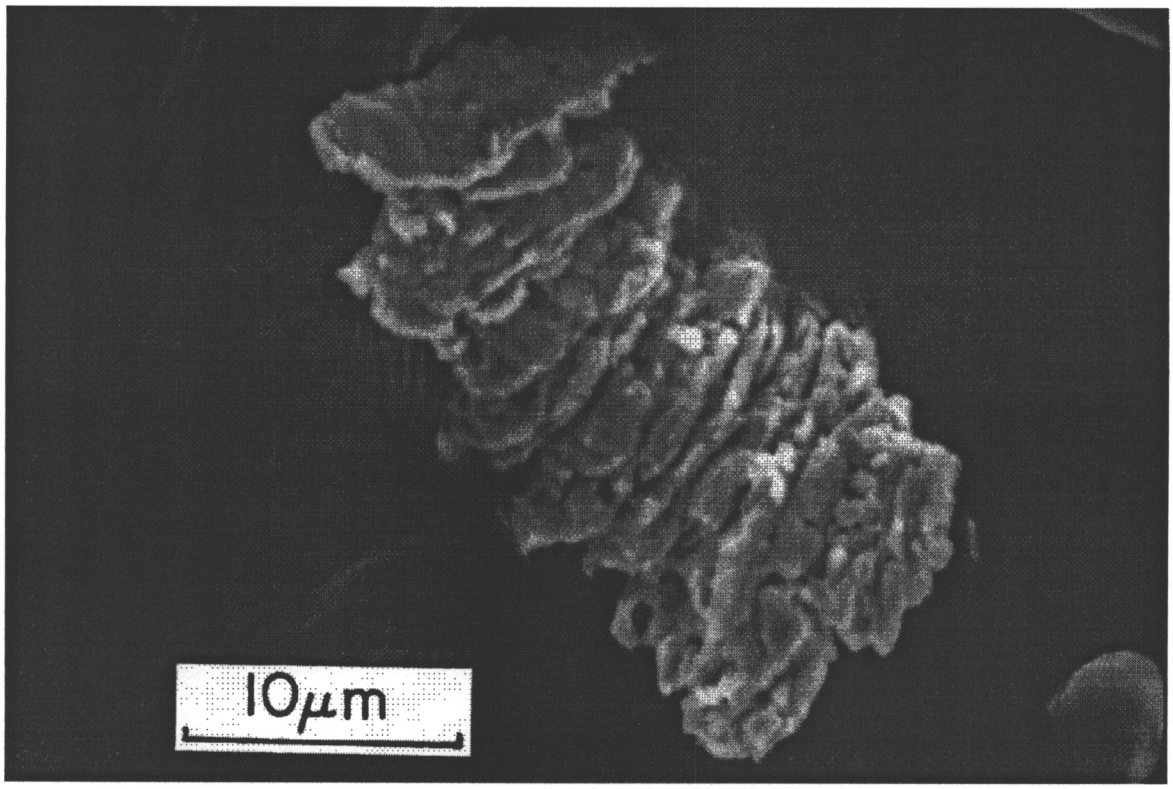

Figure 63: Wear particle from CPM10V RC 59 which may have formed by wedging.

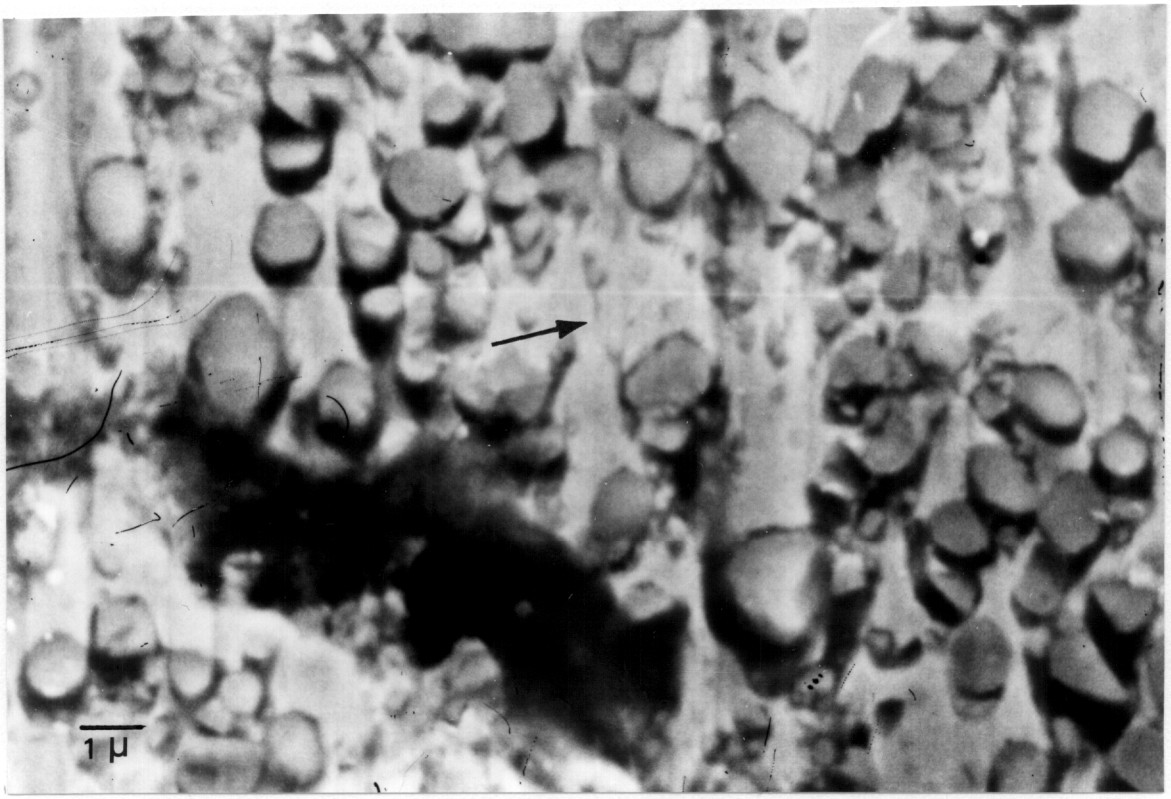

Figure 64: Cracks (arrow) in wear scar of ion nitrided CPM10V RC 55.

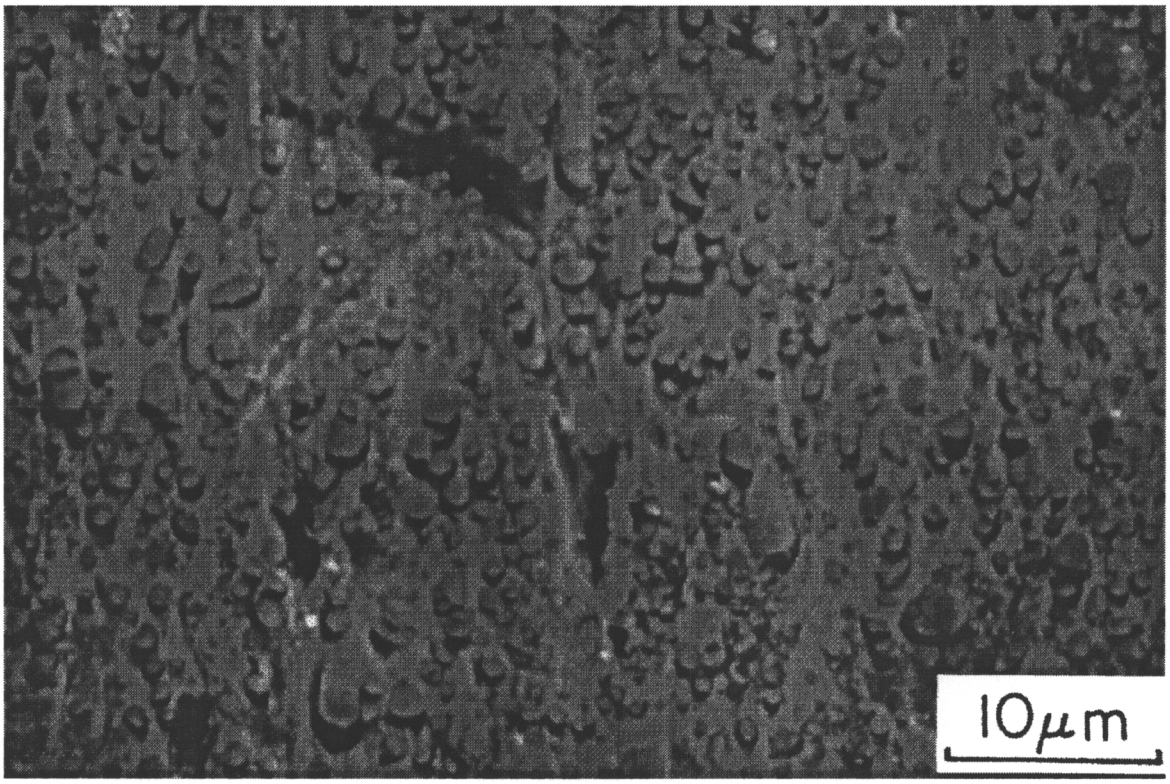

Figure 65: Pits in wear scar of ion nitrided CPM10V RC 55 (same region as Figure 64).

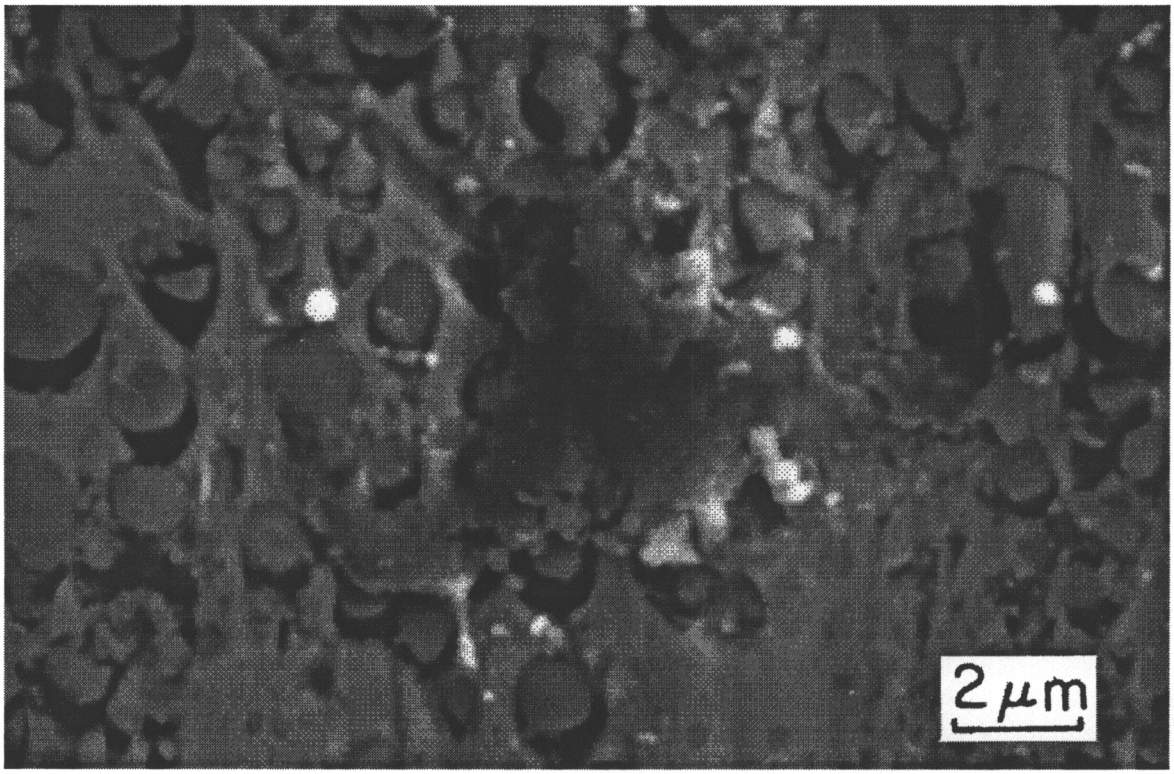

Figure 66: Loosely attached wear sheet in wear scar of ion nitrided CPM10V RC 55.

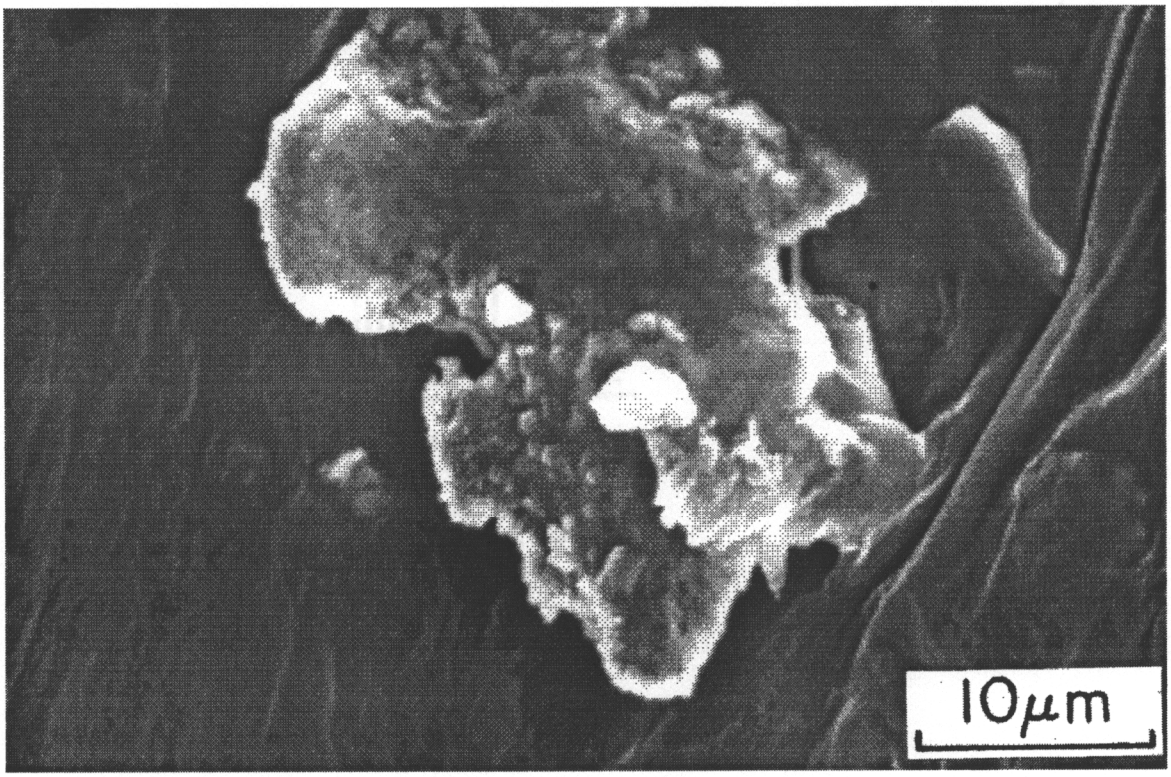

Figure 67: Sheet type wear particle in debris from ion nitrided CPM10V RC 55.

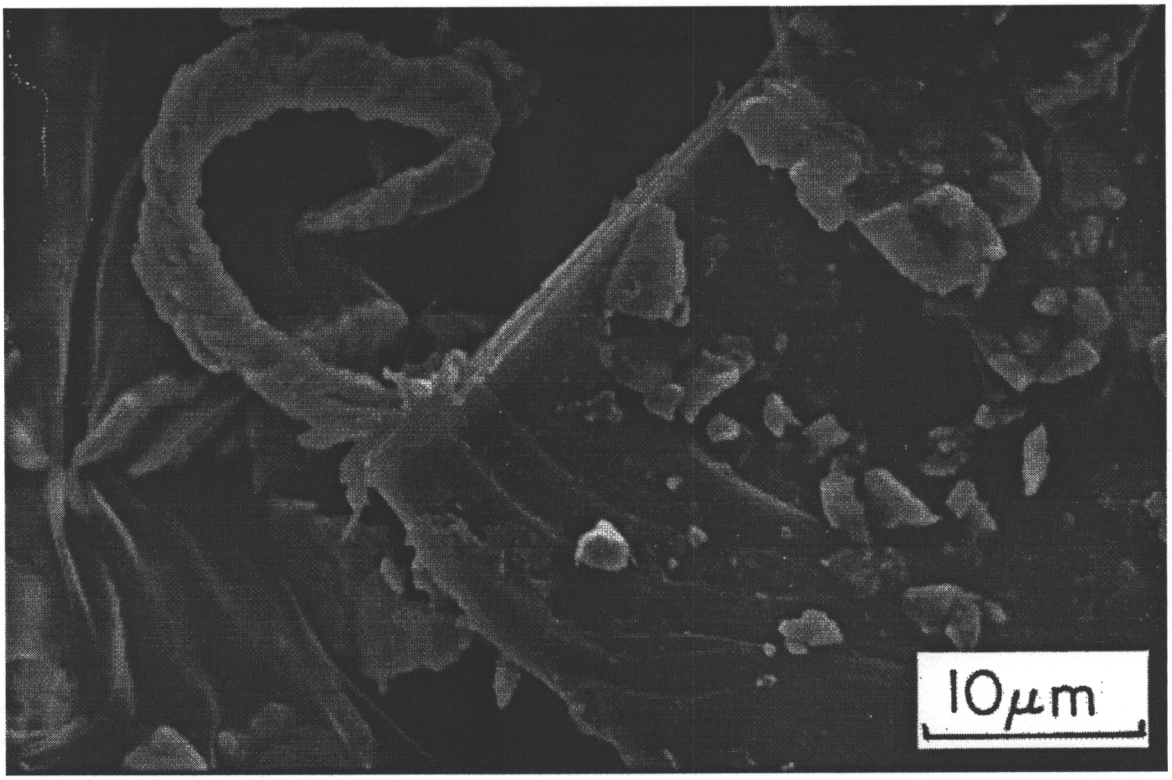

Figure 68: Microchip attached to silica fragment in debris from ion nitrided CPM10V RC 55.

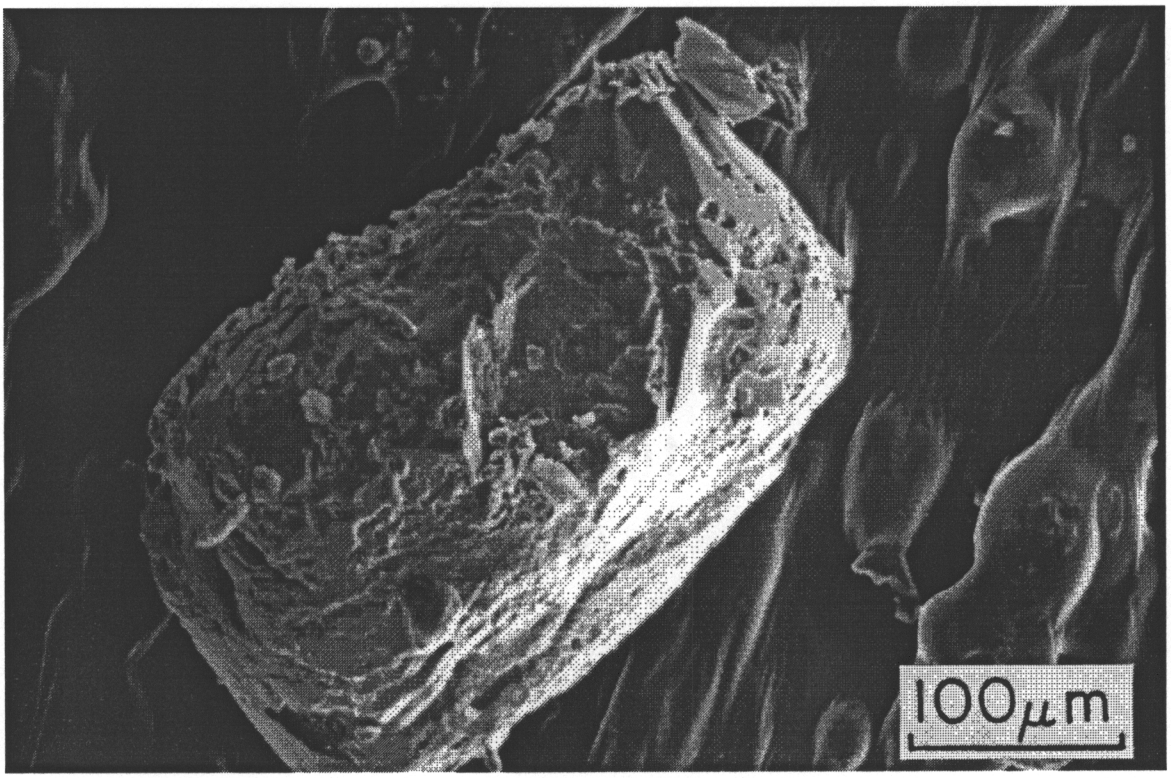

Figure 69: Used sand grain with wear debris.

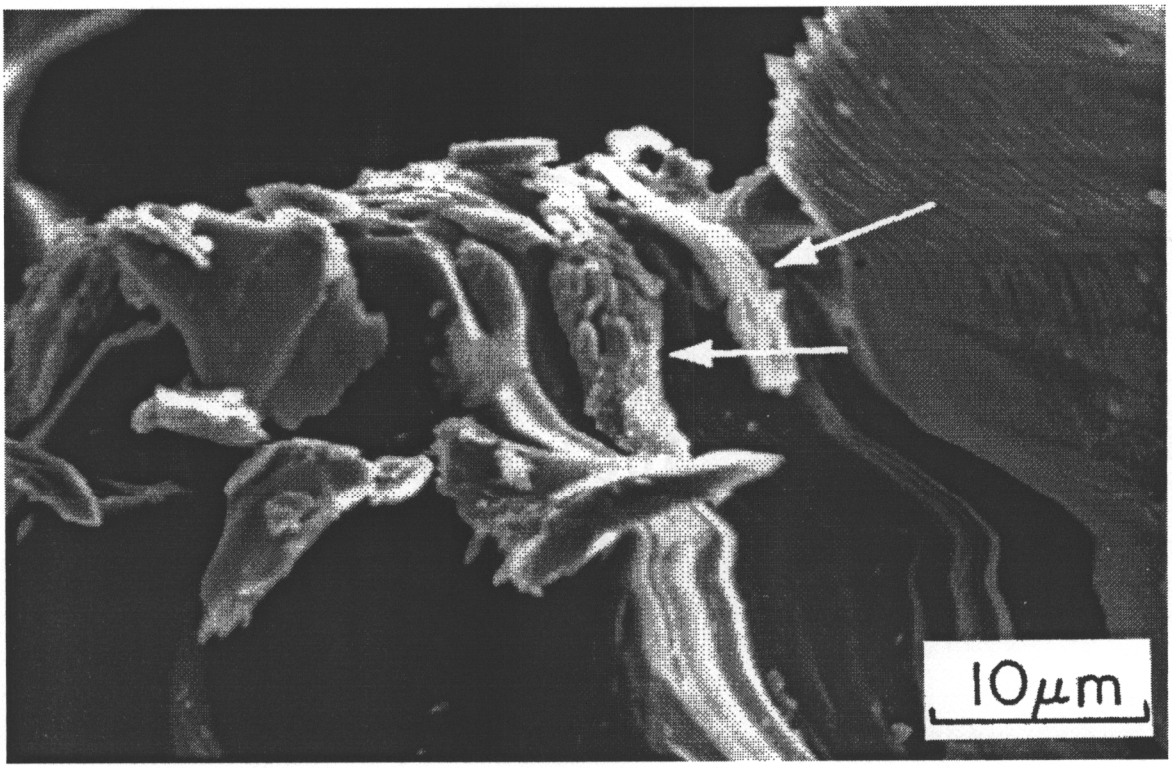

Figure 70: Enlarged view of crystal terminations on sand grain in Figure 69, showing microchips (arrows).

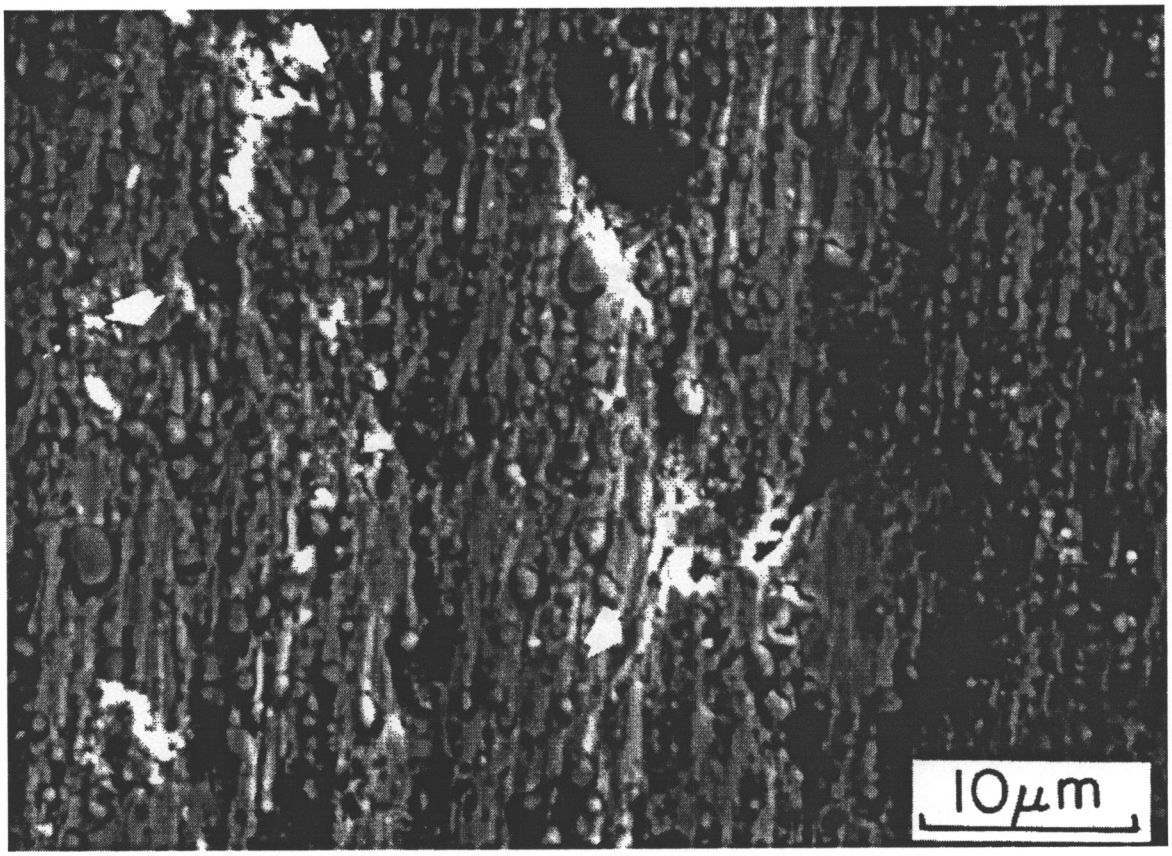

Figure 71: Wear scar on a gray sample of ion nitrided CPM10V RC 59 showing several cracks at the edge of wear sheets (arrows).

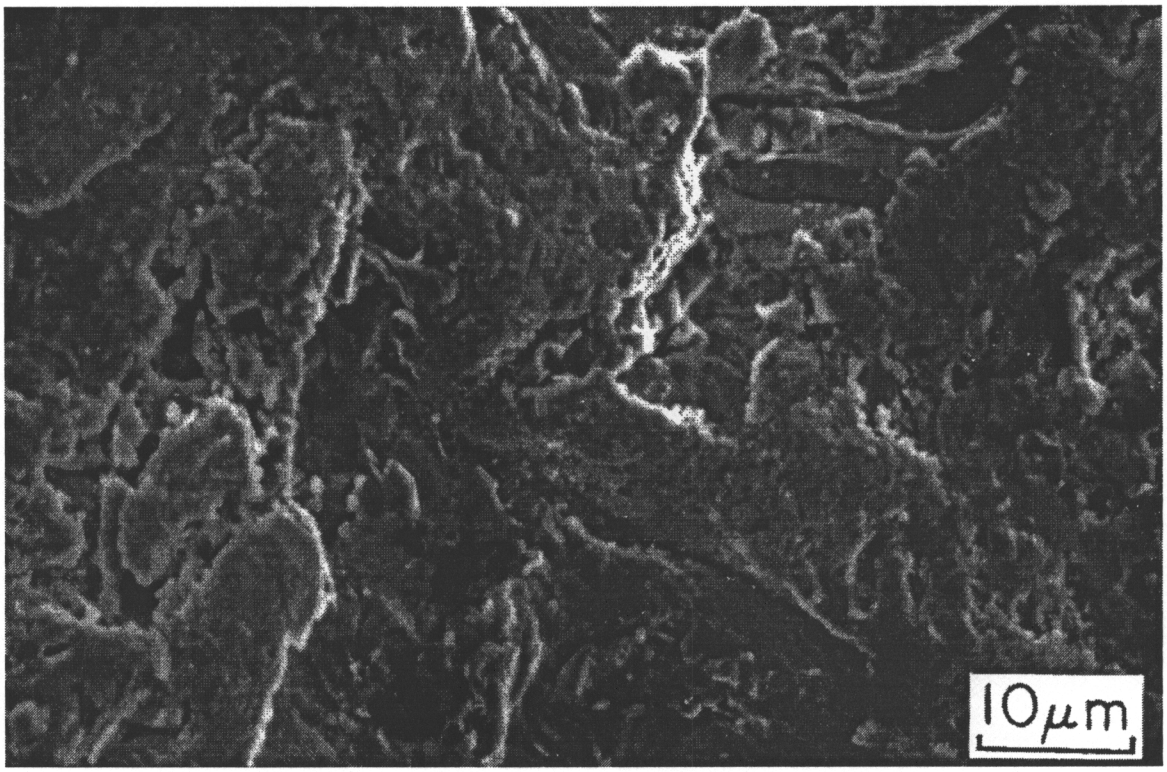

Figure 72: Unworn surface on a gray sample of ion nitrided CPM10V RC 59 showing several cracks.

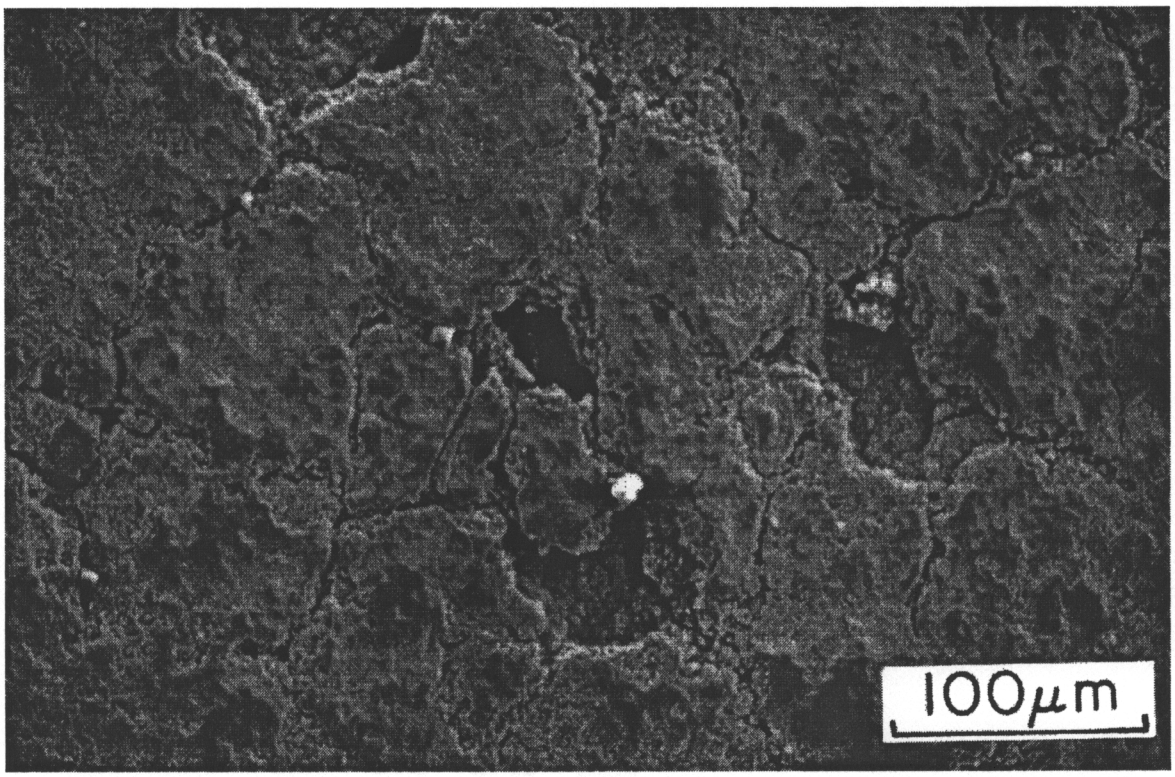

Figure 73: Entry region of wear scar on a black sample of ion nitrided CPM10V RC 59 showing surface layer spalling off.

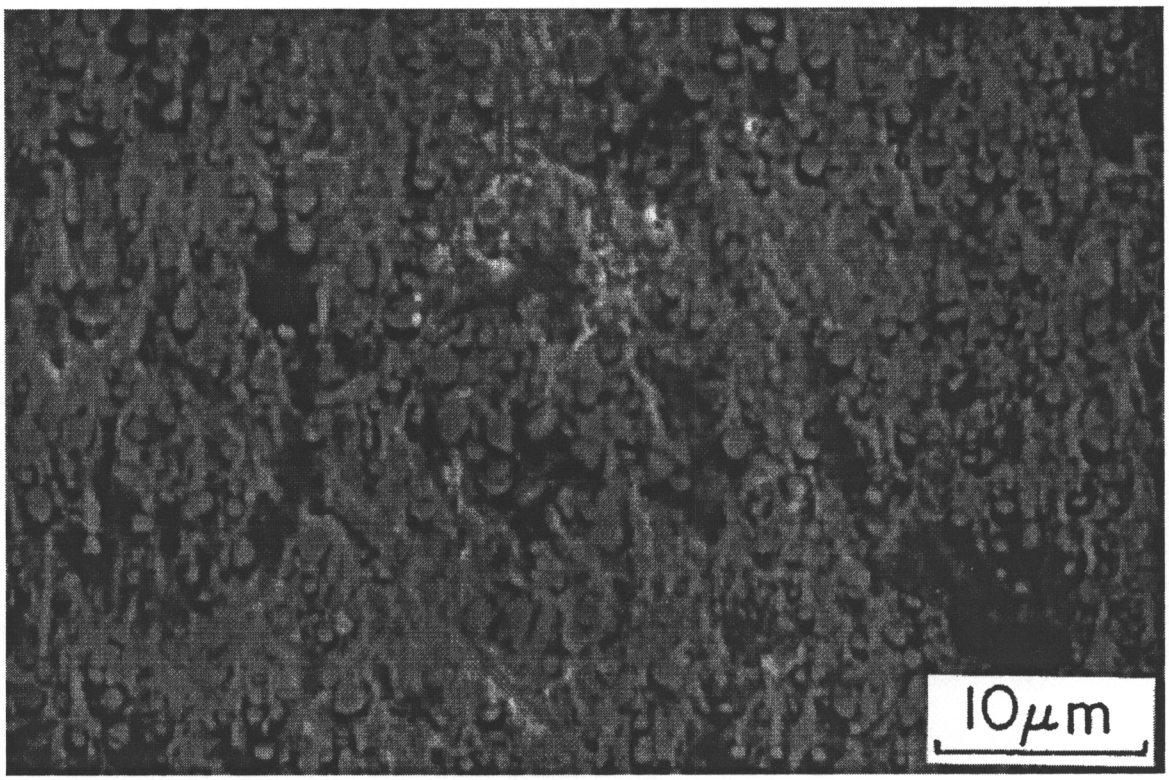

Figure 74: Center of wear scar on a black sample of ion nitrided CPM10V RC 59.

Figure 75: Transition in appearance of wear scar on ion nitrided Thyssen 4122.

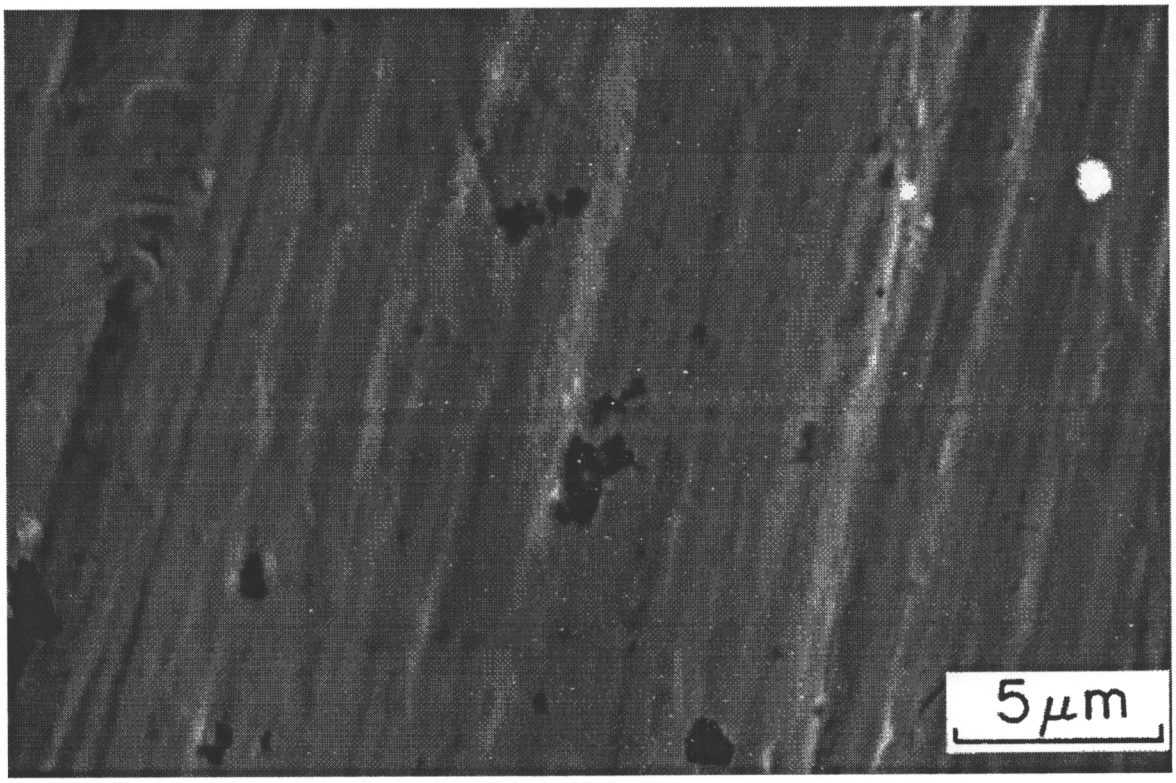

Figure 76: Linear scratches on nitride layer of wear scar on ion nitrided Thyssen 4122.

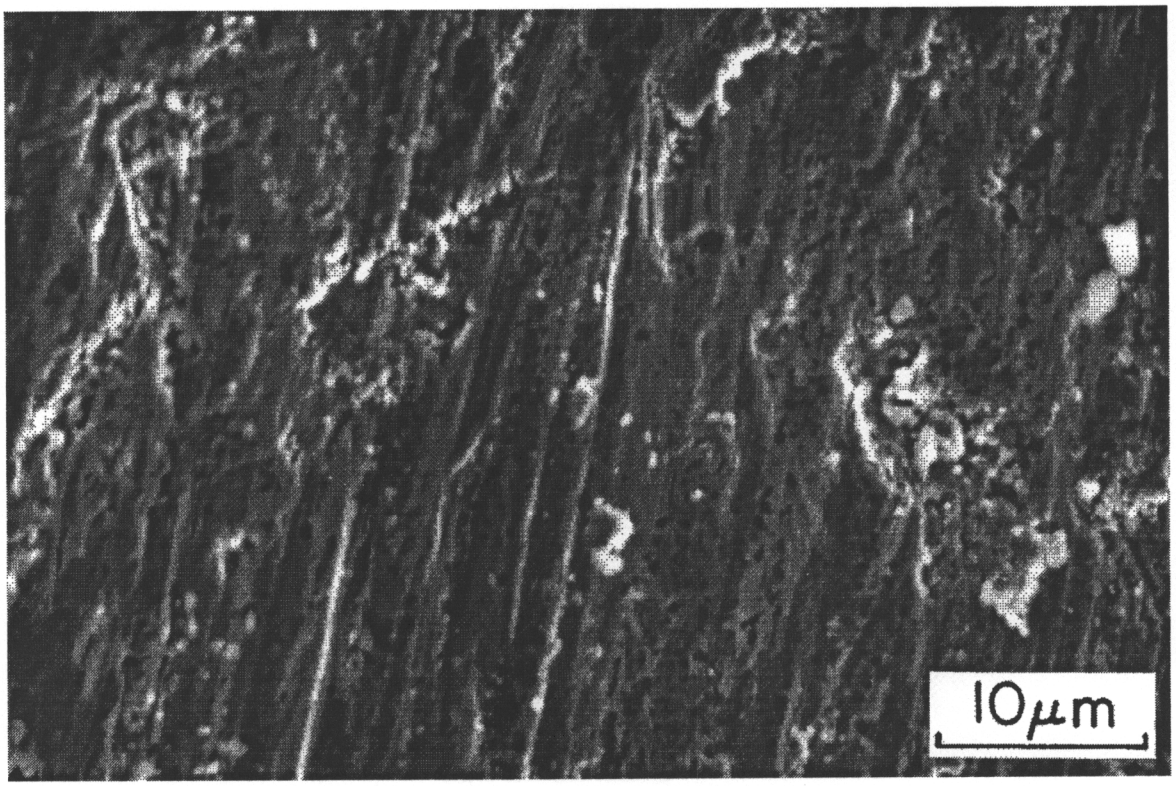

Figure 77: Sheet of loosely attached smeared metal in wear scar on ion nitrided Thyssen 4122.

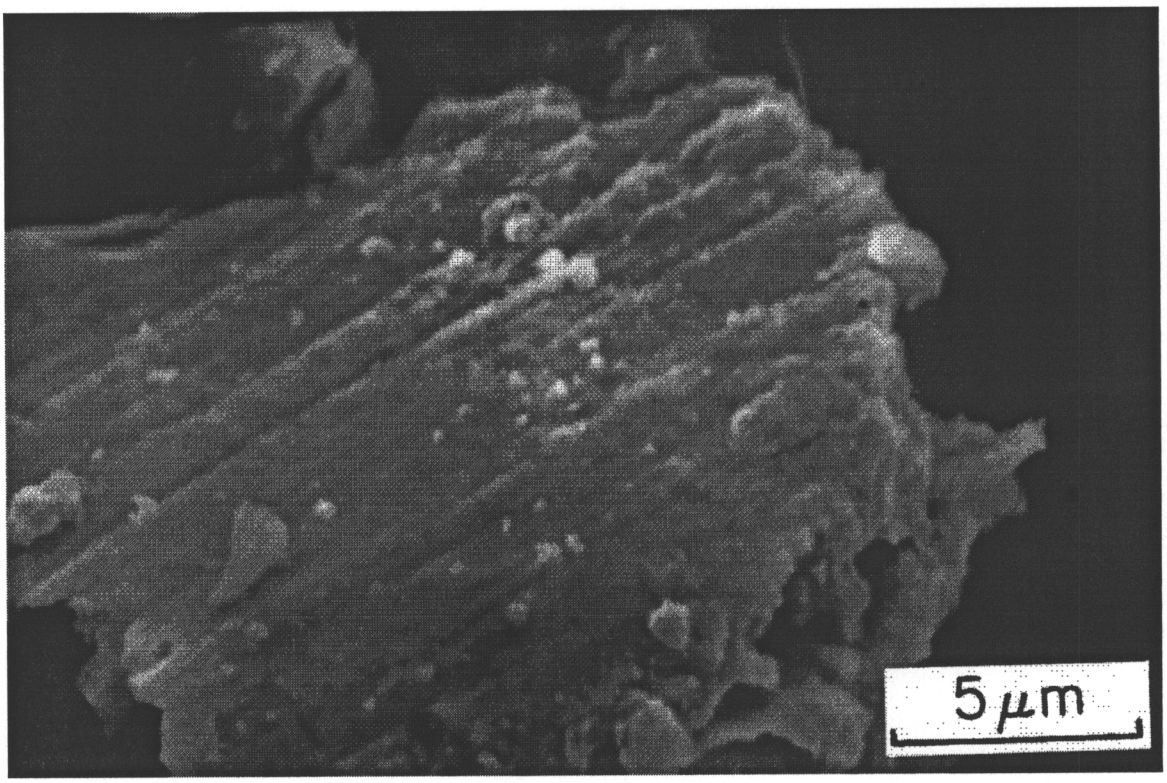

Figure 78: Wear sheet, with scratches, in debris from ion nitrided Thyssen 4122.

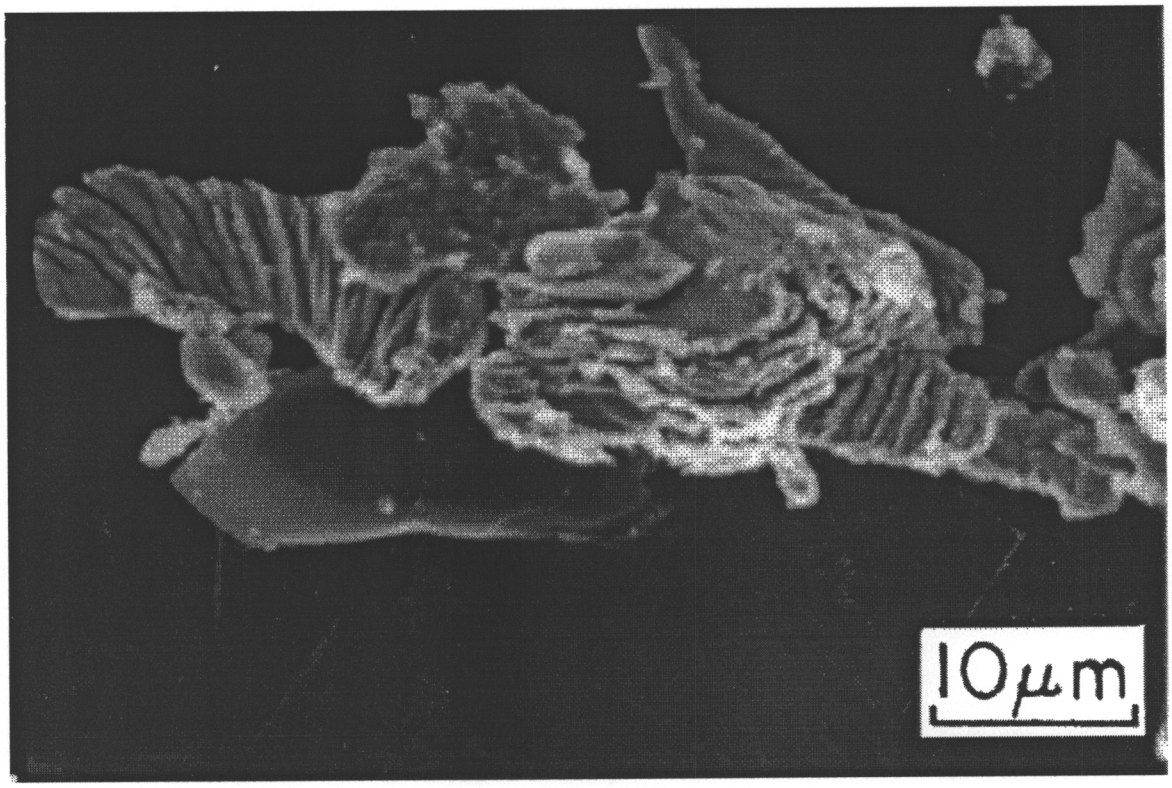

Figure 79: Microchip with thick center region in debris from ion nitrided thyssen 4122.

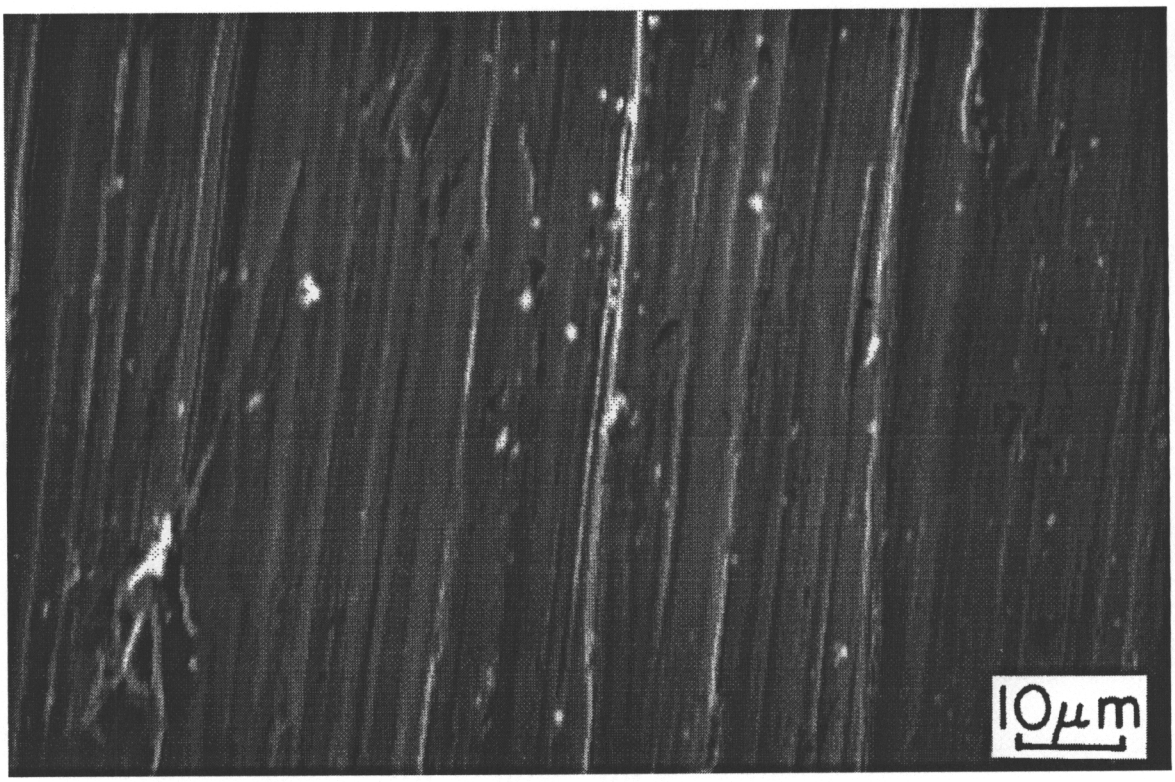

Figure 80: Sharply defined microcutting type scratches in nitride layer at ends of wear scar on ion nitrided AISI 4150.

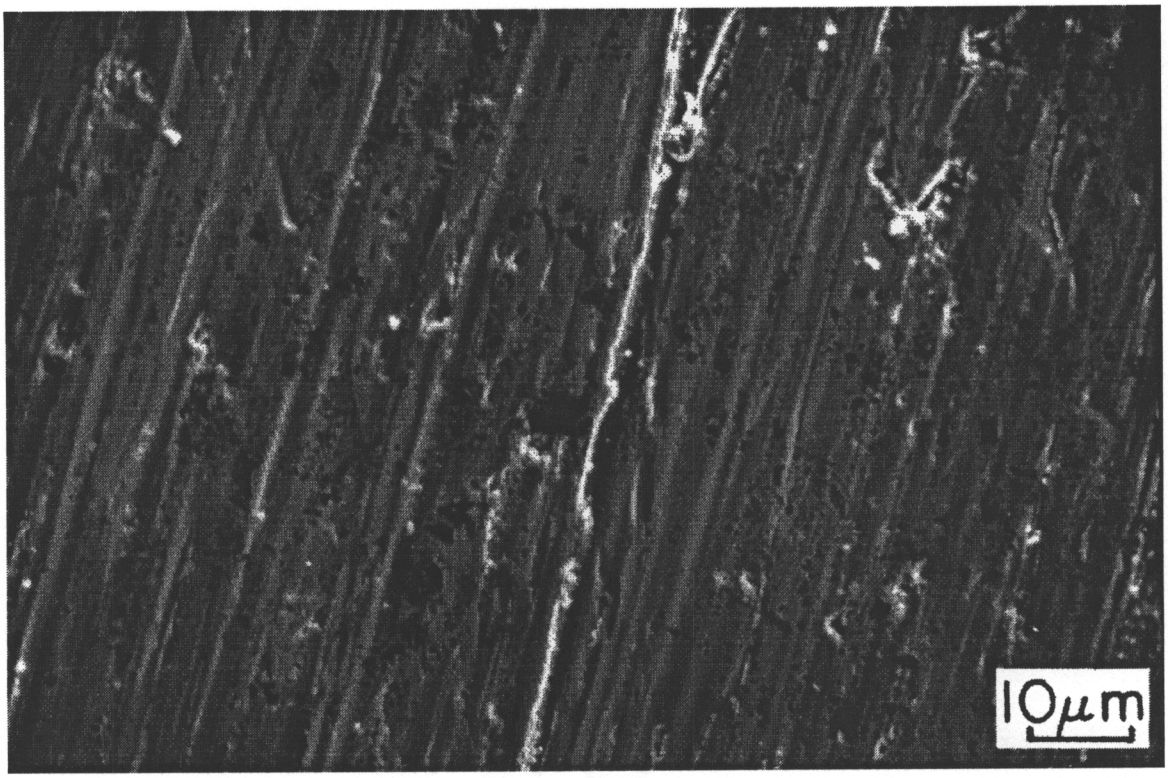

Figure 81: Smeared and dented plowing type scratches in nitride layer at the ends of wear scar on ion nitrided AISI 4150.

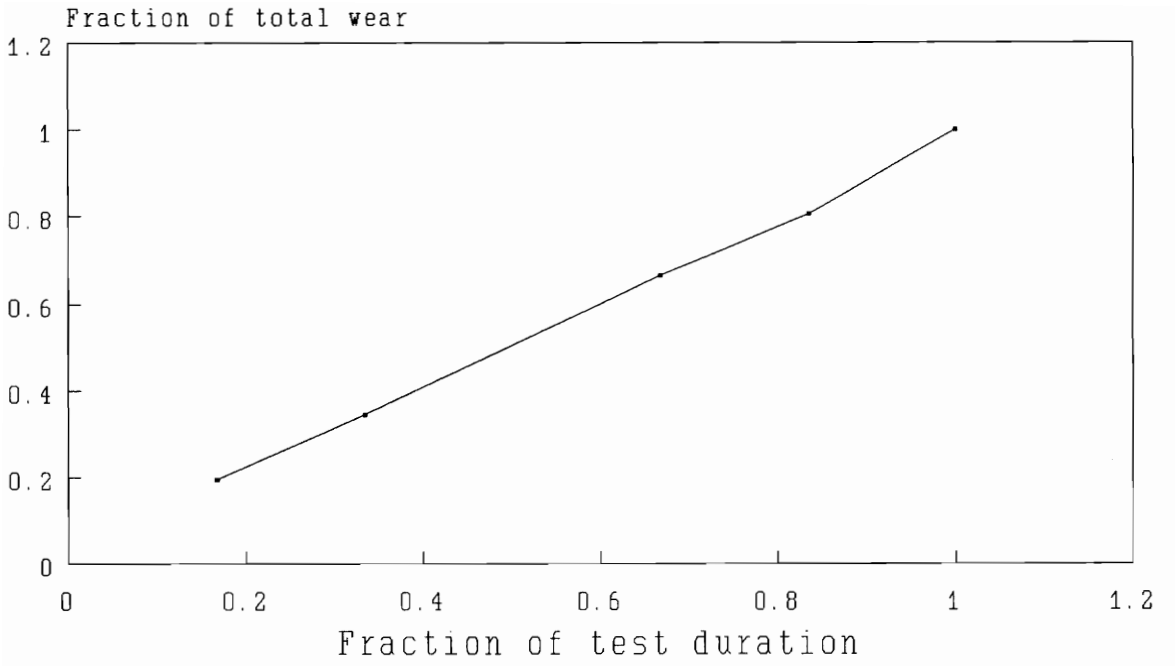

Figure 82: Interrupted tests on D-2, showing a linear relationship of wear to sliding distance.

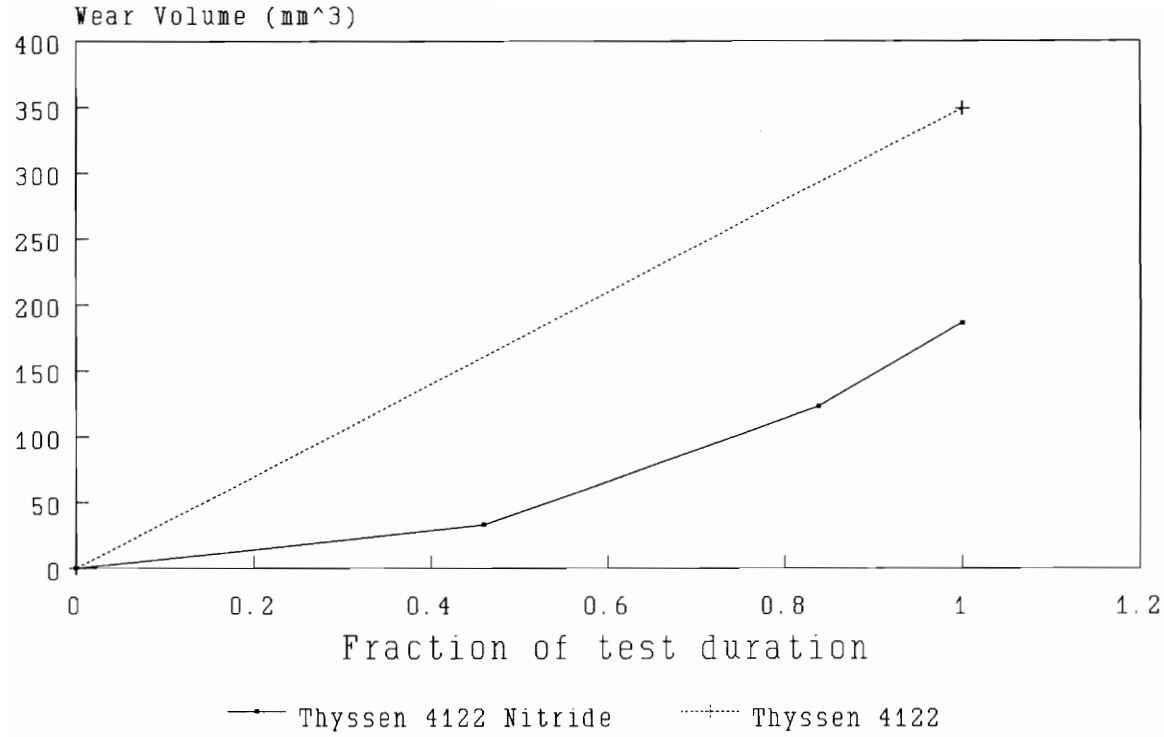

Figure 83: Interrupted tests on ion nitrided Thyssen 4122, showing a nonlinear relationship of wear rate to sliding distance.

VITA

William George Halley was born on May 22, 1951, in Steubenville, Ohio, and was raised in the steel mill town of Weirton, West Virginia.

Bill first attended Virginia Tech in 1969 as a co-op student working for Weirton Steel Division of National Steel Corporation. Bill received his B.S. degree in Metallurgical Engineering in 1974, and went to work full time for Weirton Steel.

After serving 10 year in the steel industry, Bill resigned to become involved in a leveraged buyout of a plant that National Steel was closing in New Castle, Pennsylvania, where he served as vice president. When this plant was sold to new owners in 1986, Bill left to become a consultant. After a year and a half during which he was involved in creating management and operating projections for several businesses including franchise fast foods, and the startup and operation of a plant producing polymer bonded magnets, Bill decided to return to engineering and so entered graduate school at Virginia Tech to pursue a M.S. degree in Materials Engineering.

After completing his M.S. Bill intends to continue on to get his doctorate.